# The Effect of Organic Resins on Ice Recrystallization

Ali Mohammed Saleem

A thesis submitted to the University of Ottawa in partial fulfillment of the requirements for the Master of Science degree in Chemistry

Department of Chemistry and Biomolecular Sciences
Faculty of Science
University of Ottawa

# Abstract

Over the years, methods to preserve biological samples, such as red blood cells, have been explored and researched. Currently, cryopreservation of biological samples is the most commonly used method for long-term storage of cells and tissues. Cryopreservation stores samples at very low temperatures, typically ranging between -80 ºC to -196 ºC — temperatures at which biochemical processes are effectively halted. However, at this temperature, cellular damage due to cryoinjury is a major concern. The causes of cryoinjury are mainly due to two major factors, osmotic pressure and mechanical damage due to ice formation. Both issues can be mitigated with the use of cryoprotectants, chemical additives that are added to a sample prior to preserving it at -80 ºC to -196 ºC. Moreover, some cryoprotectants exhibit properties of ice recrystallization inhibitors (IRIs), which reduce the growth rate of ice crystals and lead to a decrease in cellular damage due to the aforementioned factors.

In this thesis, the IRI activity of Wang and PEGA resins was evaluated, finding no IRI activity when compared with 2FA, a well-known IRI. As Wang and PEGA resins are commonly coupled with amino acids during solid phase synthesis, the IRI activity of the resins functionalized with different amino acids was also tested. To determine which amino acid to couple with the resin, the IRI activity of various amino acids was tested, along with some of their β-amino acid counterparts. Among the amino acids tested, *L*-phenylalanine exhibited the highest IRI active, with an $IC_{50}$ = 14.0 mM [12.3, 15.6], while *L*-glycine showed the lowest IRI active, with an $IC_{50}$ = 287.1 mM [242.3, 316.2]. Moreover, all the tested β-amino acids had less IRI activity compared to their α-amino acid isomer. Using this information, the IRI activity of functionalized Wang and PEGA resin – Wang-Gly, Wang-Gly-Phe, Wang-Gly-Lys, PEGA-Phe, and PEGA-Lys – was evaluated, finding no IRI activity when compared with 2FA.

In order to enhance the IRI activity of amino acids, the most IRI active amino acid tested, *L*-phenylalanine, was used as the starting material to synthesize and evaluate the IRI activity of acylated and alkylated amino acid derivatives. *N*-acyl-*L*-phenylalanine showed either low solubility, a decrease in IRI activity, or both when compared with *L*-phenylalanine. On the other hand, *N*-isopropyl-phenylalanine showed enhanced IRI activity, with an $IC_{50}$ = 1.3 mM [0.9, 1.7] compared to *L*-phenylalanine's $IC_{50}$ = 14.0 mM [12.3, 15.6].

As the IRI activity of some amino acids was tested, *L*-phenylalanine showed the best IRI activity compared with the other tested amino acids. However, the IRI active amino acids showed no discernable IRI activity when conjugated to insoluble organic resins, Wang and PEGA. Derivatives of *L*-phenylalanine, such as *N*-isopropyl-phenylalanine, showed high IRI activity with an $IC_{50}$ = 1.3 mM [0.9, 1.7], which could potentially be conjugated to the insoluble organic beads such as Wang and PEGA resins to test whether that would cause the resins to exhibit IRI activity.

# Acknowledgements

For the past two years, I have been doing research in the Ben lab. And throughout the many ups and downs during the semesters, there are many I would like to thank. First and foremost, I would like to thank my Professor and supervisor for this research, Professor Robert Ben. I started my graduate studies without enough information on what I was getting myself into, and without his help and support, I would have suffered a lot. Whenever I had concerns, whether they were regarding my research, time management, or life in general, he was always there to help me. I will never forget the impact he had on my life.

I would also like to thank my colleagues in the lab – Marcus Diamante, Leah McMunn, and Elly Walsh – for their guidance and support. They were always there to help me navigate the lab and teaching me many things I initially lacked. Without their assistance, my lab knowledge would not have been up to par, and the foundation of my knowledge regarding the research and lab work would have been lacking. I thank them greatly for their help, guidance, and patience. I also have to thank the undergraduate student, Simon Sinn, for assisting me in the synthesis and analysis of several compounds, accelerating the progress of my research.

Finally, I would like to thank my family and friends, who have always been there to listen when things got tough, helped me persevere through my studies, provided unwavering support — support I truly cannot imagine being without.

# Table of Contents

# List of Figures

## 1 Introduction

## 2 Organic Resins

# List of Tables

## List of Abbreviations

| | |
|---|---|
| RBC | Red blood cell |
| CPA | Cryoprotective agent |
| IIF | Intracellular ice formation |
| PVA | Polyvinyl alcohol |
| IRI | Ice recrystallization inhibitor |
| PBS | Phosphate-buffered saline |
| AFPs | Antifreeze proteins |
| AFGP | Antifreeze glycoproteins |
| TH | Thermal hysteresis |
| PEGA | Acrylamide polyethylene glycol |
| DMF | Dimethylformamide |
| HBTU | Hexafluorophosphate benzotriazole tetramethyl uronium |
| DIPEA | *N*,*N*-diisopropylethylamine |
| 2FA | *N*-(2-fluorophenyl)-d-gluconamide |
| $IC_{50}$ | Half-maximal inhibitory concentration |
| SD | Standard deviation |

# 1 Introduction

### 1.1.1 Preservation of biological samples

There are three common techniques for preserving biological samples through cooling. The first method is called hypothermic storage, which involves preserving biological samples at temperatures between 4 ºC and 10 ºC. At this temperature range, biochemical processes are slowed, which helps in preserving cellular metabolites without reaching the temperature where ice formation occurs. This method is primarily used for short-term storage (days to weeks). [1,2] However, cell death from exposure to low temperatures is a common issue when cooling biological samples. In the case of hypothermic storage, if the samples are stored for extended periods of time at temperatures between 4 ºC and 10 ºC, stress-induced cell death through apoptosis and necrosis pathways are observed. [3]

The second method of preserving biological samples through cooling involves vitrification. This is done by adding very high concentrations of cryoprotective agents (CPAs) to the biological sample, which is then rapidly cooled with liquid nitrogen. This causes the highly viscous cryomedium to transition into a "glass-like" state, avoiding the formation of ice crystals. [2,4–8] At this temperature (-196 ºC), biochemical processes are effectively halted, preventing stress-induced cell death. The difficulty with vitrification includes achieving the required high cooling rates to form the glass-like state on large biological samples. Moreover, vitrification can still cause damage to biological samples during devitrification, this is caused by ice crystal formation due to heating at a non-optimal rate during thawing. [9–14]

The third technique is cryopreservation, in which the biological sample is stored at temperatures ranging from -80 ºC to -196 ºC, effectively halting all biochemical processes in the cells, allowing the biological sample to be available for long-term storage. [15] However, at these temperatures, ice crystals will form, potentially damaging the cells. [4] Many factors can influence ice growth and, consequently, the viability of cells after cryopreservation. These factors include cooling rate, sample volume, storage temperature, warming rate when thawing, type of cells being preserved, type and amount of cryoprotectants (CPAs) used. [4,5,13,16] During cryopreservation, cell death within the preserved biological sample is still observed, but for different reasons. As cells are cooled down to sub-zero temperatures, water nucleates and forms ice crystals. These ice crystals can cause cell injury through mechanical damage or osmotic imbalance. [17] Moreover, when the cells are cooled down rapidly, ice crystals can grow within them, leading to cellular damage. In contrast, damage can also occur through slow cooling of the cell, which can cause excessive dehydration. [4,18–20]

Cryopreservation has enabled major advancements in the field of medicine. For example, the cryopreservation of red blood cells (RBCs) enables easier storage and access to rare blood types. [12,21,22] Other applications include oocyte and embryo cryopreservation for preservation of reproductive capacity, tissue banking for human leukocyte antigen typing in organ transplantation, in-vitro fertilization, and transplantation of various progenitor cells. [5]

### 1.1.2 Cryoprotective agents (CPAs)

Cryopreservation requires the use of CPAs. [4] CPAs are chemical additives that are added to a sample prior to preserving it under extreme cold temperatures (-80 ºC to -196 ºC). [2,4,5] CPAs are essential for protecting biological samples and mitigating cellular damage caused by cooling them to sub-zero temperatures. This damage is caused by osmotic pressure and mechanical damage due to ice formation. [13,17–20] A general procedure for cryopreservation entails addition of CPAs to the biological sample, followed by the controlled rate of cooling/freezing of the sample. Afterwards, the sample is thawed, and CPAs are removed. [2,13,16,23–25]

There are two types of cryoprotectants: permeating CPAs, which enter the cell, and non-permeating CPAs, which do not. [23,26,27] Permeating CPAs, such as dimethyl sulfoxide (DMSO) and glycerol, generally enter the cell as water exits during the slow cooling processes (Figure 1.1). This helps protect the cell from injury caused by both, osmotic imbalance – which could otherwise lead to cell shrinkage and death due to the toxicity of high concentrations of electrolytes – and the formation of intracellular ice crystals — which would cause mechanical damage to the cell (Figure 1.1). [28–32]

On the other hand, non-permeating CPAs – including some sugars, such as trehalose, and polymers, such as polyethylene glycol – cannot cross the cell membrane and generally have a higher molecular weight than permeating CPAs. [23,26,27,32] Non-permeating CPAs tend to dehydrate cells due to an increase in the osmolality of the extracellular solution, reducing cellular damage caused by intracellular ice formation (IIF) during the proper cooling procedure. [2,13,16,23–25] Moreover, non-permeating CPAs are generally less toxic than permeating CPAs, as the latter can directly interact with pathways and mechanisms within the cells, while the former is blocked by the cell membrane. [23,26,27]

Moreover, some CPAs can reduce the size of ice crystal growth, further increasing the likelihood of cell survival. [28–31] However, when thawing the sample, water rapidly re-enters the cell, which can cause cells to swell beyond their initial size — a concern, as cells are generally more sensitive to swelling than to shrinkage. [18–20]

### 1.1.3 Cryoinjury

Two major factors for cryoinjury are osmotic pressure and mechanical damage due to ice formation. When the cryomedium is slowly cooled to sub-zero temperatures, the water starts to freeze. As the water freezes, solutes are excluded from the ice lattice, and therefore, are concentrated in the solution between the ice crystals. This creates an osmotic imbalance between the semi-frozen cryomedium and the cell, which causes the cell to shrink as water leaves (Figure 1.1). [4,18–20,26,33] This dehydrates the cell before its biochemical activities are effectively halted due to the extremely low temperatures (-80 ºC to -196 ºC) of cryopreservation, which can be lethal to the cell. Moreover, the high solute concentration would impact the cell membrane, reducing its stability and potentially rupturing the cell membrane, which would cause cell death. [14,18,20,21,34–38]

Dehydration of the cell due to the slow cooling can be avoided by rapidly cooling the cryomedium and cells. [4,18–20] This causes the cryomedium and cells to freeze before osmosis can cause lethal damage to the cells. [17] However, as the cell is not dehydrated and water remains within the cell, IIF occurs, in which the water within the cell freezes. This disrupts the cell's normal structure to the point that it is no longer functioning as it should, which can be lethal to the cell.

Due to these factors, an optimal rate of cooling for each cell type must be achieved to minimize cell death during cryopreservation. [4,5,39] Moreover, the usage of CPAs can help prevent cryoinjury. For example, permeating CPAs are used in the cryomedium that would enter the cell and replace the water leaving it due to osmotic imbalance, which would prevent the cell from shrinking and the adverse effects that follow. [2,13,16,23–25]

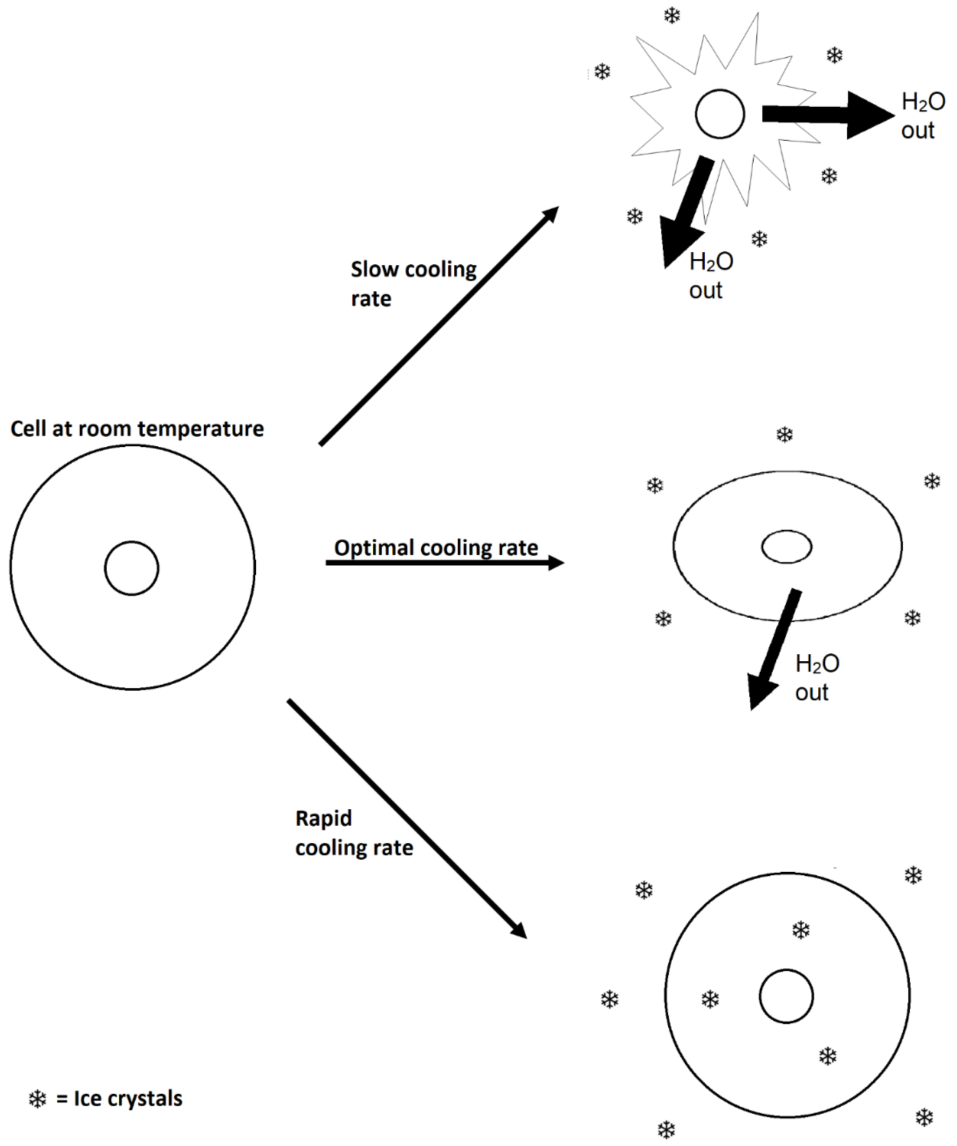

*Figure 1.1: Depiction of ice growth and osmotic effect on cells based on the cooling rate of the cryomedium* [18–20,38]

### 1.2.1 Ice Recrystallization

Ice recrystallization is defined as the growth of large ice crystals in a frozen sample at the expense of smaller ice crystals. [12,25,27,38,40,41] This is a thermodynamically driven process (Figure 1.2). [16] Ice recrystallization occurs predominantly during the warming of a frozen sample, [12–14,24,39] and is a leading cause of cell death during cryopreservation. [4–6,18–20,27,42,43]

The mechanism by which ice grows is believed to occur by either grain boundary migration or Ostwald ripening. [16,33,44,45] Grain boundary migration occurs when larger ice grains grow at the expense of smaller ones. Smaller ice grains have a greater convex surface curvature than larger ice grains, which means they will have a higher surface energy. As a result, water molecules migrate from the smaller grains to the larger ones. This process reduces the overall curvature, thus reducing the energy in the system, leading to the growth of larger ice grains (Figure 1.2). [16,33,44,45]

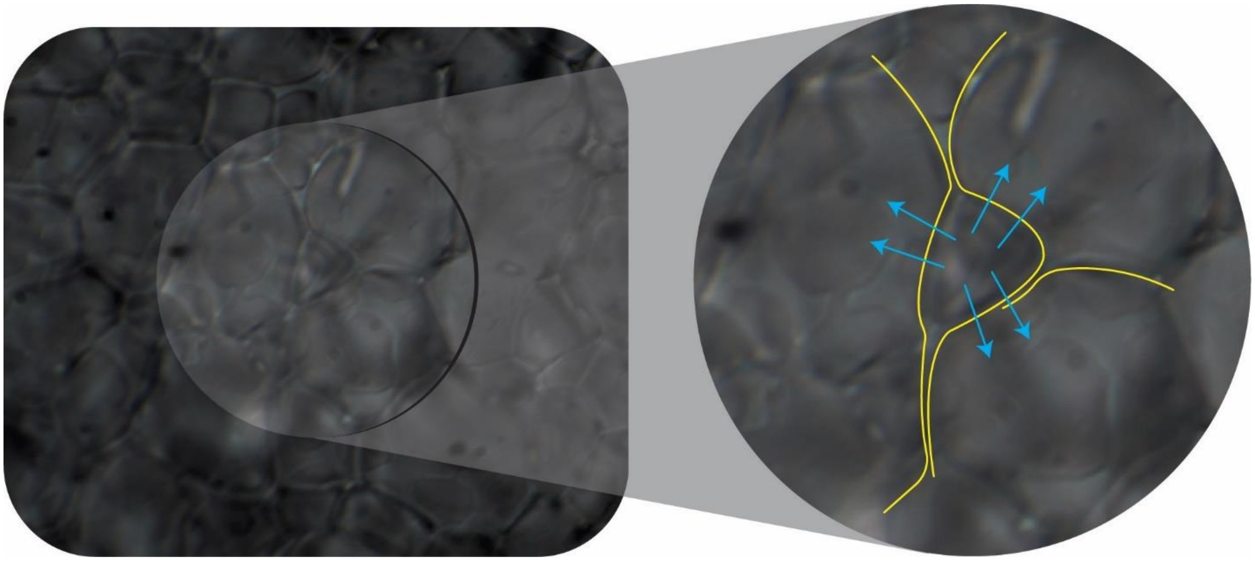

*Figure 1.2: The migration of water molecules from the smaller grain with higher convex curvature to larger ice grains with higher concave curvature (Shown in blue arrows) across a non-frozen layer (yellow line), resulting in a decrease in total system energy.* [46]

Grain boundary migration neglects the presence of bulk-water in the system. However, Ostwald ripening takes that into consideration. [45] Ostwald ripening is the thermodynamic process in which large ice crystals grow at the expense of the smaller ice crystals, reducing the total system energy. Larger ice crystals have lower surface area to volume ratio, making them more stable than smaller ice crystals, which have a greater surface area to volume ratio, since water molecules on the surface of an ice crystal are less stable than those within the ice crystal. Assuming that the overall volume of ice is constant, water molecules in the system transfer from the smaller, less stable ice crystals to the larger, more stable ice crystals. This results in an increase in the average ice crystal size, a decrease in the total number of ice crystals, and a decrease in the number of less stable water molecules at the surface of ice crystals. Hence, the system's free energy will decrease. [16,33,45,47,48]

### 1.2.2 Quantifying ice recrystallization — the splat-cooling assay

Ice crystals grow larger as they recrystallize through the mechanisms described above (Figure 1.2), which can lead to cryoinjury. [4,16,18–20,26,33,44,45] However, with the presence of some CPAs, such as antifreeze proteins (AFPs) and antifreeze glycoproteins (AFGP), it was observed that the rate of ice recrystallization decreases, which leads to a reduction in the number of damaged cells. [28–30,46,49–53] This decrease in ice recrystallization is caused by ice recrystallization inhibitors (IRIs), which can be analyzed using a splat-cooling assay, where a sample is dissolved in phosphate-buffered saline (PBS) at different concentrations in order to generate a dose-response curve for the IRI activity of the sample. In this assay, a 10 µL volume of each sample is dropped, at a height of 2 m, onto a dry-ice cooled aluminium block (approximately -80 ºC), forming an ice wafer (Figure 1.3). The wafer is then allowed to anneal for 5 minutes at -6.4 ºC, during this time, ice recrystallization occurs. The annealing time of 5 minutes was used as the growth of ice crystals is monoexponential, and the difference between the mean grain size of ice crystals between 5 and 20 minutes was not significant enough to warrant a longer wait time. [12,16,33,38,40,47,54,55] After the 5-minute annealing period, images of the ice crystals are taken using a microscope fitted with a camera; this allows images to be captured and viewed with consistent properties (Figure 1.3). Using ImageJ, the images were analyzed by manually circling the boundaries of each ice crystal, whose area was then calculated. [16] After the splat-cooling assay is conducted, the rate of ice crystal growth is calculated using the areas of the ice crystals and time spent annealing (5 minutes). Afterwards, the sample's ice crystal growth rate is normalized with that of a blank control PBS, which was used as the solvent, and a four-parameter dose-response curve is generated using the normalized growth rates of the sample. [27,40,54] The dose-response curve was drawn using GraphPad Prism 9.0.0.

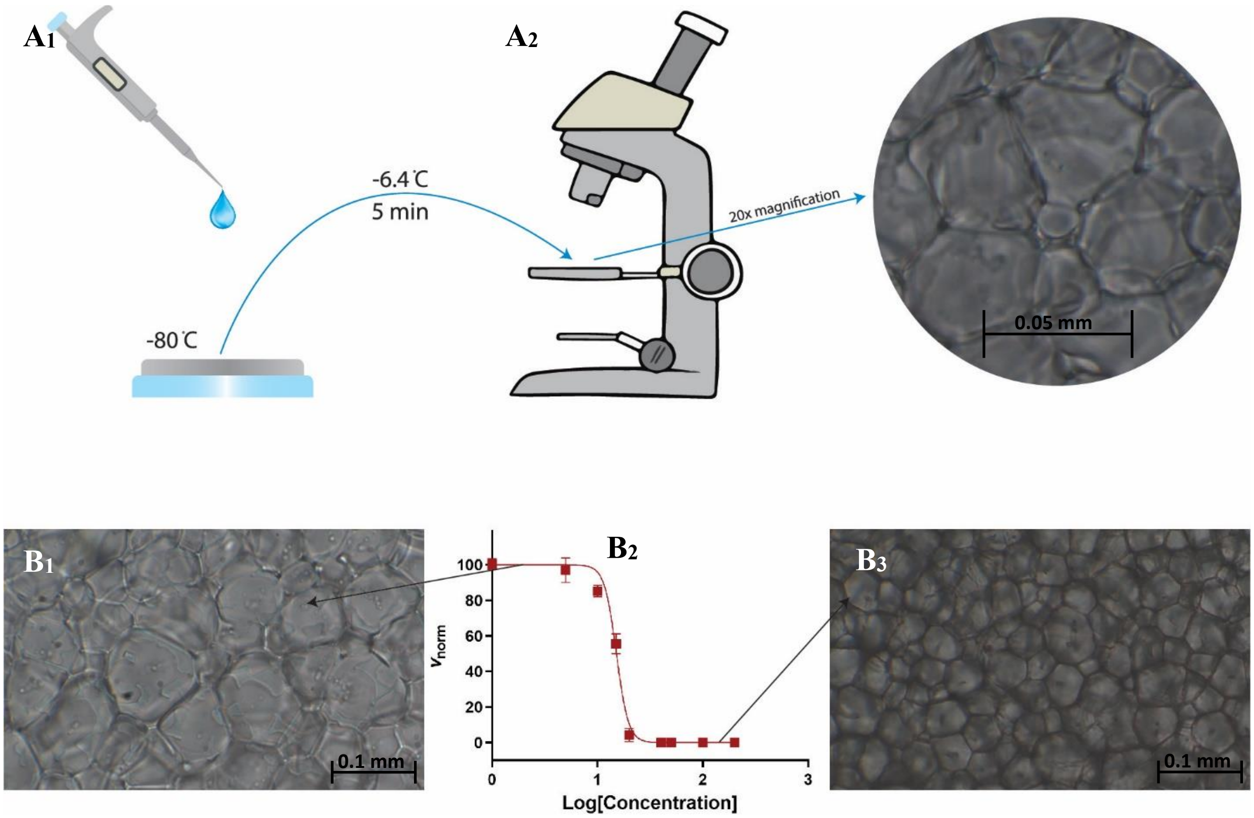

*Figure 1.3: The general procedure for a splat-cooling assay. ($A_1$) How an ice wafer is obtained from a 10 µL sample. ($A_2$) Ice crystals under a microscope annealing at -6.4 °C for 5 min. ($B_2$) Expected dose-response curve obtained from an IRI active molecule (L-phenylalanine in this case). ($B_1$) Image of an ice wafer at 20x magnification of 1 mM L-phenylalanine, ($B_3$) Image of an ice wafer at 20x magnification of 100 mM L-phenylalanine.* [54–56]

### 1.3.1 Natural ice recrystallization inhibitors (IRIs)

AFGPs (Figure 1.4) and AFPs, found in organisms inhabiting sub-zero environments, were the first discovered compounds that exhibit IRI properties.[33,40,57–61] However, these compounds are not commonly used as CPAs, as both AFPs and AFGPs also possess thermal hysteresis (TH) properties, which can lead to damage in biological samples. [62]

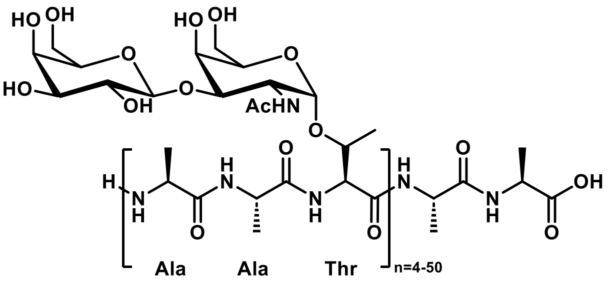

*Figure 1.4: The general structure of AFGPs.* [40]

TH is the localized freezing point depression relative to the melting point, caused by the irreversible binding of AFPs and AFGPs to ice crystals; the difference between these two points is known as the TH gap. [18,25–27,40]

AFPs and AFGPs maintain a stable ice crystal as long as the temperature is within the TH gap. However, cryopreservation temperatures are outside of the TH gap, and once the temperature drops below the TH gap, ice grows uncontrollably into long spicules that damage the cell; this ice growth phenomena is known as dynamic ice shaping. [59,60,62] This effect is hypothesized as the reason why AFPs and AFGPs preform poorly as CPAs, resulting in low post-thawing cell viability. However, the IRI properties of AFPs and AFGPs are of interest, and research was done to design IRIs which do not show dynamic ice shaping properties. [18,25,33,40,61]

### 1.3.2 Polymers as ice recrystallization inhibitors

IRI activity in synthetic polymers has been previously explored. [5,53,60–69] PVA is an example of an IRI polymer, exhibiting IRI activity at micromolar concentrations.[48,58,62,67,68] The IRI activity of PVA is hypothesized to be due to its ability to adsorb onto the surface of the ice crystals due to PVA's hydroxyl groups, and acts as an obstacle in the migration of water molecules between the ice crystals. [48,58] Moreover, the greater the molecular weight of PVA used (7.2 to 98 kDa), the more IRI activity was observed. [63,65] Acetylation of the PVA's hydroxyl group causes a decrease in its IRI activity, which supports this theory. [64] IRI activity in polymers other than PVA was also explored; for example, polyampholytes and synthetic (glyco)polymers – such as poly-*L*-lysine, polyethylene glycol, and poly-*L*-glutamic acid – have been found to exhibit IRI activity. [42,48,57,58,62–71] The potential of polymers as IRIs is vital because, unlike naturally occurring antifreeze, various polymers are easier to synthesize. [42,48,57,58,62–68,70,71]

### 1.3.3 Wang and PEGA resins

Organic resins, such as acrylamide polyethylene glycol (PEGA) and Wang resin, are commonly used for solid phase synthesis of short peptide chains. [72–76] Wang resin is a hydrophobic resin (Figure 1.5 A) while PEGA resin is a hydrophilic resin (Figure 1.5 B). These differences cause them to behave differently in a solution. [74,75,77,78] Unlike the usual polymers used as IRIs, [42,48,57,58,62–71] Wang and PEGA resins are large macromolecules, of which those used in this thesis have a mesh size ranging from 100-200 (74-149 µm) and are insoluble in PBS, creating heterogeneous suspensions. This is unusual in the study of potential IRI molecules, as IRIs are typically soluble in PBS, allowing the assumption of a homogeneous solution. [2,12,25,40,42,48,57,58,62–71,79–81] Moreover, the resins are easily modifiable by functionalizing through the conjugation of different amino acids, this opens the idea of using Wang and PEGA resins as a core that can be functionalized and its IRI activity assessed. [72–76]

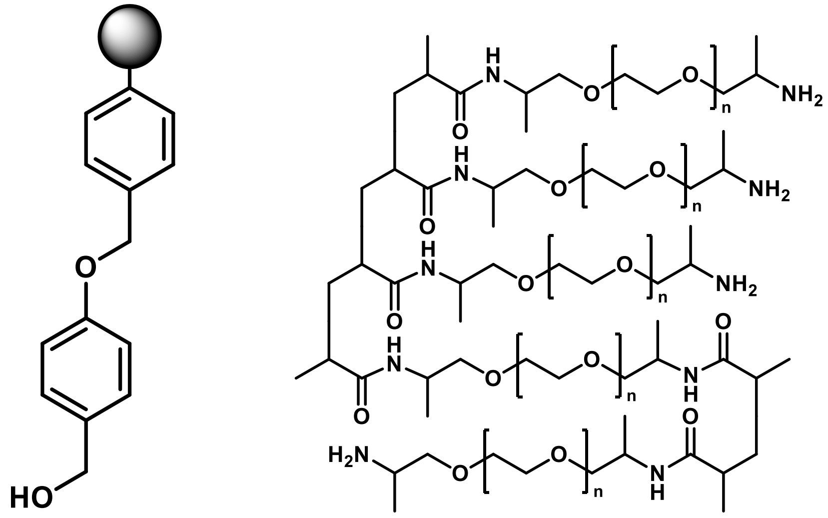

**(A) Wang Resin** **(B) PEGA resin**

*Figure 1.5: Structure of Wang resin (A) and PEGA resin (B).* [72–76]

## 1.4 Objective

Given that the use of polymers for cryopreservation has been reported to be beneficial, [42,48,57,58,62–71] the objective of this thesis is to explore the possibility of using large, PBS-insoluble resin macromolecules to inhibit ice recrystallization. [72,73] Additionally, it aims to assess the IRI activity of resins functionalized with amino acids, as well as the IRI activity of individual amino acids that could be conjugated to the resin. Finally, the research will investigate the IRI activity of amino acid derivatives that can be used to functionalize the resins, potentially assessing the IRI activity of resins functionalized with the synthesized amino acid derivatives.

# 2 Organic Resins

## 2.1 Experimental design of using insoluble resins

PBS-soluble small molecules (AMU < 450) that exhibit IRI activity, such as *N*-(2-fluorophenyl)-d-gluconamide (2FA), are assessed for IRI activity using a splat-cooling assay. [41] However, the large non-soluble polymers being explored (Wang and PEGA resins) cannot be tested using the general splat-cooling assay procedure. In contrast to typical small molecule and soluble polymer IRIs, Wang and PEGA resins are insoluble in PBS. [25,41,54,82] Hence, the sample preparation method was modified to minimize the problems that may influence the results due to the uneven distribution of the resin beads in the suspension. In a heterogenous suspension, the % w/v of the samples diluted through serial dilution is not likely to be accurate with respect to concentration. Moreover, the number of resin beads in the 10 µL drop used to create an ice wafer in a splat-cooling assay may not represent the sample.

The first step in preparing a resin-PBS suspension is to add PBS solution to the dry resin. For example, 0.8 mL PBS was added to 0.2 g Wang resin to create a 20% w/v Wang resin suspension which was then diluted multiple times to create at least five different concentrations. The five suspensions obtained are then used to generate a four-parameter dose-response curve showing the IRI activity of the sample. [54]

In a resin-PBS suspension, it was observed that the resin beads tend to form clumps and do not get properly distributed through the resin-PBS suspension (Figure 2.1 A). As a result, sonicating the resin-PBS suspension using a BRANSONIC 1510-MT sonicator at 42 KHz for 60 minutes in an attempt to evenly distribute the resin across the suspension was explored (Figure 2.1 B). After sonication, the resin-PBS suspension appeared more homogenous for a longer period of time. (Figure 2.1 $B_1$). Moreover, it was observed that the visible clumps of resin in the suspension were noticeably reduced and rarely observed in the wafers under the microscope (Figure 2.1 $B_2$).

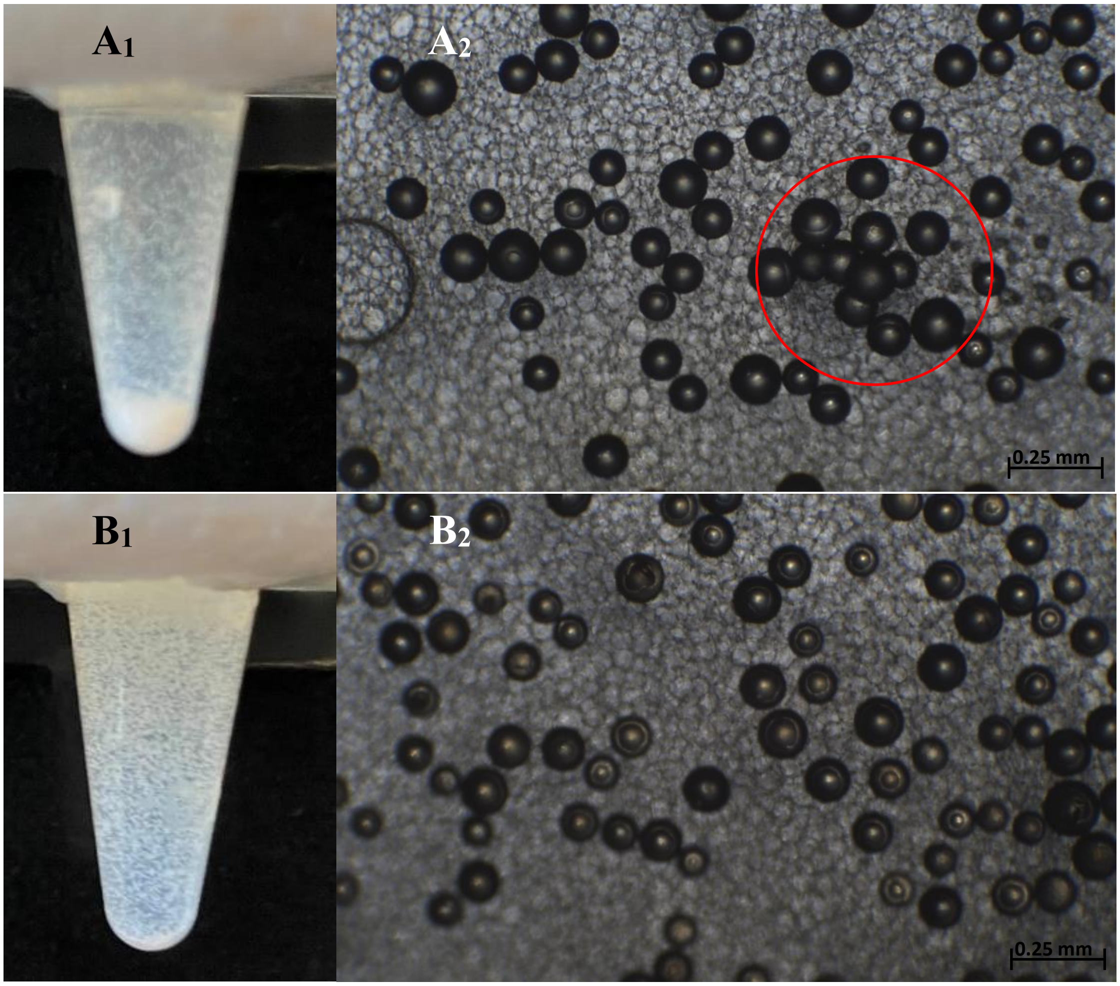

*Figure 2.1: ($A_1$, $B_1$) 10% w/v Wang resin suspension in PBS, ($A_2$, $B_2$) are 4× magnification images of frozen wafers obtained from the respective suspensions following 5 minutes of annealing at -6.4 °C. (A) shows a non-sonicated resin-PBS suspension, in which resin bead clumping was observed (circled in red). (B) shows a sonicated suspension with no visible clumping.*

Due to the heterogeneity of the resin-PBS suspension, the accuracy of the diluted sample's % w/v cannot be guaranteed due to the beads' clumping and their uneven distribution across the suspension. In order to test if dilutions are successful, a stock resin-PBS suspension with 10% w/v was diluted to 5% w/v. Afterwards, the number of beads in a 10 µL sample of the

10% and 5% w/v resin-PBS suspensions were counted through a splat-cooling assay at a lower magnification (4x) in both, sonicated and non-sonicated suspensions (Table 2.1), expecting the number of beads in the 5% w/v suspension to equal approximately half the number of beads in the 10% w/v suspension. The lower magnification was used (4x) in order to capture a larger field of view on the wafer, which would give a better understanding of the resin beads' distribution throughout the wafer. The number of beads in the field of view was counted and averaged in three different locations across each of the five wafers — one image in a location containing a high density of resin beads near the edge of the wafer, then another two images in a straight line starting at the position of the first image across the centre. The test was repeated after the resin-PBS suspension was left to rest on the bench for 2 hours – a time period long enough to conduct a splat-cooling assay – to test if the resin would form clumps after resting (Table 2.1). No clumps were observed in the sonicated resin–PBS suspension after 2 hours of rest (Figure 2.1 B), suggesting that sample analysis can feasibly proceed within this time frame.

*Table 2.1: The average number of Wang resin beads counted within the field of view of three images across the wafers at 4x magnification for resin-PBS suspensions before and after sonication.*

| | Average number of beads in the field of view | |
|---|---|---|
| Wang resin | Non-sonicated suspension | Sonicated suspension |
| 5% Wang resin | 14 ± 4 | 16 ± 4 |
| 10% Wang resin | 29 ± 11 | 26. ± 4 |
| 5% Wang resin after 2 hours | 12 ± 1 | 17 ± 3 |
| 10% Wang resin after 2 hours | 29 ± 8 | 35 ± 3 |

In order to test the validity of the diluted samples, 10% w/v Wang resin-PBS suspension was prepared and used to prepare a 5% w/v Wang resin suspension through serial dilution. Both samples were analyzed with a splat-cooling assay, and the average number of beads within the field of view of three images across each of the three wafers at 4x magnification were counted

(Table 2.1). This process was repeated using another 10% w/v Wang resin suspension, which was sonicated prior to preparing the 5% w/v Wang resin suspension. In a non-sonicated resin-PBS suspension, 10% w/v suspension had an average of 29 ± 11 resin beads within the field of view, and when diluted to 5% w/v, the number of beads was roughly halved to 14 ± 4 beads within the field of view. The same trend was seen when sonicating the suspension, with 10% w/v and 5% w/v suspensions having 26 ± 4 and 16 ± 4 beads within the field of view, respectively. After resting the resin-PBS suspension for 2 hours, this remains to be the case. In a non-sonicated suspension, 10% w/v and 5% w/v suspensions having 29 ± 8 and 12 ± 1 beads within the field of view, respectively. Meanwhile, in a sonicated suspension, 10% and 5% w/v suspension have 35 ± 3 and 17 ± 3 beads within the field of view, respectively (Table 2.1). These results indicate that the 5% w/v Wang resin suspension contains around half the number of beads found in the 10% w/v Wang resin, which meets the expected value.

After sonicating the resin suspension, the clumping observed in resin wafers was noticeably reduced, and the resin remains in suspension for a longer period of time. Hence, it was concluded that in order to properly assess if Wang resin exhibit IRI activity, the suspensions should be sonicated for 60 minutes. After sonication, the suspension was shaken manually then immediately used in a splat-cooling assay, within at most 2 hours.

## 2.2 Assessing the ability of Wang resin to inhibit ice recrystallization

Once the experimental procedure for proper mixing of a resin-PBS suspension was established, a Wang resin-PBS suspension (100-200 mesh) was evaluated for IRI activity using splat-cooling assay at 20x magnification. The large black circles in Figure 2.2 – such as the one circled in red – represent Wang resin beads. It was observed that some of the ice crystals that are close to the Wang resin bead appear smaller than the ice crystals which are further away — circled in blue (Figure 2.2). However, analysis of the IRI activity of Wang resin (Figure 2.3 A) using the splat-cooling assay showed no measurable IRI activity.

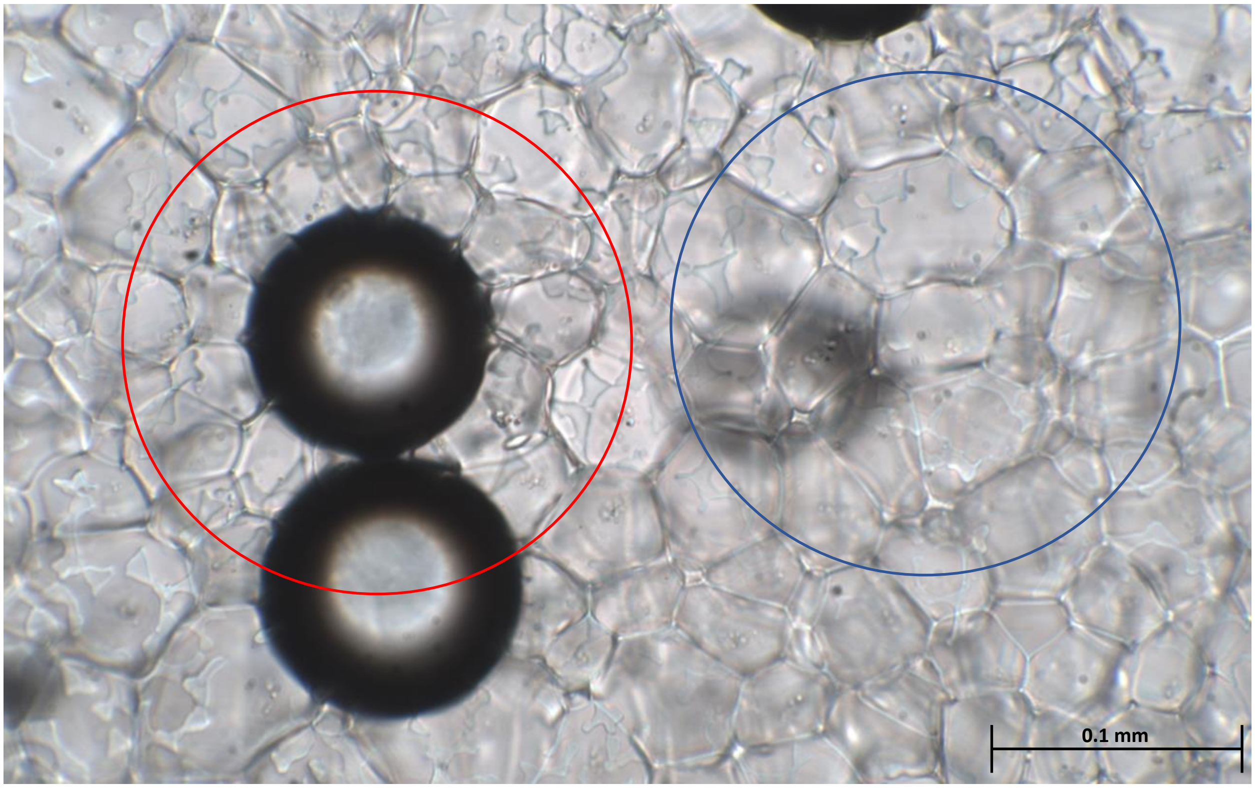

*Figure 2.2: Ice crystals from a 20% w/v Wang resin in PBS at 20x magnification. It was noted that some of the ice crystals in direct contact with the Wang resin beads (region circled in red) appear smaller than those further away (region circled in blue).*

In order to test if Wang resin is IRI active based on the proximity of the ice crystals to the resin beads, a splat-cooling assay using 15% w/v Wang resin-BS suspension was conducted, and images were analyzed based on the number of beads within the field of view. If it is assumed that Wang resin is IRI active and would decrease the size of ice crystals around the bead, then images with 5 resin beads should show more IRI activity when compared to images with one resin bead. However, when analyzing images with 1-5 resin beads within the field of view, no measurable difference in IRI activity was observed (Figure 2.3 B), concluding that Wang resin is not IRI active.

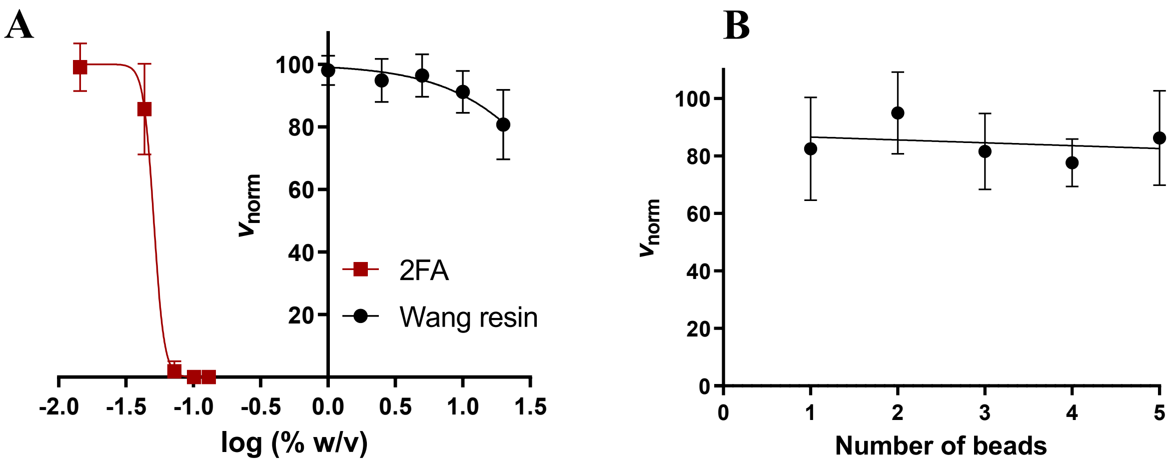

*Figure 2.3: IRI activity of 2FA and Wang resin normalized to PBS using a 4-parameter nonlinear regression, graphed using GraphPad Prism 9.0.0. (A) compares the IRI activity of Wang resin and 2FA based, each point having a different w/v %. (B) Shows the IRI activity of 15% w/v Wang resin based on the number of beads within the analyzed field of view.*

Due to the observed change in crystal size around the Wang resin beads (Figure 2.2), another method to interrogate the data was explored, which studies the distribution of ice crystals based on ice crystal size, rather than the normalized rate of ice crystal growth, this increase in resolution is required to detect minor IRI activity that would have normally gone unnoticed in a dose-response curve.

When calculating $V_{norm}$ in figure 2.3, the rate of growth was calculated by first distributing the ice crystals into bins starting from 0 mm$^2$, with 0.001 mm$^2$ intervals. The area of the first bin (0 mm$^2$ – 0.001 mm$^2$) proportional to the total area of ice crystals was divided by annealing time (5 minutes) to obtain the rate of growth. This rate was then normalized using growth rate of blank PBS to obtain $V_{norm}$.

The new method to interrogate the data suggested was done by comparing the distribution of ice crystal size in the sample with PBS by sorting the ice crystals into bins with size ranging from 0 mm$^2$ to 0.004 mm$^2$, with 0.0002 mm$^2$ intervals between each bin. The smaller bin sizes will allow better visualization of how the ice crystals' size distribution changes in the sample compared to PBS. The binning approach was done for a set of Wang resin-PBS suspension at 20% w/v, a blank PBS standard, and 2FA – a known IRI active small molecule with an $IC_{50}$ = 1.8 mM [1.7, 1.8] – for comparison (Figure 2.4). [41]

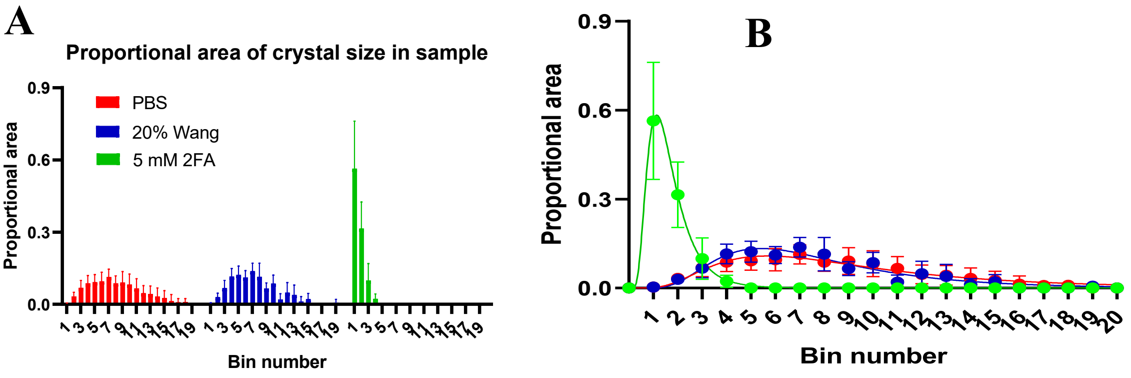

*Figure 2.4: The distribution of ice crystal population in a 20% w/v suspension of Wang resin in PBS (blue), PBS (Red) and 5 mM 2FA (Green). (A) shows the size distribution of ice crystal population sorted into 20 bins. The smallest bin (bin 1) is for ice crystals with size (0-0.0002) mm$^2$, with an incremental increase of 0.0002 mm$^2$ until bin 20, with ice crystals size (0.0038 – 0.0040) mm$^2$. (B) shows a simplified version of (A) for ease of comparison, this was done using a nonlinear lognormal regression of the data in (A).*

The data obtained show that the ice crystals in the PBS control have the highest distribution at the 7th bin. This indicated that most of the area within the field of view in a PBS sample was occupied by ice crystals that have an area of (0.0012 to 0.0014) mm$^2$. However, the amplitude was relatively low (11.3 ± 3.2) %, this is because the size of ice crystals is distributed across a broad range, as 78.4% of the area occupied by ice crystals found in PBS populate bins 3 through 11, with crystal sizes ranging from (0.0004 to 0.0024) mm$^2$. On the other hand, for 2FA (an IRI active molecule), 87.8% of the area was occupied by ice crystals populating the first 2 bins, with crystal sizes ranging from (0 to 0.0004) mm$^2$. The amplitude of the first bin was higher than that of PBS (56.3 ± 19.8) %, this is because 2FA prevents the growth of ice crystals, resulting in all ice crystals to be small and of similar size, generating a narrow crystal size distribution. Meanwhile, for Wang resin, 84.1% of the area occupied by ice crystals populate bins 3 through 11, peaking at (13.8 ± 3.3) % at the 7th bin, similar to PBS, and different from 2FA. Looking at this data, the control PBS and 20% w/v Wang resin suspension showed similar distribution of ice crystal size. Using t-test to compare PBS with 20% w/v Wang resin resulted in a $p$-value > 0.1, indicating no statistically significant difference between them. Meanwhile, the percentage of ice crystal population of 5 mM 2FA solution was mostly in the first 2 bins. When compared with PBS, 2FA showed statistical difference with a $p$-value < 0.05. Based on these results, it is concluded that Wang resin without any functionalization is IRI inactive.

## 2.3 Assessing the ability of amino acids to inhibit ice recrystallization

Wang resin is commonly used for solid phase synthesis of short peptide chains. This process was done by a cycle of coupling the amino acids to the resin, followed by deprotection. [64] Wang resin was deemed IRI inactive; however, IRI activity in Wang resin functionalized with amino acids was not yet explored. To evaluate potential amino acids for conjugation with Wang resin, the IRI activities of several amino acids were assessed using splat-cooling assay using PBS as control (Table 2.2).

*Table 2.2: The IRI activity of various amino acids and their corresponding IC50 values within the 95% confidence interval*

| Amino Acid | Chemical Structure | $IC_{50}$ (mM) |
|---|---|---|
| Glycine | 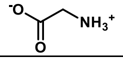 | 287.1 [242.3, 316.2] |
| *L*-alanine | 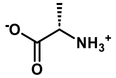 | 115.7 [105.2, 123.4] |
| β-alanine | 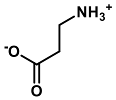 | 241.4 [193.6, 274.5] |
| *L*-phenylalanine | 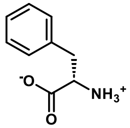 | 14.0 [12.3, 15.6] |
| *D*-phenylalanine | 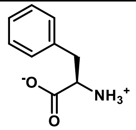 | 15.1 [13.9, 16.0] |
| β-phenylalanine | 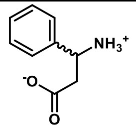 | 56.2 [52.1, 66.7] |
| *L*-leucine | 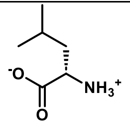 | 33.0 [27.0, 39.9] |
| β-leucine | 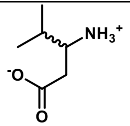 | 71.0 [61.2, 82.0] |
| *L*-valine | 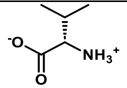 | 39.4 [37.5, 40.7] |
| *L*-lysine | 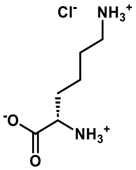 | 79.2 [69.7, 89.3] |

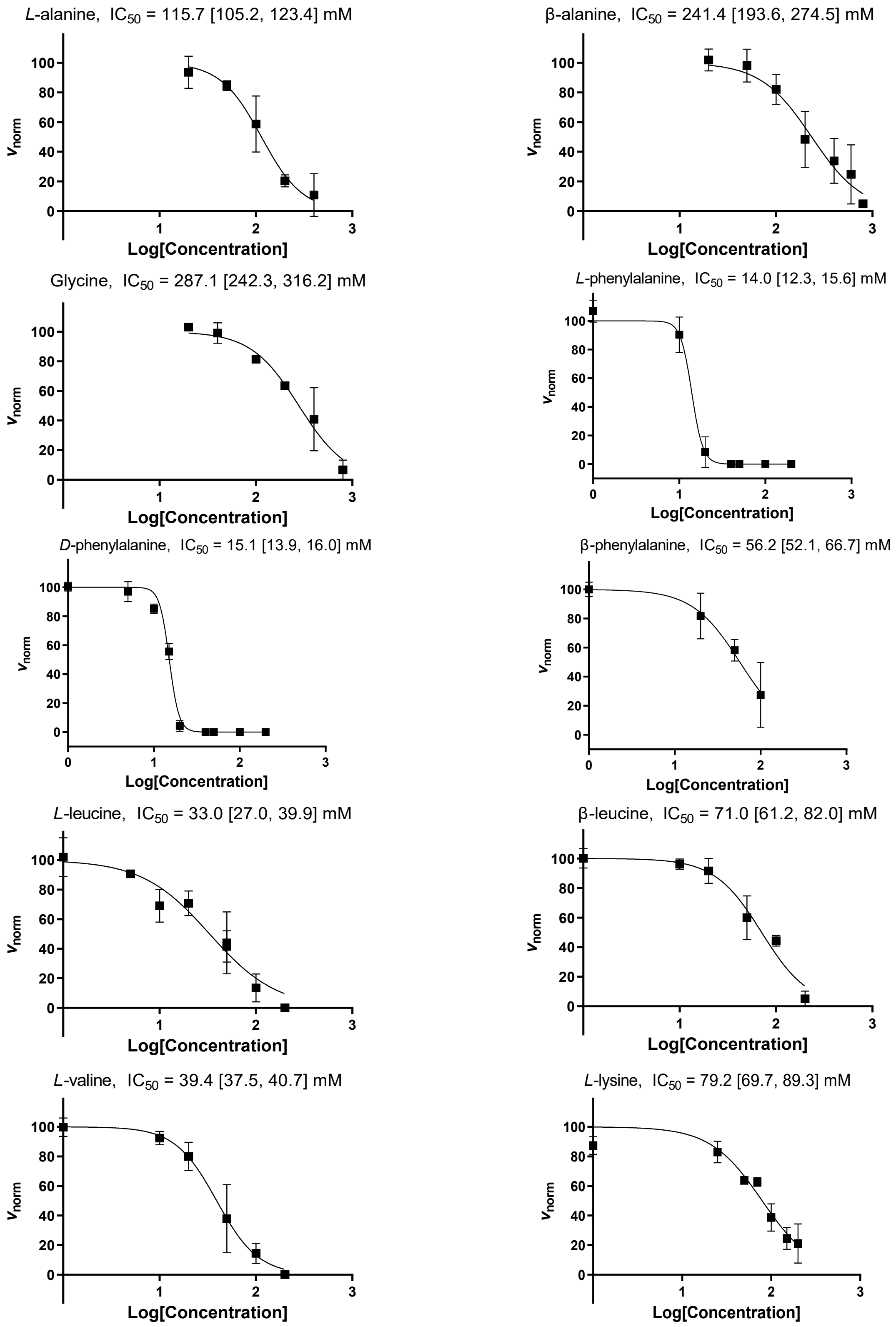

*L*-alanine, $IC_{50}$ = 115.7 [105.2, 123.4] mM

β-alanine, $IC_{50}$ = 241.4 [193.6, 274.5] mM

Glycine, $IC_{50}$ = 287.1 [242.3, 316.2] mM

*L*-phenylalanine, $IC_{50}$ = 14.0 [12.3, 15.6] mM

*D*-phenylalanine, $IC_{50}$ = 15.1 [13.9, 16.0] mM

β-phenylalanine, $IC_{50}$ = 56.2 [52.1, 66.7] mM

*L*-leucine, $IC_{50}$ = 33.0 [27.0, 39.9] mM

β-leucine, $IC_{50}$ = 71.0 [61.2, 82.0] mM

*L*-valine, $IC_{50}$ = 39.4 [37.5, 40.7] mM

*L*-lysine, $IC_{50}$ = 79.2 [69.7, 89.3] mM

*Figure 2.5: $IC_{50}$ dose-response curves of all the amino acids in Table 2.2.*

Glycine was the first amino acid to be tested through a splat-cooling assay for IRI activity, as it lacks additional functional groups and serves as a baseline for comparison with other amino acids. The IRI activity of *L*-alanine was investigated next in order to explore the effect of amino acid side chains on IRI activity, beginning with the simplest side chain — a methyl group. Subsequently, the IRI activity of β-alanine was investigated to compare the IRI activity of amino acids with β-amino acids, as β-alanine is the simplest β-amino acid. Prior research by the Gibson lab observed that *L*-alanine showed IRI activity at 100 mM, and its isomer, β-alanine, showed no activity at that concentration. [83] The results obtained match this observation, *L*-alanine showed higher IRI activity than glycine and β-alanine (Figure 2.6). *L*-alanine had the lowest $IC_{50}$ = 115.7 mM [105.2, 123.4], while glycine and β-alanine had an $IC_{50}$ = 287.1 mM [242.3, 316.2] and 241.4 mM [193.6, 274.5], respectively. When comparing *L*-alanine with glycine, the addition of a methyl side chain caused the IRI activity to double. However, when comparing β-alanine with glycine, the change in $IC_{50}$ was less pronounced.

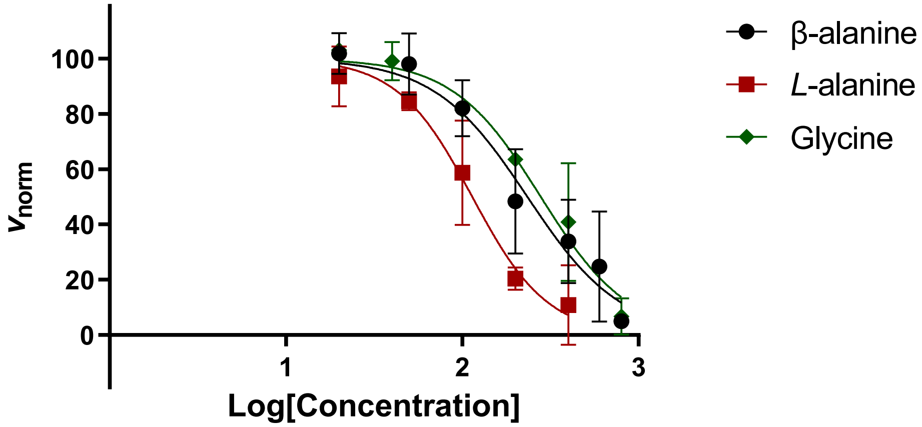

*Figure 2.6: IRI dose-response curves of L-alanine (red), β-alanine (black), and glycine (green).*

Phenylalanine was tested to explore the effect of a phenyl substituent on *L*-alanine, and how it would impact IRI activity compared to glycine and *L*-alanine. Phenylalanine had the best IRI activity of all the tested amino acids, with an $IC_{50}$ = 14.0 mM [12.3, 15.6] and 15.1 mM [13.9, 16.0] for *L* and *D* enantiomers, respectively. When compared to *L*-alanine, the addition of a phenyl group caused enhanced IRI activity by approximately 8 times, from an $IC_{50}$ = 115.7 mM [105.2, 123.4] to 14.0 mM [12.3, 15.6].

Both enantiomers of phenylalanine – *L*-phenylalanine and *D*-phenylalanine – were tested to evaluate whether chirality influences the IRI activity of amino acids. While many of the enantiomer's physical properties are identical, each will have a different optical rotation. Moreover, enantiomers interact differently with enzymes within biological systems due to the enzyme's chiral active sites formed by chiral amino acids. This stereospecific binding can lead to different biological responses from each enantiomer.[86]

However, in the context of IRI, no statistically significant difference in activity was found between *L*-phenylalanine and *D*-phenylalanine (Figure 2.7). This outcome was expected as the IRI assay occurs in a non-chiral water-based solution.[84,85] These results are consistent with previous research conducted in the Ben lab using *D*-fucose, *L*-fucose, *D*-galactose, and *L*-galactose.[26]

Racemic β-phenylalanine was also tested to compare its IRI activity with that of *L*-phenylalanine. Similar to the results obtained for *L*-alanine and β-alanine, *L*-phenylalanine showed better IRI activity than β-phenylalanine, with an $IC_{50}$ = 14.0 mM [12.3, 15.6] and 56.2 mM [52.1, 66.7], respectively (Figure 2.7). Additionally, similar to the relationship between *L*-phenylalanine and *L*-alanine, β-Phenylalanine showed better IRI activity when compared to β-alanine, with an $IC_{50}$ = 241.4 mM [193.6, 274.5] and 56.2 mM [52.1, 66.7], respectively. When compared to β-alanine, the addition of a phenyl group caused an increase in the IRI activity by approximately four times, from an $IC_{50}$ = 241.4 mM [193.6, 274.5] to 56.2 mM [52.1, 66.7].

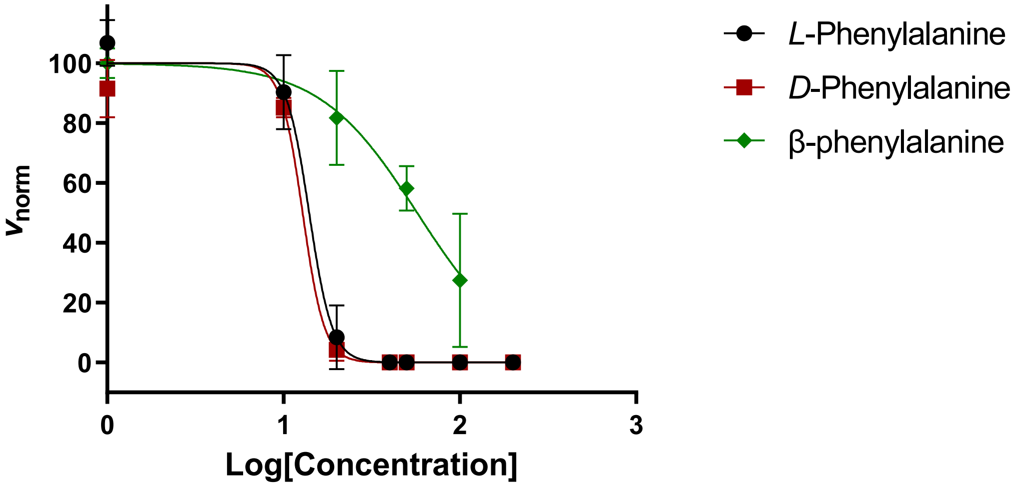

*Figure 2.7: IRI dose-response curve of L-phenylalanine (black), D-phenylalanine (red), and β-phenylalanine (green).*

*L*-leucine, racemic β-leucine, and *L*-valine were tested to evaluate the effect of isopropyl R-groups on IRI activity, and compare the effect of branching alkyl R-groups to phenyl R-groups (Table 2.2). Among the three amino acids, *L*-leucine exhibited the highest IRI activity, with an $IC_{50}$ = 33.0 mM [27.0, 39.9]. Valine, with an R-group containing one less carbon than leucine, showed a similar $IC_{50}$ = 39.4 mM [37.5, 40.7]. Racemic β-leucine showed far less IRI activity than *L*-valine and *L*-leucine, with an $IC_{50}$ = 71.0 mM [61.2, 82.0] (Figure 2.8). The isopropyl group in Leucine, β-leucine, and *L*-valine showed an increase in activity compared to *L*-alanine and β-alanine's single carbon side chain. However, the isopropyl side chain showed less IRI activity when compared to a phenylalanine's phenyl group. This implies that a phenyl side chain enhances IRI activity more than an isopropyl side chain.

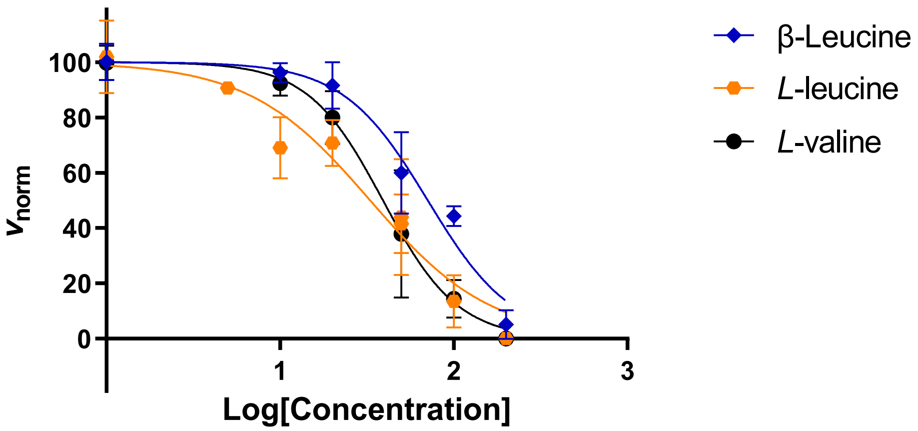

*Figure 2.8: IRI dose-response curve of Leucine (Yellow), β-Leucine (Blue), and Valine (Black).*

When comparing amino acids alongside their β isomers (Table 2.2) (Figures 2.6, 2.7, 2.8), all the amino acids tested have a lower $IC_{50}$ compared to their β isomer. This suggests that α-amino acids are more IRI active than their β isomer. The difference in IRI activity between amino acids and their β counterpart may be attributed to the effect of amphiphilicity on IRI activity, as small compounds with longer alkyl chains tend to show better IRI activity than those with shorter alkyl chains. [26,27,60,87,88] This is demonstrated by *N*-octyl-*D*-gluconamide (NOGlc) — an IRI active glucose derivative with an octyl group. Reducing the length of the octyl group causes a decrease in IRI activity. [26] Since α-amino acids have longer alkyl chains in their R-group compared to β-amino acids, this could explain the observed difference.

*L*-lysine, an amino acid with a long chain hydrophilic R-group, which would form an ionic $-NH_3^+$ group when dissolved in PBS, was then tested to see the impact of the protonated amine. *L*-lysine had an $IC_{50}$ = 79.2 mM [69.7, 89.3] (Figure 2.9). Compared to the other tested amino acids, *L*-lysine showed less IRI activity than the tested amino acids with hydrophobic R-groups, such as *L*-valine, leucine, and phenylalanine. This is consistent with the hypothesis regarding the effect of amphiphilicity on the IRI activity of amino acids, as the R-group of *L*-lysine contains a hydrophilic functional group and exhibits lower IRI activity than the tested amino acids with hydrophobic R-groups.

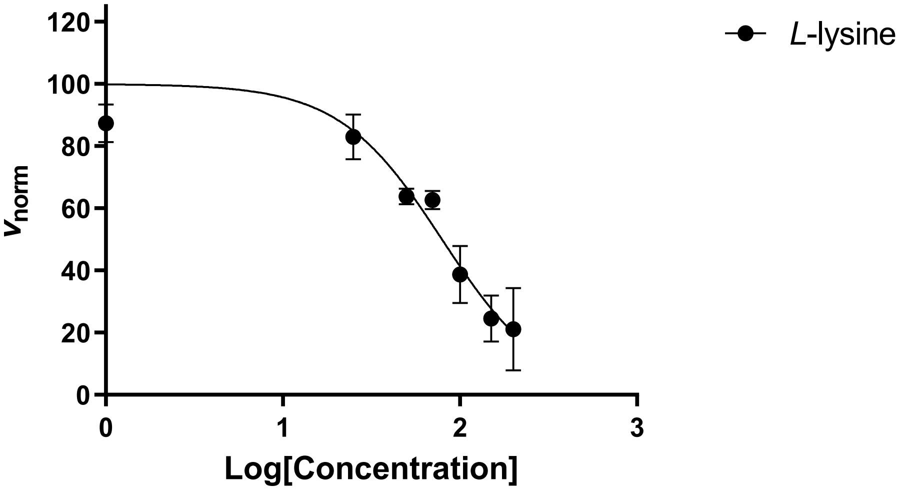

*Figure 2.9: IRI dose-response curve of L-lysine, with an $IC_{50}$ = 79.2 mM.*

As the amino acids show IRI activity, especially *L*-phenylalanine with an $IC_{50}$ = 14.0 mM [12.3, 15.6], the use of amino acids as cryoprotectants is plausible. However, other IRI active small molecules, such as 2FA, have better IRI activity than all the tested amino acids, with an $IC_{50}$ = 1.8 mM [1.7, 1.8] compared to *L*-phenylalanine's $IC_{50}$ = 14.0 mM [12.3, 15.6].

On the other hand, amino acids can be used to synthesize derivatives that may have better IRI activity than 2FA. Among the tested amino acids, phenylalanine showed promising IRI activity, which opens a potential route of using L-phenylalanine as a starting material to synthesize derivatives and explore their IRI activity.

## 2.4 Assessing the ability of phenylalanine derivatives to inhibit ice recrystallization

Amino acids showed promising IRI activity, and – as earlier research in the Ben lab showed – small molecule derivatives could also have enhanced IRI activity. [12,25–27,38,40,41] As *L*-phenylalanine showed the highest IRI activity among the amino acids tested (Table 2.2), it was used as the starting material to synthesize the amino acid derivatives, along with β-phenylalanine for further comparison between amino acids and β-amino acids. *N*-Acyl and *N*-alkyl derivatives of phenylalanine were explored with the aim of enhancing the IRI activity of the starting material, and to later use to functionalize organic resins.

### 2.4.1 Assessing the IRI activity of acyl derivatives of *L*-Phenylalanine

Five different acyl groups were explored for *N*-acyl-*L*-phenylalanine and *N*-acyl-β-phenylalanine (Figure 2.10). The first acyl derivative of interest was *N*-acetyl-*L*-phenylalanine, as the short carbon chain can be used as a baseline to compare with the other derivatives. *N*-benzoyl-*L*-phenylalanine was tested next, as the IRI activity of a phenyl group was found to be the most IRI active when testing amino acids (Table 2.2). Subsequently, the IRI activity of *N*-isobutyric-*L*-phenylalanine was assessed, based on the observation that an isopropyl group showed higher IRI activity than a methyl group when comparing *L*-leucine and *L*-alanine (Table 2.2). Other hydrocarbon derivatives were tested to obtain a wider variety of results; *N*-valeryl-*L*-phenylalanine to test the IRI activity of a longer unbranched hydrocarbon chain and Boc-*L*-phenylalanine to test the effect of IRI activity of further branching compared to *N*-isobutyric-*L*-phenylalanine.

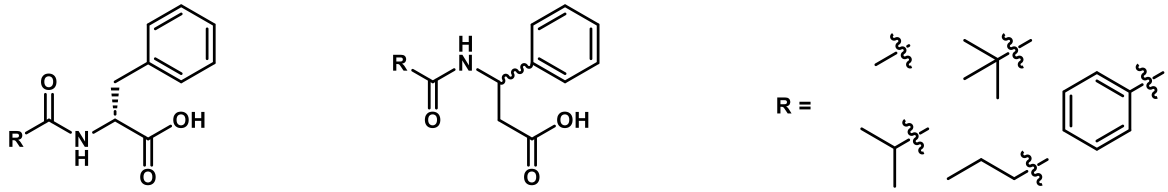

*Figure 2.10: General structures of N-acyl-L-phenylalanine (left) and N-acyl-β-phenylalanine (right)*

*Table 2.3: Maximum solubility of all the synthesized acyl-phenylalanine and acyl-β-phenylalanine in PBS.*

| | 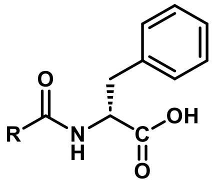 | 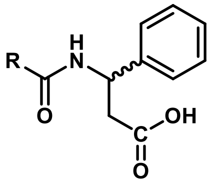 |
|---|---|---|
| R | *N*-acetyl-α-*L*-phenylalanine | *N*-acetyl-β-phenylalanine |
| | Max solubility in PBS (mM) | |
|  | 27 | 44 |
| 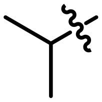 | 21 | 8 |
| 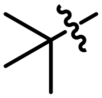 | 93 | 5 |
| 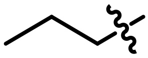 | 5 | 14 |
| 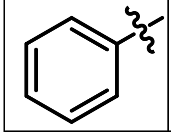 | 2 | < 1 |

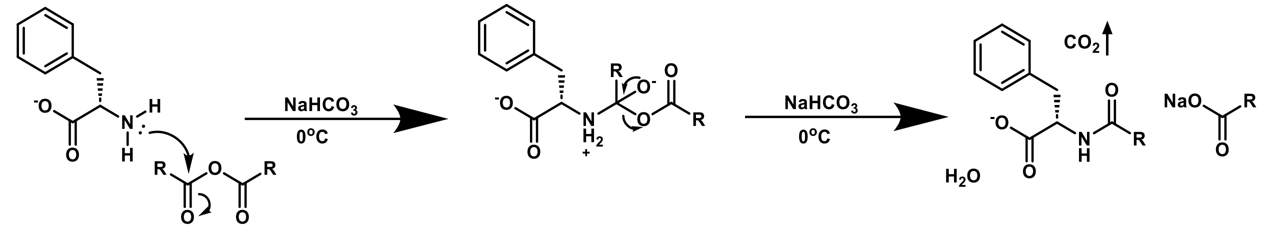

R = methyl, propyl, isopropyl, t-butyl, phenyl

*Figure 2.11: Mechanism of the amide coupling of L-phenylalanine, in which R is an alkyl group.* [89]

For the amide coupling of *L*-phenylalanine and β-phenylalanine, various alkyl R-groups were synthesized and tested for their IRI activity. However, due to the low solubility of *N*-acyl-*L*-phenylalanine and *N*-acyl-β-phenylalanine (Table 2.3), none of the tested molecules were soluble enough in PBS to obtain an $IC_{50}$ value (Figure 2.12). The IRI activity of the synthesized *N*-acyl-*L*-phenylalanine and *N*-acyl-β-phenylalanine derivatives was analyzed at their maximum solubility in PBS (Table 2.3) using the splat-cooling assay (Figure 2.12)

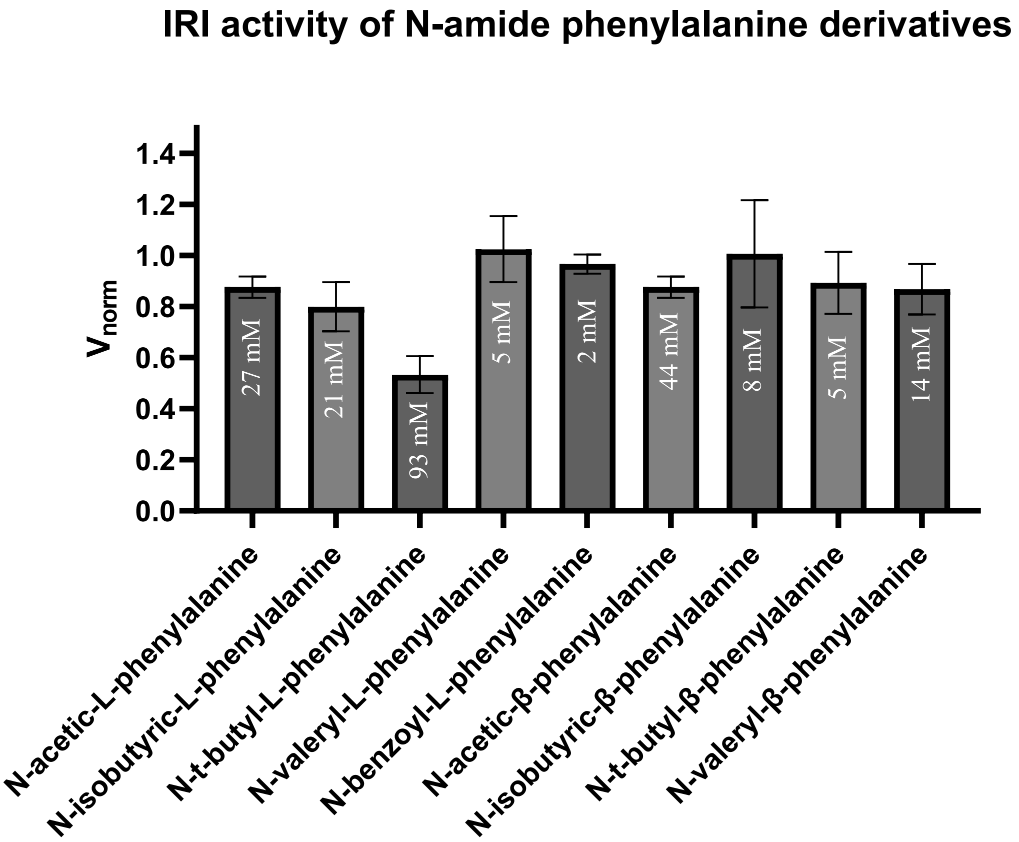

*Figure 2.12: IRI activity of all the synthesized N-acyl-phenylalanine and N-acyl-β-phenylalanine at their limit of solubility in PBS (Table 2.5).*

Other than *N*-$^t$butyl-*L*-phenylalanine, *N*-isobutyrc-*L*-phenylalanine, and *N*-acetyl-*L*-phenylalanine, all other tested *N*-acyl-phenylalanine derivatives exhibited no IRI activity at their maximum solubility in PBS. *N*-isobutyrc-*L*-phenylalanine, *N*-acetyl-*L*-phenylalanine, and *N*-$^t$butyl-*L*-phenylalanine demonstrated a relatively low IRI activity, with a $V_{norm}$ of (79.9 ± 9.6) % at 21 mM, (87.7 ± 4.2) % at 27 mM, and (53.3 ± 7.2) % at 93 mM, respectively. However, this IRI activity was observed at a concentration higher than *L*-phenylalanine, with an $IC_{50}$ = 14.0 mM [12.3, 15.6]. As such, due to their low solubility and diminished IRI activity compared to the starting material, the use of *N*-acyl derivatives appears to hold little promise.

### 2.4.2 Assessing the IRI activity of alkyl derivatives of *L*-Phenylalanine

When *N*-acyl-*L*-phenylalanine was tested for IRI activity, a lack of solubility and a decrease in IRI activity were observed when compared with *L*-phenylalanine, which had an $IC_{50}$ = 14.0 mM [12.3, 15.6]. Hence, a different substituent was explored. Secondary amines generally exhibit greater solubility than structurally similar amides, as the amide's nitrogen is conjugated with the adjacent carbonyl oxygen, while the secondary amine's nitrogen has a more accessible lone pair. This allows the *N*-alkyl derivatives to be more readily available to form hydrogen bonding with water compared to *N*-acyl derivatives. The IRI activity of *N*-alkyl-*L*-phenylalanine derivatives was explored next (Figure 2.13). [90]

*Figure 2.13: Structures of N-isopropyl-L-phenylalanine (left) and N-isopropyl-β-phenylalanine (right).*

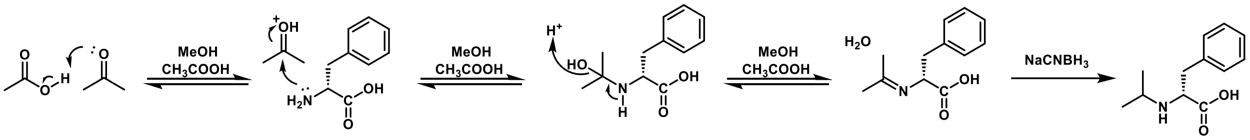

Figure 2.14: Mechanism of the reductive amination of L-phenylalanine and acetone, reduced by sodium cyanoborohydride, using acetic acid catalyst and methanol solvent. [91]

Earlier work in Ben lab showed enhanced IRI activity when comparing small molecules before and after the addition of an isopropyl group. [26,27] Hence, the effect of an isopropyl group on phenylalanine was explored. *N*-isopropyl-*L*-phenylalanine and *N*-isopropyl-β-phenylalanine were synthesized through a reductive amination reaction, in which the amino acid was reacted with acetone, and then reduced using $NaCNBH_3$, using methanol as the solvent with catalytic glacial acetic acid (Figure 2.14). [91]

After *N*-isopropyl-*L*-phenylalanine and *N*-isopropyl-β-phenylalanine were synthesized, their IRI activity was tested using a splat-cooling assay. It was found that *N*-isopropyl-*L*-phenylalanine is more IRI active than *L*-phenylalanine, having an $IC_{50}$ = 1.3 mM [0.9, 1.7] compared to the *L*-phenylalanine's $IC_{50}$ = 14.0 mM [12.3, 15.6]. Moreover, *N*-isopropyl-β-phenylalanine is less IRI active than β-phenylalanine, having an $IC_{50}$ = 84.8 mM [63.7, 106.0] compared to β-phenylalanine's $IC_{50}$ = 56.2 mM [52.1, 66.7] (Figure 2.15). *N*-isopropyl-*L*-phenylalanine showed a much better IRI activity when compared to *N*-isopropyl-β-phenylalanine, with an $IC_{50}$ = 1.3 mM [0.9, 1.7] and 82.5 mM [63.7, 106.0], respectively. This implies that modifying amino acids by synthesizing amino acid derivatives could be an effective method to enhance their IRI activity. However, different amino acids can have vastly different outcomes, as demonstrated by *N*-isopropyl-*L*-phenylalanine exhibited higher IRI activity than *L*-phenylalanine, while *N*-isopropyl-β-phenylalanine have lower IRI activity when compared to β-phenylalanine.

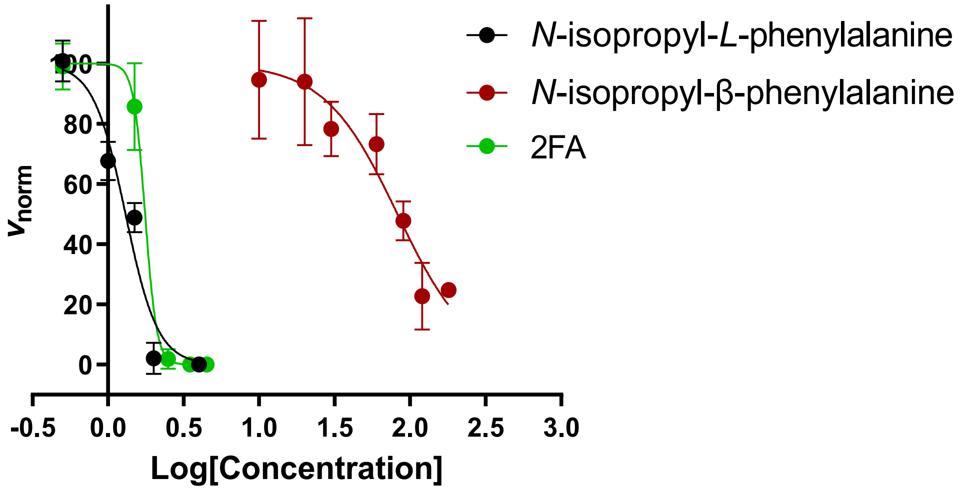

*Figure 2.15: Dose-response curve of the N-isopropyl-L-phenylalanine, N-isopropyl-β-phenylalanine, and 2FA with $IC_{50}$ values equaling 1.3 mM, 82.5 mM, and 1.8 mM, respectively.*

The use of amino acid derivatives as cryoprotectants is plausible given their IRI activity, as *N*-isopropyl-phenylalanine IRI activity is comparable to that of 2FA, with an $IC_{50} = 1.3$ mM [0.9, 1.7] and 1.8 mM [1.7, 1.8], respectively (Figure 2.15). Among the tested amino acids and amino acid derivatives, *N*-isopropyl-phenylalanine had the highest IRI activity, and shows promise for further research in using *N*-alkyl derivatives of amino acid, by exploring different alkyl groups or alternative amino acids.

## 2.5 Assessing the ability of amino acid functionalized Wang resin to inhibit ice recrystallization

Non-functionalized Wang resin does not show any measurable IRI activity. However, functionalizing the resin by coupling IRI active amino acids might cause the resin to exhibit IRI activity by interacting differently with the water molecules.

The first functionalized Wang resin tested for IRI was Wang-Gly-Fmoc (Figure 2.16). This molecule was used as the starting material to all the functionalized Wang resins synthesized in this research, hence, its IRI activity was tested as the baseline control. Following the same experimental procedure as Wang resin, the area of the ice crystals in wafers of 1%, 5%, 7.5%, 10% and 20% w/v Wang-Gly-Fmoc in PBS was calculated to generate a dose-response curve. The highest w/v suspension, 20% w/v, was then binned and compared with control PBS for any significant difference in crystal size population (Figure 2.17).

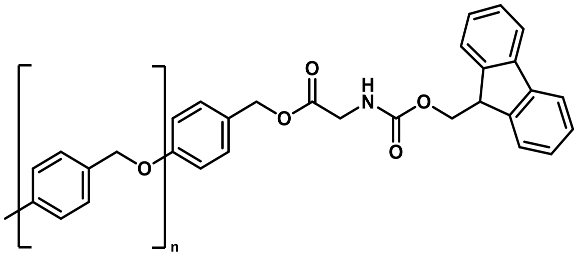

*Figure 2.16: Structure of Wang-Gly-Fmoc.*

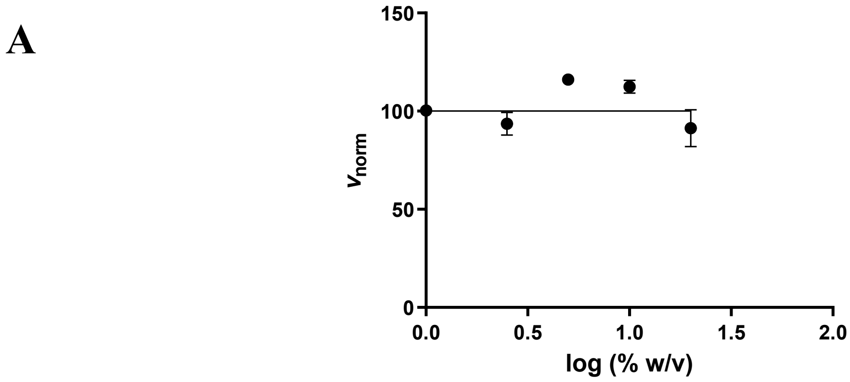

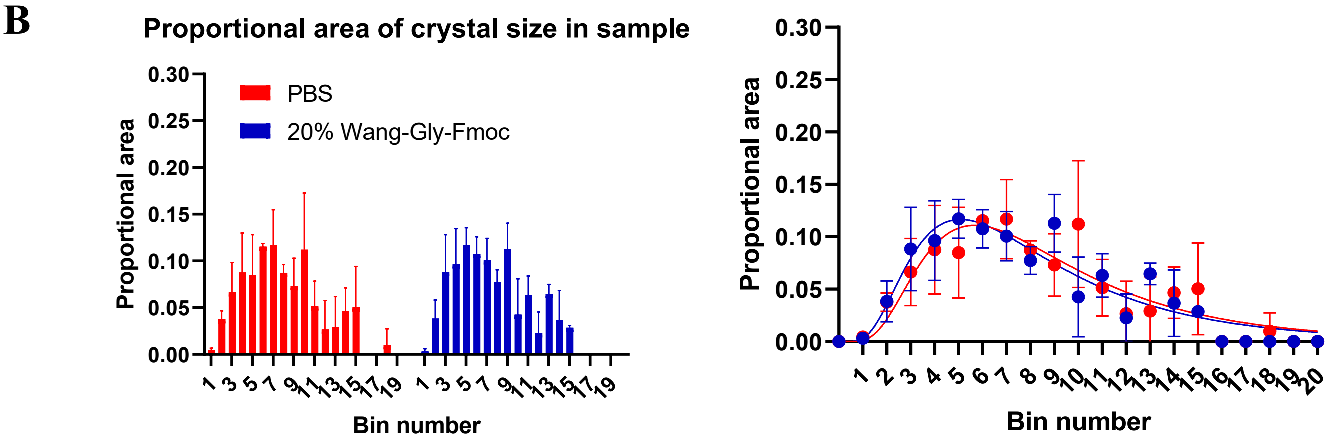

*Figure 2.17: Analysis of Wang-Gly-Fmoc. (A) Dose–response curve showing the IRI activity of Wang-Gly- at 1%, 5%, 7.5%, 10%, and 20% w/v. (B) shows the distribution based on crystal size of the proportional area of ice crystals sorted into 20 bins, the smallest bin (bin 1) is for ice crystals with size (0-0.0002) $mm^2$, with an incremental increase of 0.0002 $mm^2$ until bin 20, with ice crystals size (0.0038 – 0.0040) $mm^2$. The figure compares 20% w/v Wang-Gly-Fmoc (Blue), with control PBS (Red), which are graphed using nonlinear lognormal regression curve.*

When the distribution of ice crystal size of 20% w/v Wang-Gly-Fmoc was compared to PBS, no statistically significant difference was observed, with a *p*-value > 0.1, indicating that 20% w/v Wang-Gly-Fmoc is IRI inactive.

Following the determination that Wang-Gly-Fmoc showed no measurable IRI activity, the Fmoc protecting group was removed, and Wang-Gly-$NH_2$ (Figure 2.18) was subsequently tested for IRI activity, yielding similar results (Figure 2.19).

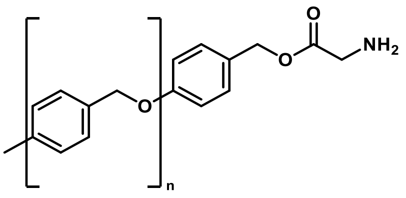

*Figure 2.18: Structure of Wang-Gly-$NH_2$.*

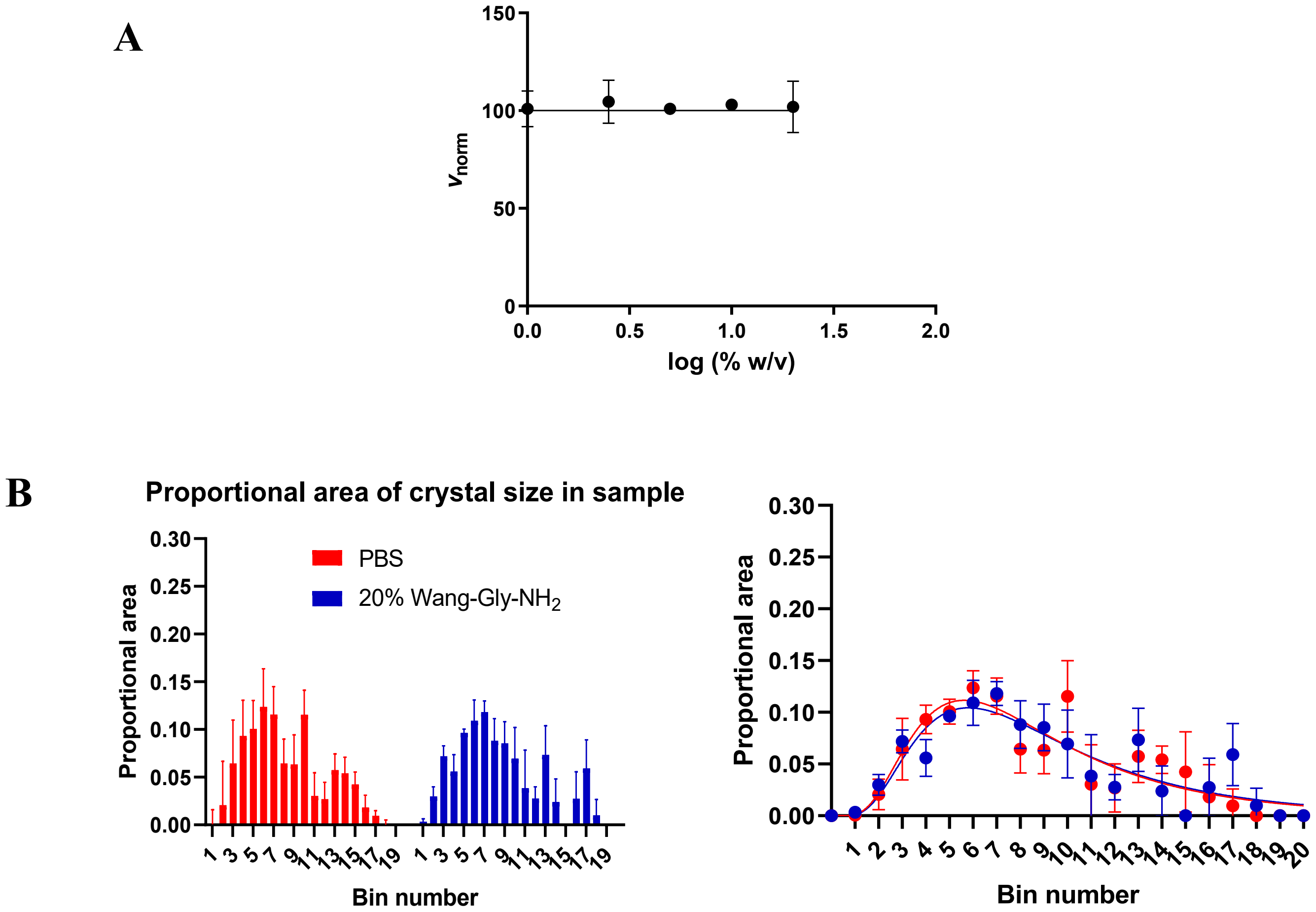

*Figure 2.19: Analysis of Wang-Gly-NH$_2$. (A) Dose–response curve showing the IRI activity of Wang-Gly- at 1%, 5%, 7.5%, 10%, and 20% w/v. (B) shows the distribution based on crystal size of the proportional area of ice crystals sorted into 20 bins, the smallest bin (bin 1) is for ice crystals with size (0-0.0002) mm$^2$, with an incremental increase of 0.0002 mm$^2$ until bin 20, with ice crystals size (0.0038 – 0.0040) mm$^2$. The figure compares 20% w/v Wang-Gly-NH$_2$ (Blue), with control PBS (Red), which are graphed using nonlinear lognormal regression curve.*

When the ice crystal size distribution of 20% w/v Wang-Gly-NH$_2$ was compared to PBS, no statistically significant difference was observed, with a p-value > 0.1, indicating that 20% w/v Wang-Gly-NH$_2$ is IRI inactive.

Wang-Gly-Phe-Fmoc (Figure 2.20) was tested next, as *L*-phenylalanine was the most IRI active amino acid among those previously tested. However, 20% w/v Wang-Gly-Phe-Fmoc showed no statistically significant difference from the control PBS, with a $p$-value > 0.1 (Figure 2.21).

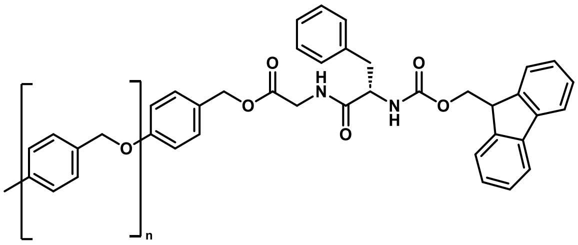

*Figure 2.20: Structure of Wang-Gly-Phe-Fmoc.*

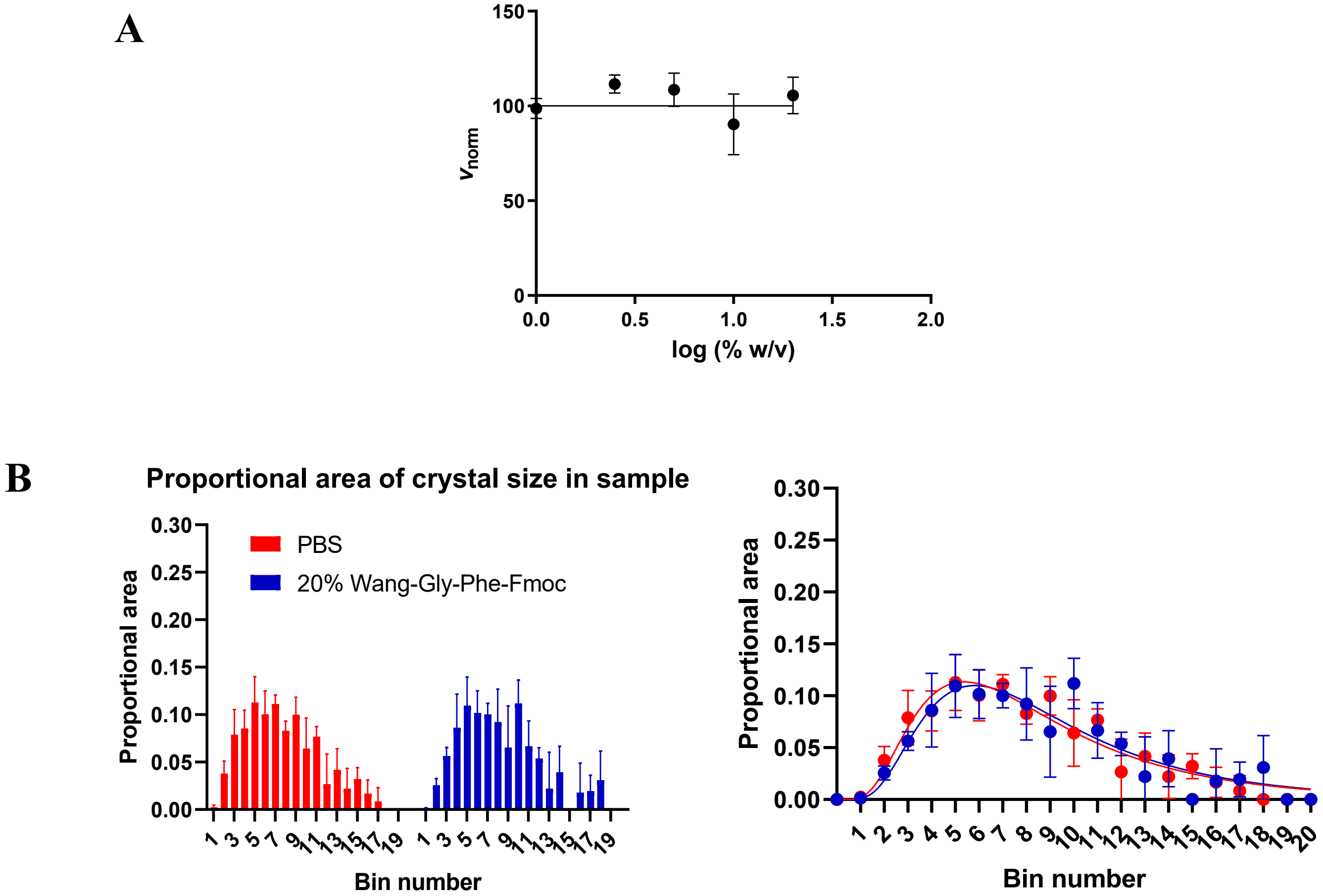

*Figure 2.21: Analysis of Wang-Phe-Fmoc. (A) Dose–response curve showing the IRI activity of Wang-Phe-Fmoc at 5%, 7.5%, 10%, and 20% w/v. (B) shows the distribution based on crystal size of the proportional area of ice crystals sorted into 20 bins, the smallest bin (bin 1) is for ice crystals with size (0-0.0002) mm$^2$, with an incremental increase of 0.0002 mm$^2$ until bin 20, with*

*ice crystals size (0.0038 – 0.0040) mm$^2$. The figure compares 20% w/v Wang-Phe-Fmoc (Blue), with control PBS (Red), which are graphed using nonlinear lognormal regression curve.*

The Fmoc protecting group in Wang-Gly-Phe-Fmoc was subsequently removed, resulting in Wang-Gly-Phe-$NH_2$ (Figure 2.22), which was then tested for its IRI activity. The ice crystal size distribution of 20% w/v Wang-Gly-Phe-$NH_2$ showed no statistically significant difference from the control PBS, with a *p*-value < 0.1 (Figure 2.23).

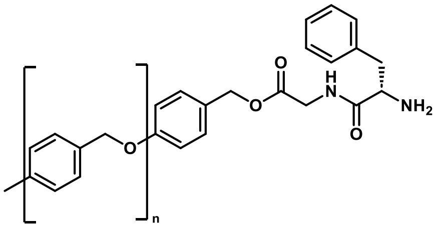

*Figure 2.22: Structure of Wang-Gly-Phe-$NH_2$.*

**A**

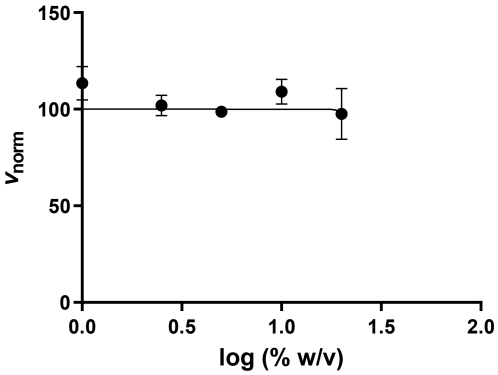

**B**

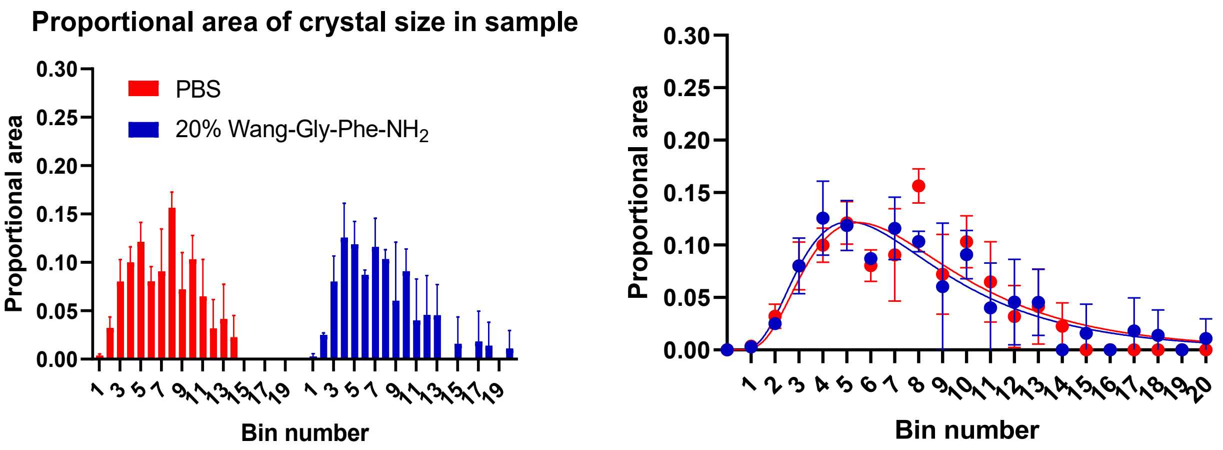

*Figure 2.23: Analysis of Wang-Phe-$NH_2$. (A) Dose–response curve showing the IRI activity of Wang-Phe-$NH_2$ at 1%, 5%, 7.5%, 10%, and 20% w/v. (B) shows the distribution based on crystal size of the proportional area of ice crystals sorted into 20 bins, the smallest bin (bin 1) is for ice crystals with size (0-0.0002) $mm^2$, with an incremental increase of 0.0002 $mm^2$ until bin 20, with ice crystals size (0.0038 – 0.0040) $mm^2$. The figure compares 20% w/v Wang-Phe-$NH_2$ (Blue), with control PBS (Red), which are graphed using nonlinear lognormal regression curve.*

As *L*-phenylalanine – an amino acid with a hydrophobic R-group – cojugated to Wang resin showed no IRI activity. *L*-lysine was used next to functionalized Wang-resin (Figure 2.24), which contains a hydrophilic R-group instead of the hydrophobic *L*-phenylalanine. The ice crystal size distribution of 20% w/v Wang-Gly-Lys-$NH_2$ showed no statistically significant IRI activity when compared to the control PBS, with a *p*-value > 0.1 (Figure 2.25).

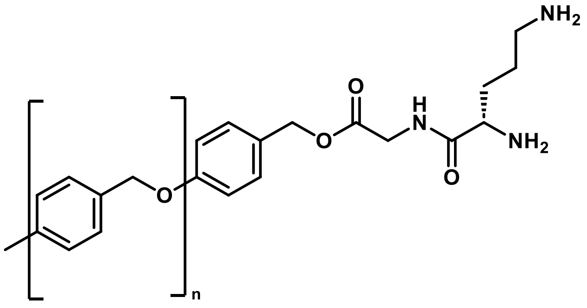

*Figure 2.24: Structure of Wang-Gly-Lys-$NH_2$.*

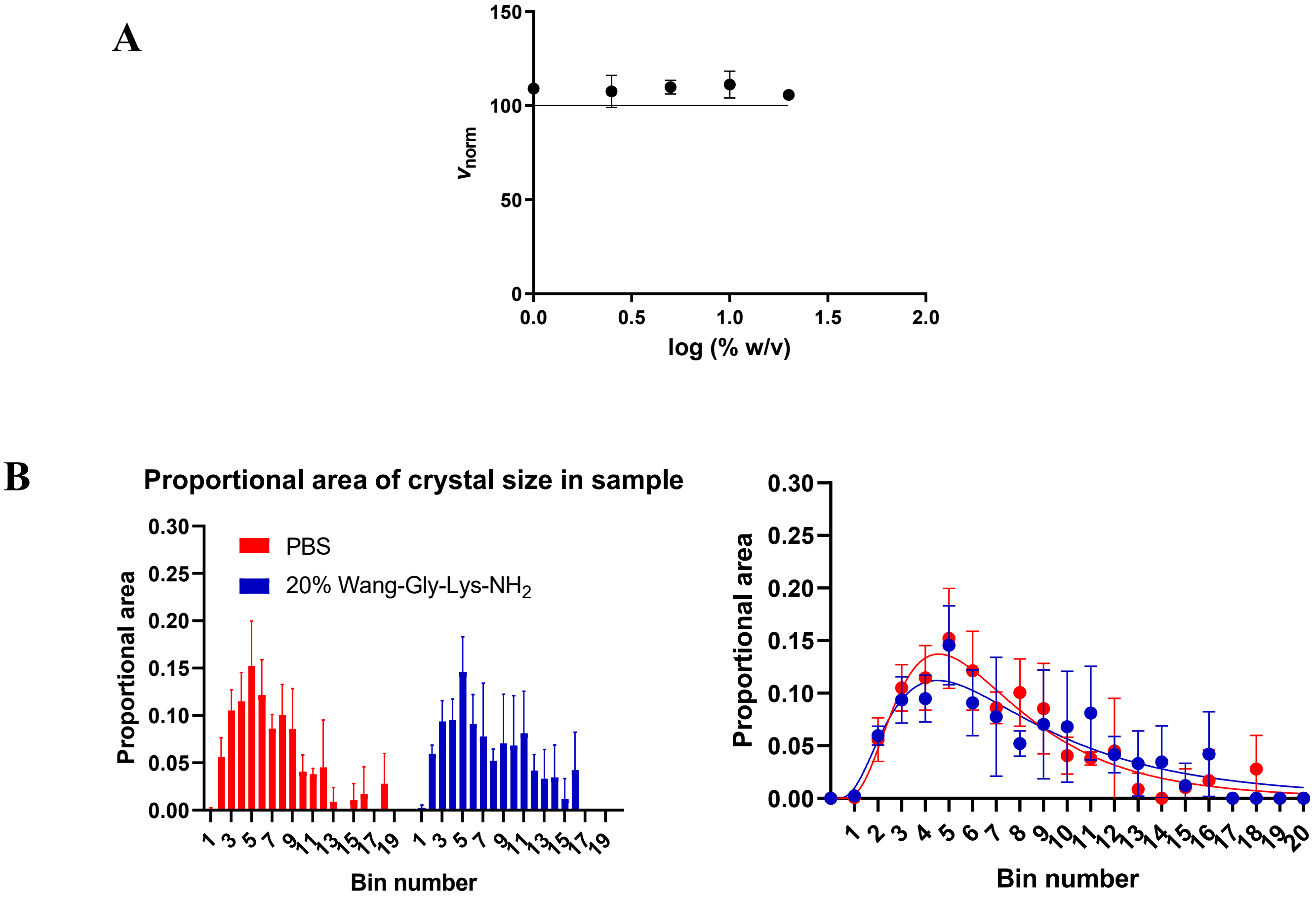

*Figure 2.25: Analysis of Wang-Lys-$NH_2$. (A) Dose–response curve showing the IRI activity of Wang- Lys-$NH_2$ at 1%, 5%, 7.5%, 10%, and 20% w/v. (B) shows the distribution based on crystal size of the proportional area of ice crystals sorted into 20 bins, the smallest bin (bin 1) is for ice crystals with size (0-0.0002) $mm^2$, with an incremental increase of 0.0002 $mm^2$ until bin 20, with ice crystals size (0.0038 – 0.0040) $mm^2$. The figure compares 20% w/v Wang- Lys-$NH_2$ (Blue), with control PBS (Red), which are graphed using nonlinear lognormal regression curve.*

The bin population distribution among all the functionalized Wang resins – Wang-Gly-Fmoc, Wang-Gly-$NH_2$, Wang-Gly-Phe-Fmoc, Wang-Gly-Phe-$NH_2$, and Wang-Gly-Lys-$NH_2$ – alongside 2FA as an IRI active control, were all normalized using their respective blank PBS and compared (Figure 2.26). The higher the normalized proportional area in the first two bins (1 and 2), the more IRI active the sample is. All the tested functionalized Wang resins showed no IRI activity when compared to 2FA, with 2FA having a normalized proportional area of 187.3 in the first bin, while the resin-PBS suspensions never exceeded 10 (Figure 2.26). These results coincide with the data obtained when comparing the functionalized Wang resin with PBS, as none of the resins showed any IRI activity.

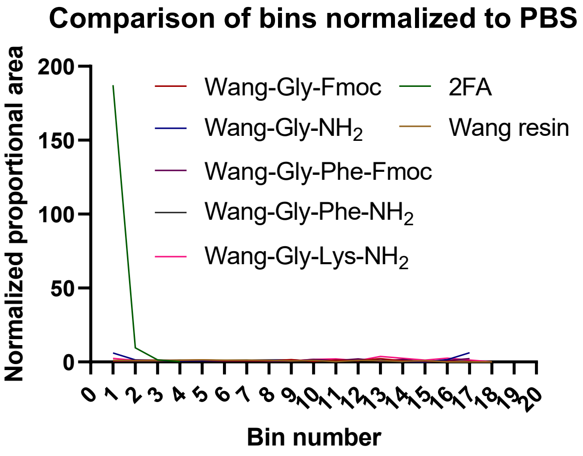

*Figure 2.26: Comparing the bin distribution of the functionalized Wang resin as a function of normalized proportional area.*

These results (Figures 2.17, 2.19, 2.21, 2.23, 2.25, and 2.26) indicate that Wang-Gly-Fmoc, Wang-Gly-$NH_2$, Wang-Gly-Phe-Fmoc, Wang-Gly-Phe-$NH_2$, and Wang-Gly-Lys-$NH_2$ are not IRI active. When comparing the data acquired for the normalized proportional area of ice crystals between the functionalized Wang resin and 2FA, the area occupied by smaller ice crystals was statistically equivalent to that of PBS. Hence, it is concluded that the tested Wang resin and functionalized Wang resin do not show any IRI activity. However, different resins, such as the hydrophilic PEGA resin, can be explored, as PEGA resin is a hydrophilic organic resin and will interact differently with PBS compared to Wang resin. [72–76]

## 2.6 Assessing the ability of PEGA resin to inhibit ice recrystallization

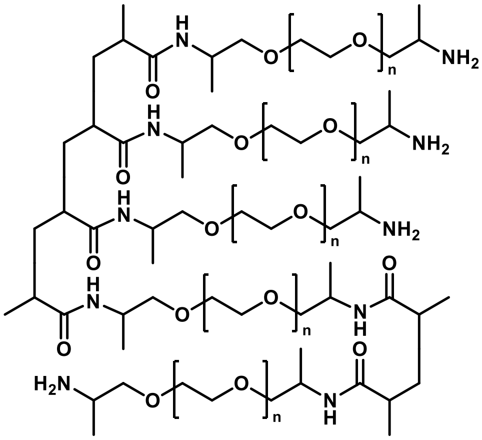

Figure 2.27: Structure of PEGA resin [72–76]

As the tested Wang resin and functionalized Wang resin were found to be IRI inactive, the IRI activity of a different resin was explored. Given that Wang resin is hydrophobic, a hydrophilic alternative was selected. PEGA resin (Figure 2.27) is a large, hydrophilic, PBS-insoluble resin that mixes more readily in PBS compared to Wang resin. (Figure 2.28). [72–76]

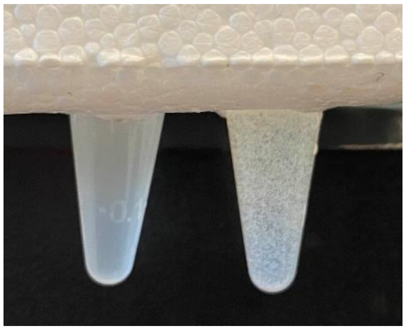

Figure 2.28: Image of 5% w/v PEGA resin (left) and 5% w/v Wang resin (right) in PBS.

PEGA resin was analyzed using the same methodology as Wang resin and functionalized Wang resin. However, unlike Wang resin, PEGA resin suspensions greater than 5% w/v in PBS formed a sludge-like mixture. When this suspension was frozen during the splat-cooling assay, a thick ice wafer was formed, making IRI analysis at concentrations above 5% w/v extremely difficult. As a result, generating a full dose-response curve ranging from 1% to 20% w/v – as was used for Wang resin – was not feasible. However, creating this dose-response curve was not required, as a single % w/v resin-PBS suspension alongside blank PBS provides sufficient data to assess the IRI activity of PEGA resin. When 5% w/v PEGA resin in PBS was analyzed using the splat-cooling assay, ice crystals around the bead appeared smaller than those further away (Figure 2.29).

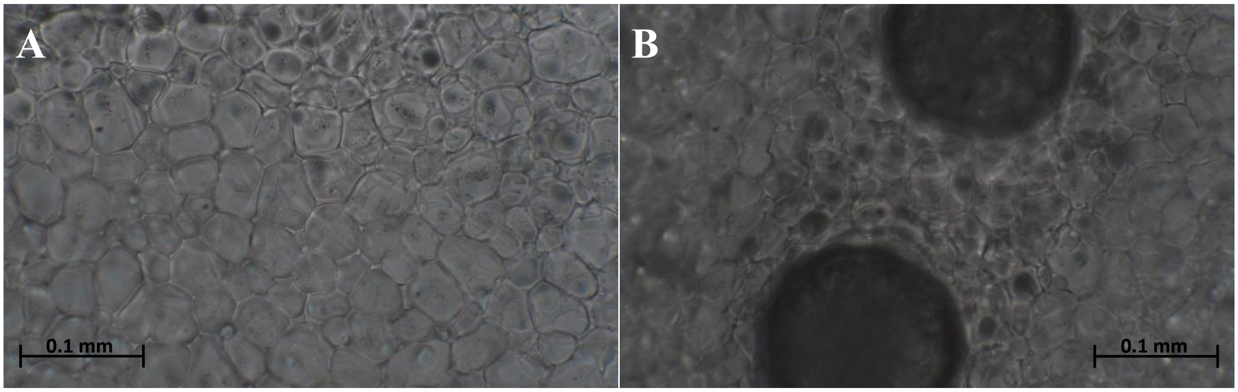

*Figure 2.29: Images taken from the same frozen wafer of a 5% w/v PEGA-PBS suspension at 20x magnification, comparing regions with and without PEGA resin beads visible within the field of view. (A) Shows a region with no visible PEGA resin beads, (B) Shows a region with at least one PEGA resin bead (2 PEGA beads in this case).*

PEGA resin, PEGA-Phe-$NH_2$, and PEGA-Lys-$NH_2$ at 5% w/v in PBS were assessed for their IRI activity using a splat-cooling assay, with blank PBS for comparison. Multiple images from each wafer were analyzed, including at least one image without any resin beads, and another image with a minimum of one resin bead. (Figure 2.29). After those images were captured, the area of each ice crystal in both images was calculated, binned, and then compared to the blank PBS.

The data obtained showed that 5% w/v PEGA resin, PEGA-Phe-$NH_2$, and PEGA-Lys-$NH_2$ suspensions in PBS had slightly smaller ice crystals than the control blank PBS. The 5% w/v PEGA-PBS suspension has (67.5 ± 6.0) % of ice crystal areas with size less than 0.001 $mm^2$ (first five bins), while the blank PBS has (45.5 ± 4.6) % within the same range. This trend was consistent with PEGA-Lys-$NH_2$ and PEGA-Phe-$NH_2$, with (57.5 ± 4.8) % and (74.2 ± 5.8) % ice crystal areas with size less than 0.001 $mm^2$, respectively (Figure 2.29). However, when compared to an IRI active molecule, 2FA, which has (87.7 ± 4.2) % of ice crystals with size less than 0.0004 $mm^2$ (first two bins), it is concluded that PEGA resin is IRI inactive.

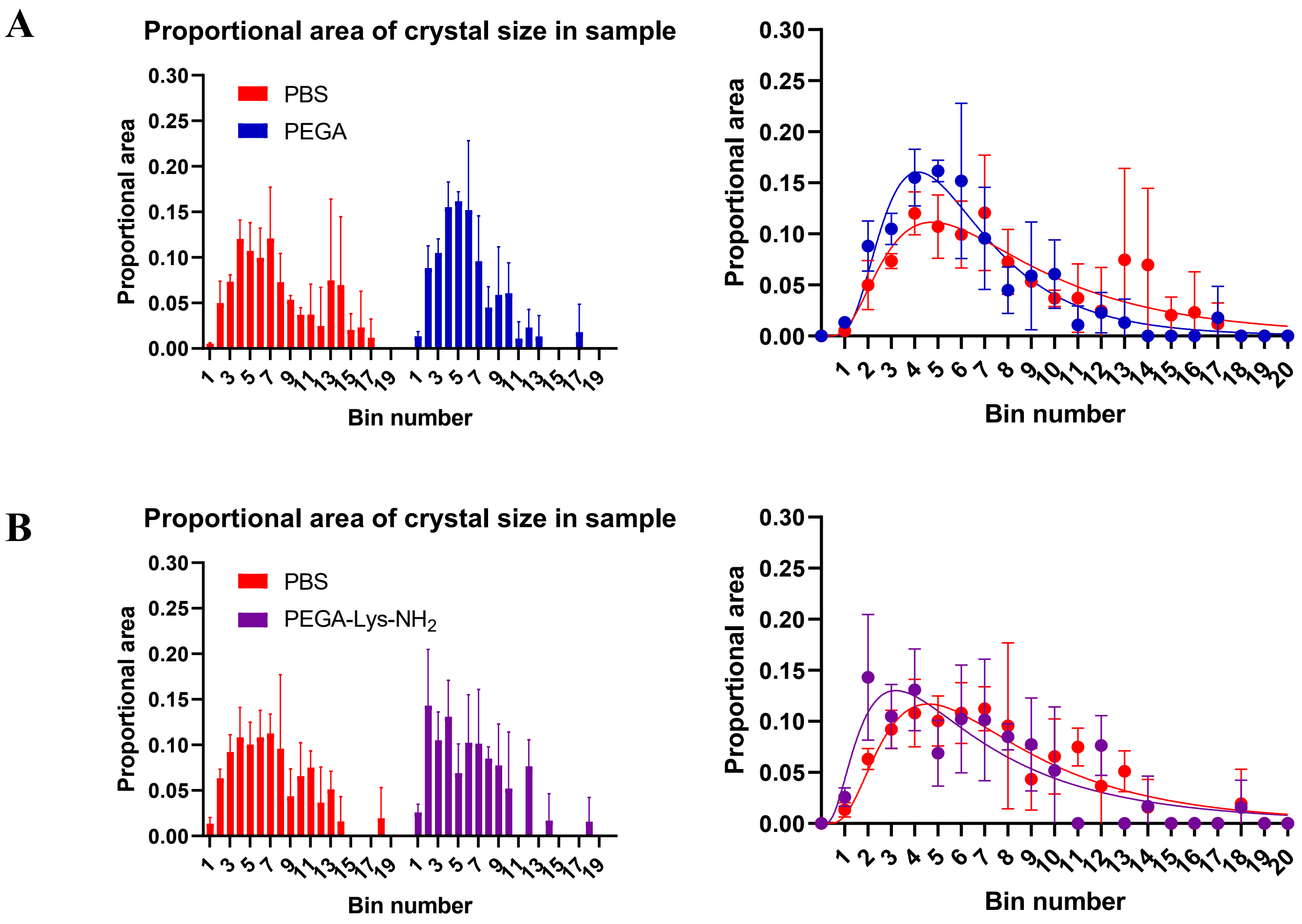

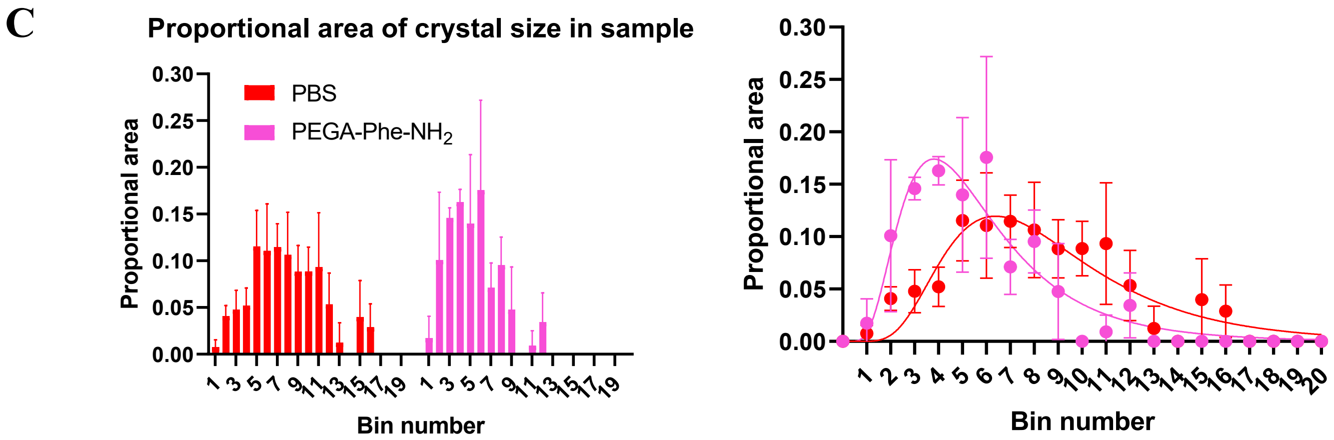
C
Proportional area of crystal size in sample
Proportional area
0.30
0.25
0.20
0.15
0.10
0.05
0.00
PBS
PEGA-Phe-NH2
1 3 5 7 9 11 13 15 17 19 1 3 5 7 9 11 13 15 17 19
Bin number
Proportional area
0.30
0.25
0.20
0.15
0.10
0.05
0.00
1 2 3 4 5 6 7 8 9 10 11 12 13 14 15 16 17 18 19 20
Bin number

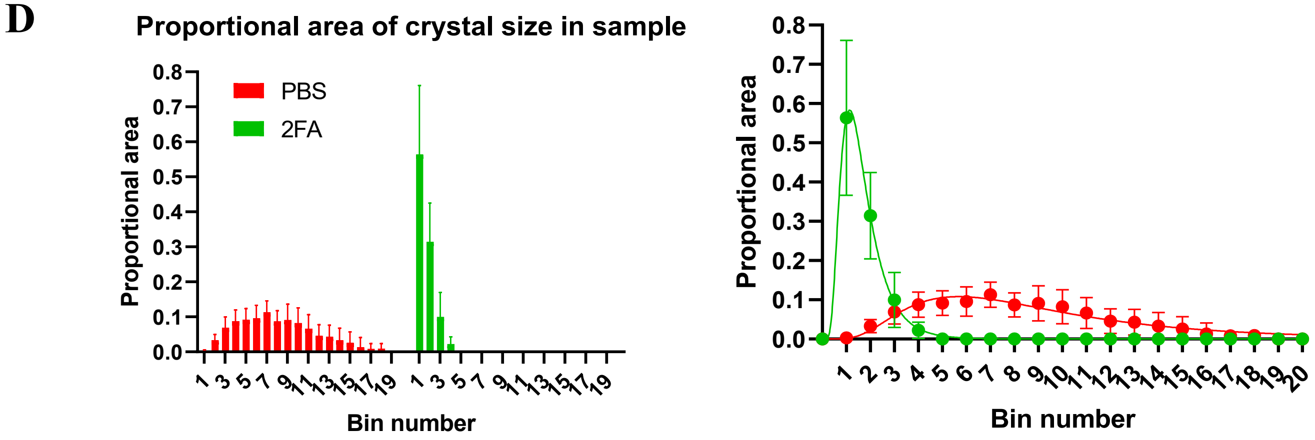
D
Proportional area of crystal size in sample
Proportional area
0.8
0.7
0.6
0.5
0.4
0.3
0.2
0.1
0.0
PBS
2FA
1 3 5 7 9 11 13 15 17 19 1 3 5 7 9 11 13 15 17 19
Bin number
Proportional area
0.8
0.7
0.6
0.5
0.4
0.3
0.2
0.1
0.0
1 2 3 4 5 6 7 8 9 10 11 12 13 14 15 16 17 18 19 20
Bin number

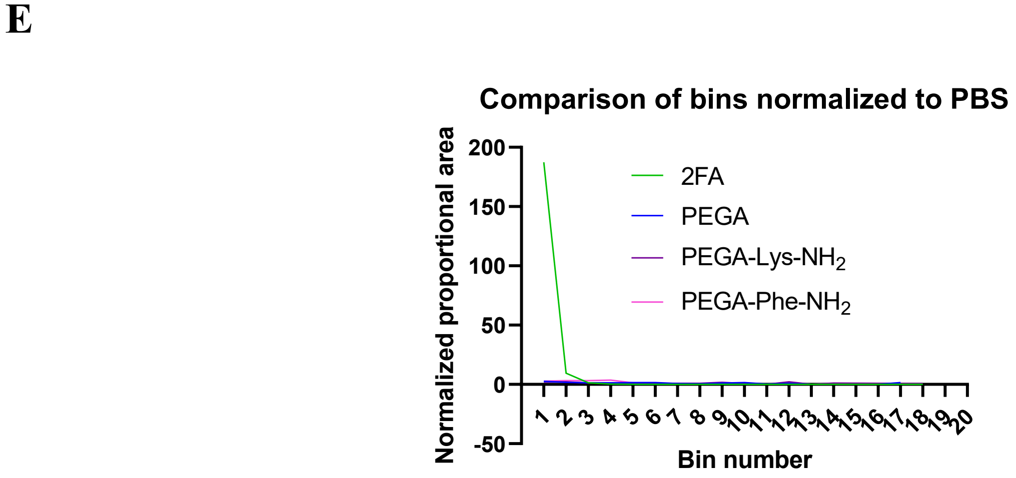
E
Comparison of bins normalized to PBS
Normalized proportional area
200
150
100
50
0
-50
2FA
PEGA
PEGA-Lys-NH2
PEGA-Phe-NH2
1 2 3 4 5 6 7 8 9 10 11 12 13 14 15 16 17 18 19 20
Bin number

*Figure 2.30: Distribution based on the proportional area of ice crystals sorted into 20 bins, the smallest bin (bin 1) is for ice crystals with size (0-0.0002) mm$^2$, with an incremental increase of 0.0002 mm$^2$ until bin 20, with ice crystals size (0.0038 – 0.0040) mm$^2$. (A) shows the bin population distribution comparing PEGA resin and blank PBS, (B) shows the bin population distribution comparing PEGA-Lys-NH$_2$ resin and blank PBS, (C) shows the bin population distribution comparing PEGA-Lys-NH$_2$ resin and blank PBS, (D) shows the bin population distribution comparing 2FA and blank PBS, (E) comparing the bin population distribution of the PEGA resin, PEGA-Lys-NH$_2$ resin, PEGA-Phe-NH$_2$ resin, and 2FA as a function of normalized proportional area.*

Using PEGA resin as an IRI active molecule showed marginally better results than Wang resin. However, the IRI activity is not significant when compared with 2FA. Functionalizing PEGA resin with *L*-phenylalanine caused the resin to show better IRI activity when compared to non-functionalized PEGA resin (Figure 2.30). This indicates the possibility of PEGA resin showing IRI activity if functionalized with different molecules, such as *N*-isopropyl-phenylalanine.

# 3 Conclusion and future work

This thesis investigated the effect of organic resins – Wang and PEGA resins – on ice recrystallization. Wang resin, along with Wang resin functionalized with Gly-Fmoc, Gly-Phe-Fmoc, Gly-$NH_2$, Gly-Phe-$NH_2$, and Gly-Lys-$NH_2$ (Figures 2.16 – 2.26) exhibited no measurable IRI activity. Similarly, PEGA resin and PEGA resin functionalized with Phe-$NH_2$ and Lys-$NH_2$ (Figure 2.30) showed no IRI activity when compared to an IRI active molecule, 2FA. However, analysis of ice crystal size distribution revealed that PEGA-PBS and functionalized PEGA-PBS suspensions exhibited a greater skew toward smaller ice crystals compared to Wang resin and functionalized Wang resin — most notably when compared to PEGA-Phe-$NH_2$ (Figure 2.30). Further exploration is needed on the effect of PEGA resin beads on IRI activity, by functionalizing the PEGA resin with small molecules exhibiting greater IRI activity than *L*-phenylalanine, such as *N*-isopropyl-*L*-phenylalanine.

Meanwhile, the amino acids tested in this thesis demonstrated varying degrees of IRI activity, with *L*-phenylalanine being the most effective, exhibiting an $IC_{50}$ = 14.0 mM [12.3, 15.6] The IRI activity of β-amino acids (β-alanine, β-leucine, β-phenylalanine) was also tested; however, they exhibited lower IRI activity compared to their corresponding α-isomer. To confirm and better understand this trend, a broader variety of β-amino acids and their α-isomers should be investigated.

The amino acid tested with the highest IRI activity, *L*-phenylalanine, was further investigated by synthesizing and testing the IRI activity of its *N*-acyl (Figure 2.10) and *N*-alkyl (Figure 2.13) derivatives. The *N*-acyl derivatives of *L*-phenylalanine either exhibited less IRI activity than the parent amino acid, or no measurable IRI activity. Due to *N*-acyl derivative's low solubility in PBS and poor IRI activity, the focus shifted toward a more soluble derivative of *L*-

phenylalanine, *N*-alkyl-*L*-phenylalanine. The tested *N*-alkyl derivative, *N*-isopropyl-*L*-phenylalanine, showed promising results with an $IC_{50}$ = 1.3 mM [0.9, 1.7], demonstrating significantly greater IRI activity than *L*-phenylalanine ($IC_{50}$ = 14.0 mM [12.3, 15.6]). Future research should explore the IRI activity of additional secondary amine derivatives.

# 4 Experimental

## 4.1 Splat-cooling assay

For a general splat-cooling assay, a sample solution of known concentration was prepared by dissolving the sample in phosphate-buffered saline (PBS), a solution made by dissolving 1.44 g $Na_2HPO_4$, 8.00 g NaCl, 0.24 g $KH_2PO_4$, and 0.20 g KCl in 1 L $H_2O$ with its pH adjusted to 7.32 using NaOH. The stock sample solution prepared was then diluted to prepare more solutions of lower concentrations through serial dilution. [54]

In case of the non-soluble resin samples, the samples ware prepared in a suspension at a known % w/v, for example, 0.2 g Wang resin in 0.8 mL PBS to make 20% Wang resin suspension. The suspension was then sonicated for 1 hour, with manual shaking performed every 10 minutes for a few seconds to ensure uniform mixing. After sonication, the suspension was ready for splat-cooling assay.

The splat-cooling assay was performed by first preparing a polished aluminum block, which was cooled using dry-ice, maintaining a temperature around -80 °C. A 10 µL drop of the sample was then dropped from a height of 2 meters onto the block. However, if the sample was an insoluble resin suspension, it was manually shaken for a few seconds beforehand. Upon contact, a single-layer ice wafer approximately 1 cm in diameter was formed. The wafer was then transferred to a cover slip and placed on a pre-cooled Peltier platform set to -6.4 °C for 5 minutes, where it was allowed to anneal. Following this, images were taken using a microscope at 20x magnification. The images were analyzed by manually circling each ice crystal and measuring their areas using ImageJ. After calculating the areas, the ice crystals were categorized into bins in Excel, with bin sizes increasing in increments of 0.0002 $mm^2$, up to 0.004 $mm^2$, followed by graphing the data using GraphPad Prism 9.0.0. [54]

## 4.2 Functionalised Wang and PEGA resins using solid phase synthesis

1) Wang-Gly-Fmoc → Wang-Gly-Phe-$NH_2$

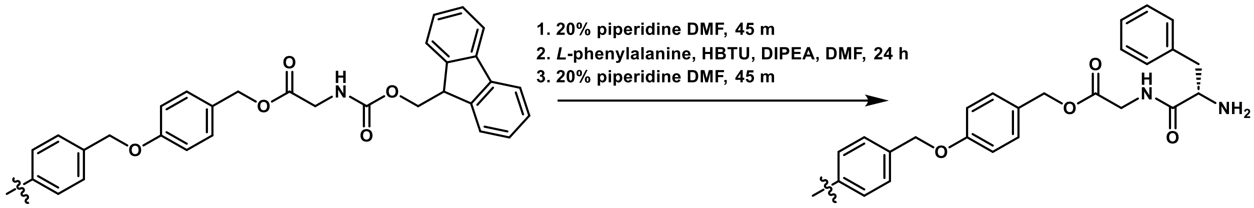

Wang-Gly-Fmoc (0.2072 g, 0.145 mmol) was first swollen in 5 mL DMF for 45 minutes, the swollen resin was washed using 3 mL DMF three times, followed by gentle mixing using a lab shaker with 3 mL of 20% piperidine in DMF solution for 45 minutes, the gentle mixing was repeated three times. After the third 20% piperidine cycle concluded, the resin was washed with 3 mL DMF three times. Resulting in Wang-Gly-$NH_2$ (0.0625 g). The acquired resin was gently mixed with *L*-Phenylalanine-Fmoc (0.1587 g, 0.410 mmol), HBTU (0.1540 g, 0.406 mmol), and DIPEA (0.15 mL, 0.861 mmol) in 3 mL DMF overnight. The resin was subsequently washed with 3 mL DMF five times to remove the excess reagents. The obtained resin was then mixed gently using a lab shaker with 3 mL of 20% piperidine in DMF solution for 45 minutes, this was repeated three times. After the third 20% piperidine cycle concluded, the resin was washed with 3 mL DMF three times. A Kaizer test was then performed to confirm reaction completion. The final product was dried under vacuum, obtaining 0.0408 g Wang-Gly-Phe-$NH_2$. [78]

2) Wang-Gly-Fmoc → Wang-Gly-Lys-$NH_2$

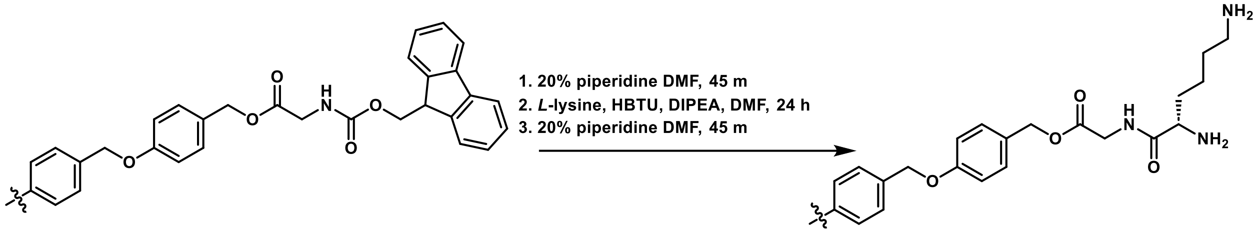

Wang-Gly-Fmoc (0.1452 g, 0.102 mmol) was first swollen in 5 mL DMF for 45 minutes, the swollen resin was washed using 3 mL DMF three times, followed by gentle mixing using a lab shaker with 3 mL of 20% piperidine in DMF solution for 45 minutes, the gentle mixing was repeated three times. After the third 20% piperidine cycle concluded, the resin was washed with 3 mL DMF three times. The acquired resin was gently mixed with *L*-lysine(Fmoc)-Fmoc (0.3581 g, 0.606 mmol), HBTU (0.3471 g, 0.915 mmol), and DIPEA (0.15 mL, 0.861 mmol) in 3 mL DMF overnight. The resin was subsequently washed with 3 mL DMF five times to remove the excess reagents. The obtained resin was then mixed gently using a lab shaker with 3 mL of 20% piperidine in DMF solution for 45 minutes, this was repeated three times. After the third 20% piperidine cycle concluded, the resin was washed with 3 mL DMF three times. A Kaizer test was then performed to confirm reaction completion. The final product was dried under vacuum, obtaining 0.0505 g Wang-Gly-Lys-$NH_2$. [78]

3) PEGA-Fmoc → PEGA-Phe-$NH_2$

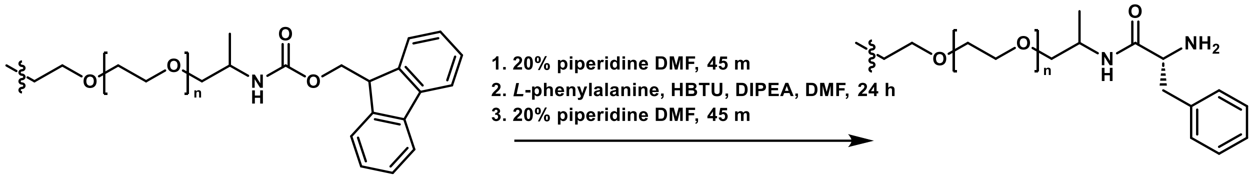

PEGA-Fmoc (0.08380 g, 0.034 mmol) was first swollen in 5 mL DMF for 45 minutes, the swollen resin was washed using 3 mL DMF three times, followed by gentle mixing using a lab shaker with 3 mL of 20% piperidine in DMF solution for 45 minutes, the gentle mixing was repeated three times. After the third 20% piperidine cycle concluded, the resin was washed with 3 mL DMF three times. The acquired resin was gently mixed with *L*-Phenylalanine-Fmoc (0.0150 g, 0.0387 mmol), HBTU (0.0262 g, 0.069 mmol), and DIPEA (0.04 mL, 0.230 mmol) in 3 mL DMF overnight. The resin was subsequently washed with 3 mL DMF five times to remove the excess reagents. The obtained resin was then mixed gently using a lab shaker with 3 mL of 20% piperidine in DMF solution for 45 minutes, this was repeated three times. After the third 20% piperidine cycle concluded, the resin was washed with 3 mL DMF three times. A Kaizer test was then performed to confirm reaction completion. The final product was dried under vacuum, obtaining 0.0241 g PEGA-Phe-$NH_2$.[78]

4) PEGA-Fmoc → PEGA-Lys-$NH_2$

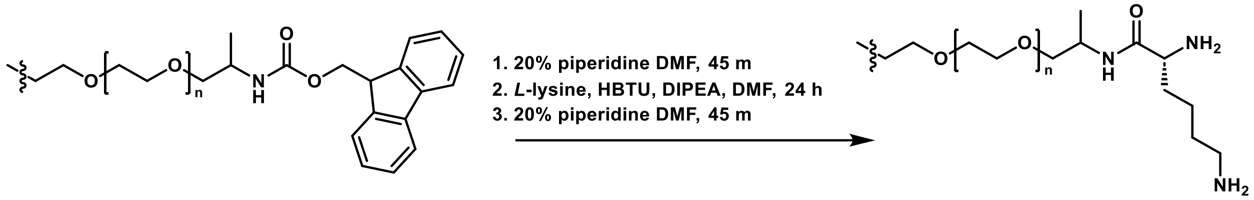

PEGA-Fmoc (0.1002 g, 0.040 mmol) was first swollen in 5 mL DMF for 45 minutes, the swollen resin was washed using 3 mL DMF three times, followed by gentle mixing using a lab shaker with 3 mL of 20% piperidine in DMF solution for 45 minutes, the gentle mixing was repeated three times. After the third 20% piperidine cycle concluded, the resin was washed with 3 mL DMF three times. The acquired resin was gently mixed with *L*-lysine(Fmoc)-Fmoc (0.0.0364 g, 0.0616 mmol), HBTU (0.0334 g, 0.088 mmol), and DIPEA (0.05 mL, 0.287 mmol) in 3 mL DMF overnight. The resin was subsequently washed with 3 mL DMF five times to remove the excess reagents. The obtained resin was then mixed gently using a lab shaker with 3 mL of 20% piperidine in DMF solution for 45 minutes, this was repeated three times. After the third 20% piperidine cycle concluded, the resin was washed with 3 mL DMF three times. A Kaizer test was then performed to confirm reaction completion. The final product was dried under vacuum, obtaining 0.0492 g PEGA-Phe-$NH_2$.[78]

## 4.3 Acylation of phenylalanine

The *L*-phenylalanine, β-phenylalanine, and all anhydrides used in this experiment were purchased from Sigma-Aldrich. The sodium bicarbonate used was purchased from ACP chemicals.

1) Synthesis of *N*-acetyl-*L*-phenylalanine

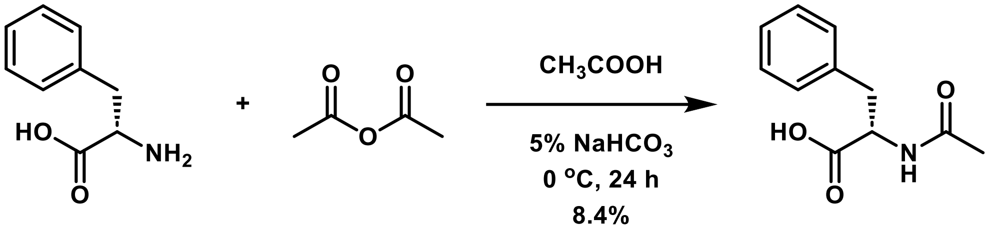

*L*-phenylalanine (0.3000 g, 1.82 mmol) was dissolved in 5.00 mL of 5% $NaHCO_3$ in $H_2O$. Subsequently, acetic anhydride (0.267 mL, 2.82 mmol) was added to the solution and stirred at 0 ºC overnight. Reaction completion was tested using TLC; if the reaction was incomplete, additional acetic anhydride was added. Once the reaction was completed, the solution was acidified to a pH of 2 by adding 6 M HCl dropwise, which caused the product to precipitate. The resulting mixture was then refrigerated overnight, followed by filtration and washing with cold H2O. The acquired white solid was then dried under vacuum and weighed. *N*-acetyl-*L*-phenylalanine (0.0323 g, 0.15 mmol) was obtained, with a total yield of 8.2%. [89] $^1$H NMR (600 MHz, $CDCl_3$): $\delta$ 7.22-7.26 (t, $J$ = 7.2 Hz, 2H), 7.18-7.21 (t, $J$ = 7.2 Hz, 1H), 7.11-7.08 (d, $J$ = 7.2 Hz, 2H), 4.73-4.79 (d, $J$ = 5.5 Hz, 1H), 4.75-4.80 (q, $J$ = 6.0 Hz, 1H), 3.14-3.20 (dd, $J$ = 8.6, 5.6 Hz, 1H), 3.04-3.10 (dd, $J$ = 8.6, 5.6 Hz, 1H), 1.94-1.91 (s, 3H) ppm.

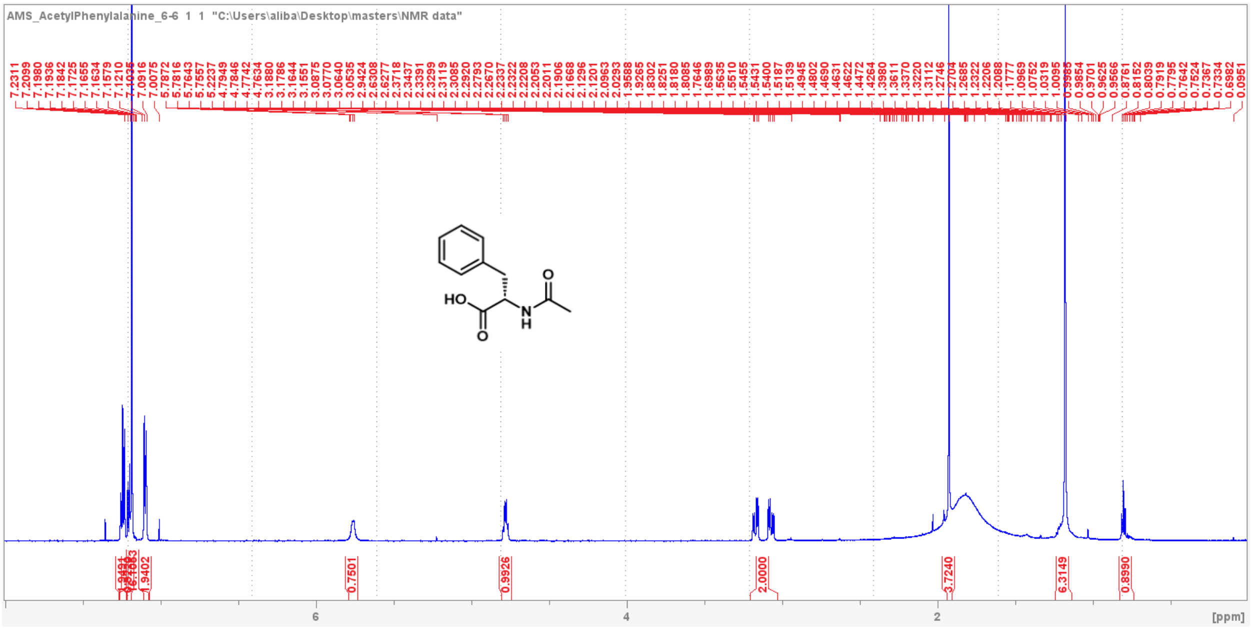

2) Synthesis of *N*-isobutyric-*L*-phenylalanine

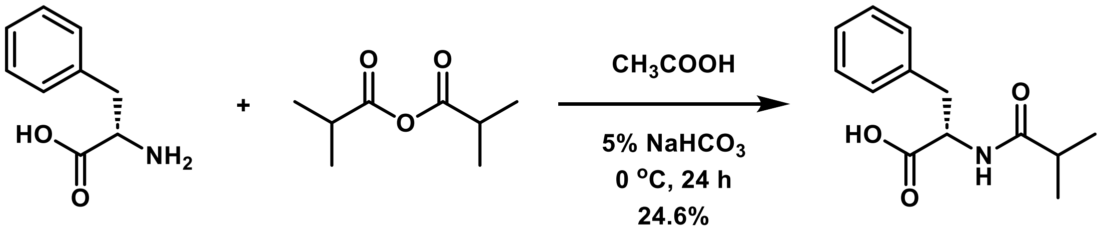

*L*-phenylalanine (0.3030 g, 1.83 mmol) was dissolved in 5.00 mL of 5% $NaHCO_3$ in $H_2O$. Subsequently, isobutyric anhydride (0.267 mL, 2.82 mmol) was added to the solution and stirred at 0 °C overnight. Reaction completion was tested using TLC; if the reaction was incomplete, additional isobutyric anhydride was added. Once the reaction was completed, the solution was acidified to a pH of 2 by adding 6 M HCl dropwise, which caused the product to precipitate. The resulting mixture was then refrigerated overnight, followed by filtration and washing with cold H2O. The acquired white solid was then dried under vacuum and weighed. *N*-isobutyric-*L*-phenylalanine (0.1053 g, 0.45 mmol) was obtained, with a total yield of 24.6%. [89] $^1$H NMR (600

MHz, DMSO-d6): *δ* 12.30-13.00 (br s, 1H), 7.98-8.03 (d, *J* = 8.3 Hz, 1H), 7.17-7.28 (m, 5H), 4.38-4.40 (ddd, *J* = 4.8, 3.1, 1.6 Hz, 1H), 3.03-3.08 (dd, *J* = 9.2, 4.3 Hz, 1H), 2.82-2.88 (dd, *J* = 9.9, 3.8 Hz, 1H), 2.32-2.40 (sept, *J* = 6.8 Hz, 1H), 0.91-0.94 (d, *J* = 6.8 Hz, 3H), 0.82-0.85 (d, *J* = 6.8 Hz, 3H) ppm. $^{13}$C NMR (600 MHz, DMSO-d6): δ 175.2, 172.8, 137.0, 128.5, 127.4, 125.7, 52.5, 36.2, 33.0, 18.9, 18.5 ppm.

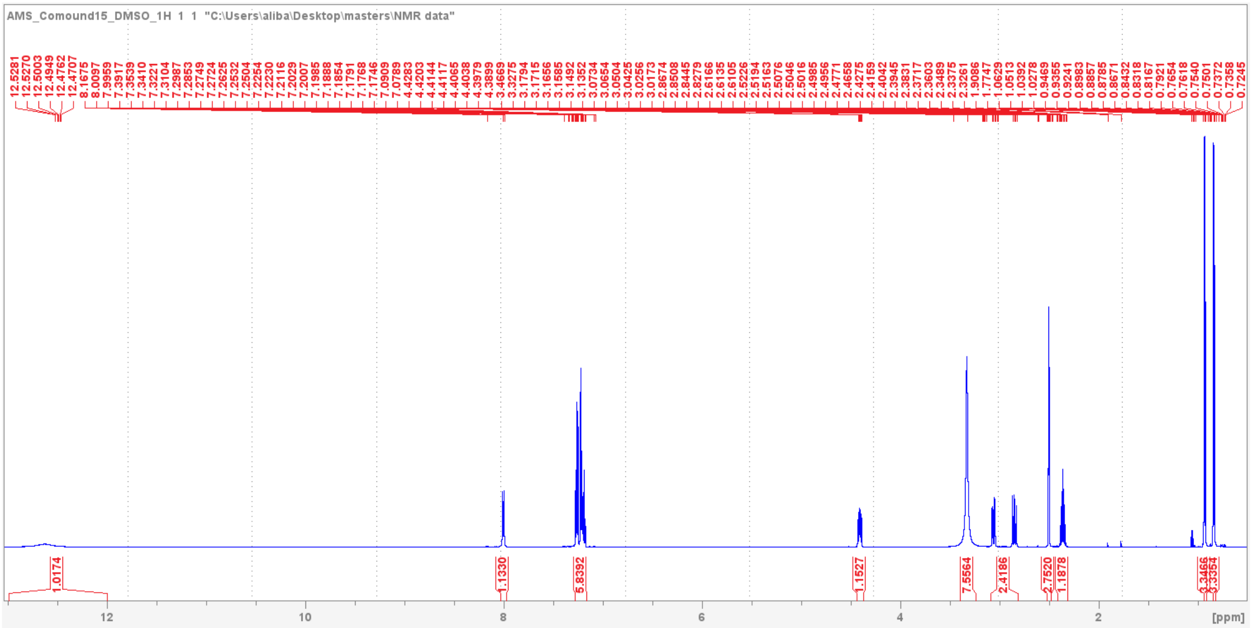

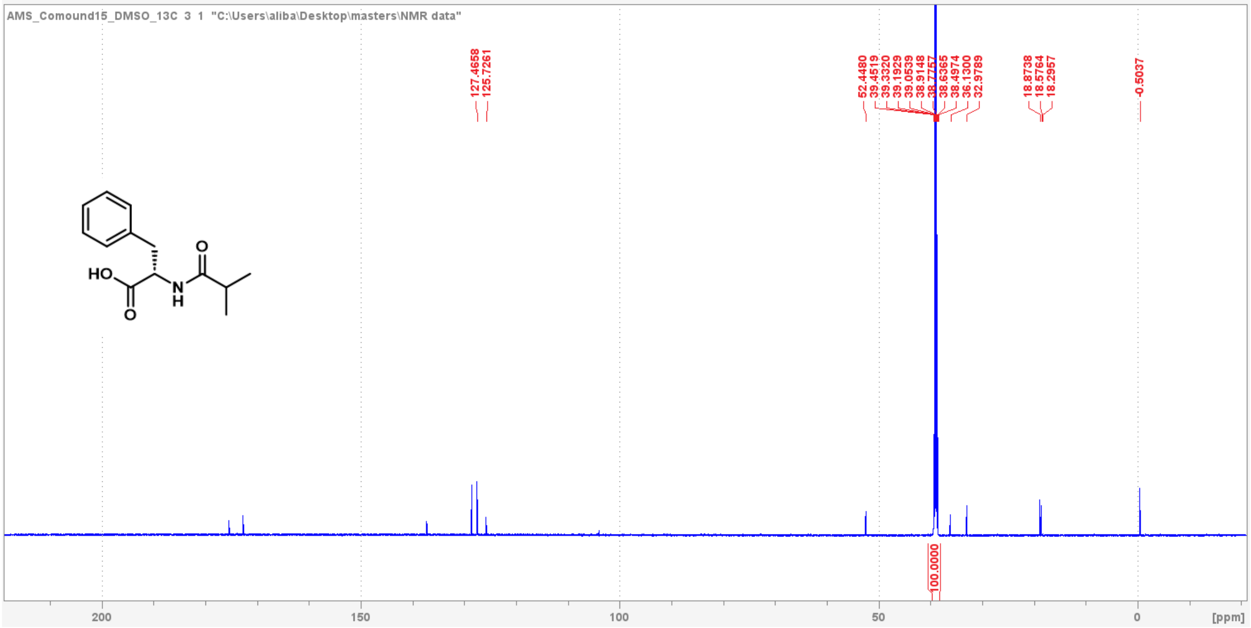

3) Synthesis of Boc-*L*-phenylalanine

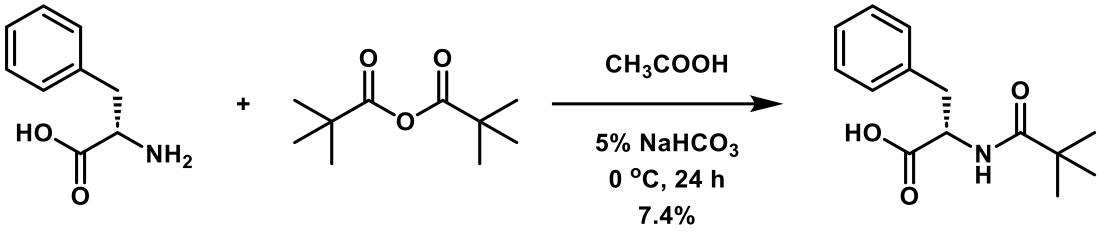

*L*-phenylalanine (0.3003 g, 1.82 mmol) was dissolved in 5.00 mL of 5% $NaHCO_3$ in $H_2O$. Subsequently, trimethylacetic anhydride (0.445 mL, 2.19 mmol) was added to the solution and stirred at 0 °C overnight. Reaction completion was tested using TLC; if the reaction was incomplete, additional trimethylacetic anhydride was added. Once the reaction was completed, the solution was acidified to a pH of 2 by adding 6 M HCl dropwise, which caused the product to precipitate. The resulting mixture was then refrigerated overnight, followed by filtration and washing with cold H2O. The acquired white solid was then dried under vacuum and weighed. Boc-*L*-phenylalanine (0.00335 g, 0.134 mmol) was obtained, with a total yield of 7.4%. [89] $^1H$ NMR (600 MHz, DMSO-d6): δ 12.54-12.74 (br s, 1H), 7.50-7.55 (d, $J$ = 6.8 Hz, 1H), 7.27-7.20 (m, 5H), 4.38-4.40 (ddd, $J$ = 4.7, 3.8, 2.1 Hz, 1H), 3.03-3.08 (dd, $J$ = 9.2, 4.3 Hz, 1H), 2.82-2.88 (dd, $J$ = 9.2, 4.3 Hz, 1H), 1.00-0.99 (s, 9H) ppm.

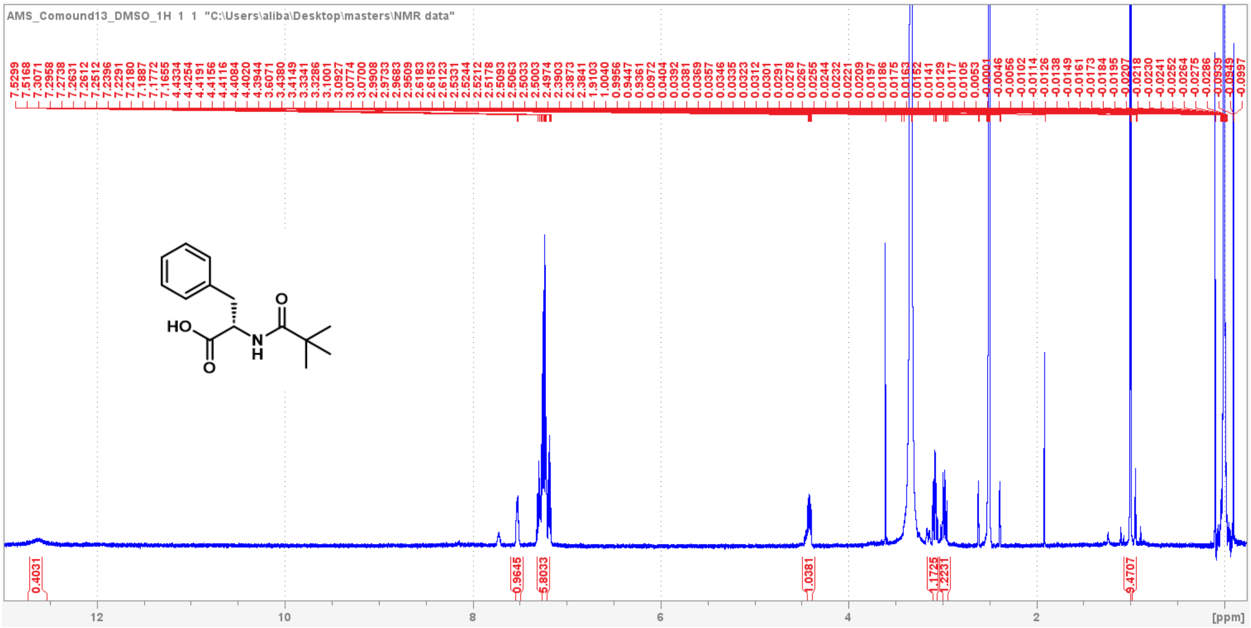

### 4) Synthesis of *N*-butyric-*L*-phenylalanine

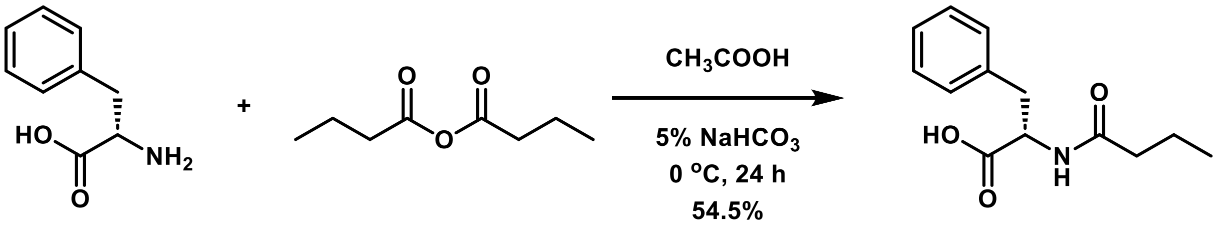

*L*-phenylalanine (0.2727 g, 1.65 mmol) was dissolved in 5.00 mL of 5% $NaHCO_3$ in $H_2O$. Subsequently, butyric anhydride (0.324 mL, 1.98 mmol) was added to the solution and stirred at 0 °C overnight. Reaction completion was tested using TLC; if the reaction was incomplete, additional butyric anhydride was added. Once the reaction was completed, the solution was acidified to a pH of 2 by adding 6 M HCl dropwise, which caused the product to precipitate. The resulting mixture was then refrigerated overnight, followed by filtration and washing with cold H2O. The acquired white solid was then dried under vacuum and weighed. *N*-butyric-*L*-phenylalanine (0.2113 g, 0.899 mmol) was obtained, with a total yield of 54.5%. [89] $^1$H NMR

(600 MHz, CDCl$_3$): $\delta$ 7.26-7.22 (m, 2H), 7.20 -7.22 (m, 1H), 7.12-7.09 (m, 2H), 5.72-5.77 (d, *J* = 7.0 Hz, 1H), 4.75-4.80 (q, *J* = 7.0 Hz, 1H), 3.16-3.21 (dd, *J* = 8.6, 5.6 1H), 3.04-3.09 (dd, *J* = 8.6, 5.6 Hz, 1H), 2.07-2.11 (td, *J* = 5.8, 2.1 Hz, 2H), 1.50-1.58 (sx, *J* = 7.4 Hz, 2H), 0.81-0.85 (t, *J* = 7.4 Hz, 3H) ppm.

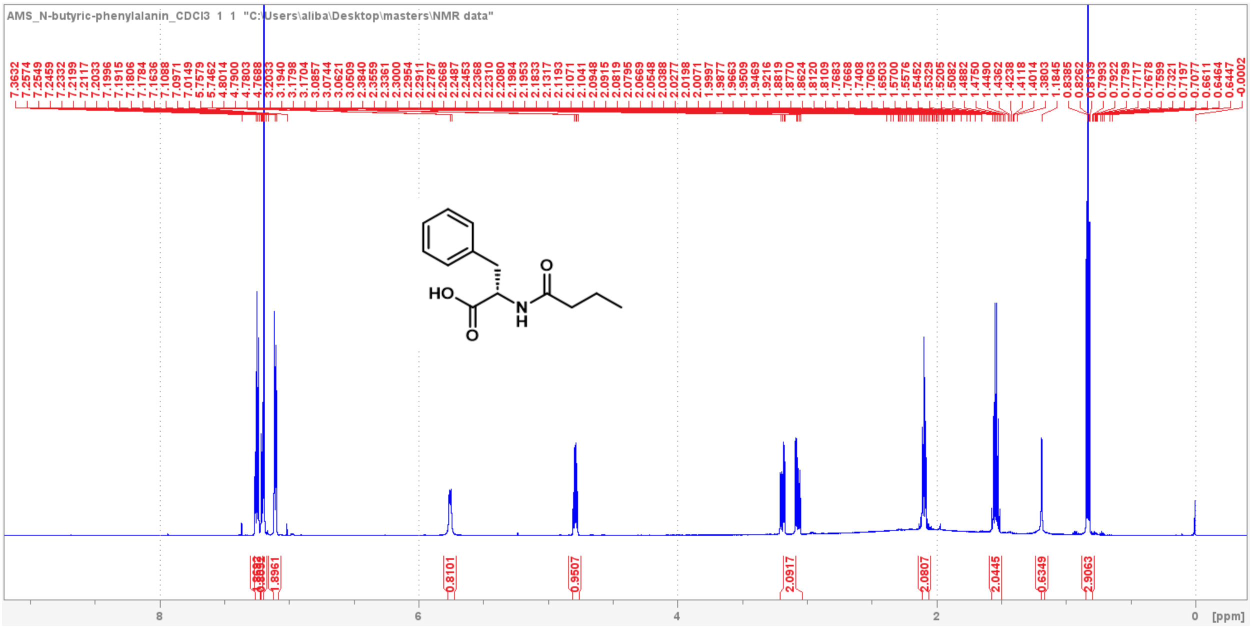

## 5) Synthesis of *N*-benzoyl-*L*-phenylalanine

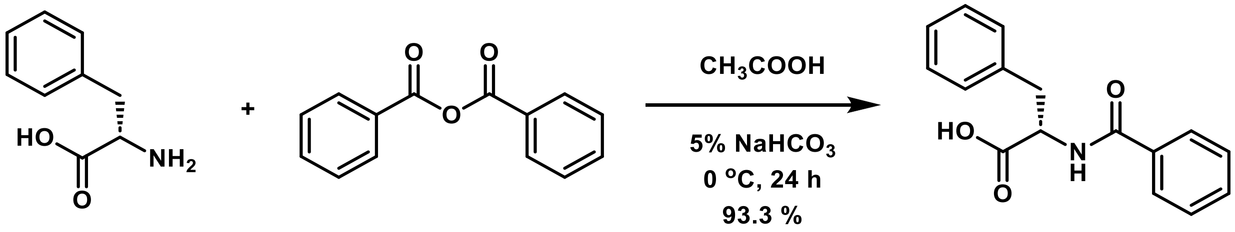

*L*-phenylalanine (0.3412 g, 2.07 mmol) was dissolved in 5.00 mL of 5% NaHCO$_3$ in H$_2$O. Subsequently, benzoic anhydride (0.3713 g, 1.64 mmol) was added to the solution and stirred at 0 ºC overnight. Reaction completion was tested using TLC; if the reaction was incomplete, additional benzoic anhydride was added. Once the reaction was completed, the solution was acidified to a pH of 2 by adding 6 M HCl dropwise, which caused the product to precipitate. The resulting mixture was then refrigerated overnight, followed by filtration and washing with cold H2O. The acquired white solid was then dried under vacuum and weighed. *N*-benzoyl-*L*-phenylalanine (0.4111 g, 1.53 mmol) was obtained, with a total yield of 93.3%. [89] $^1$H NMR (600 MHz, $CDCl_3$): $\delta$ 7.83-7.86 (m, 2H), 7.58-7.61 (m, 1H), 7.50-7.56 (m, 1H), 7.42 -7.46 (m, 2H), 7.36 -7.40 (m, 1H), 7.22-7.35 (m, 3H), 3.93-3.97 (dt, $J$ = 4.8, 2.9 Hz, 1H), 3.22-3.33 (dd, $J$ = 9.1, 15.54 Hz, 1H), 3.00-3.10 (dd, $J$ = 9.1, 11.0 Hz, 1H) ppm.

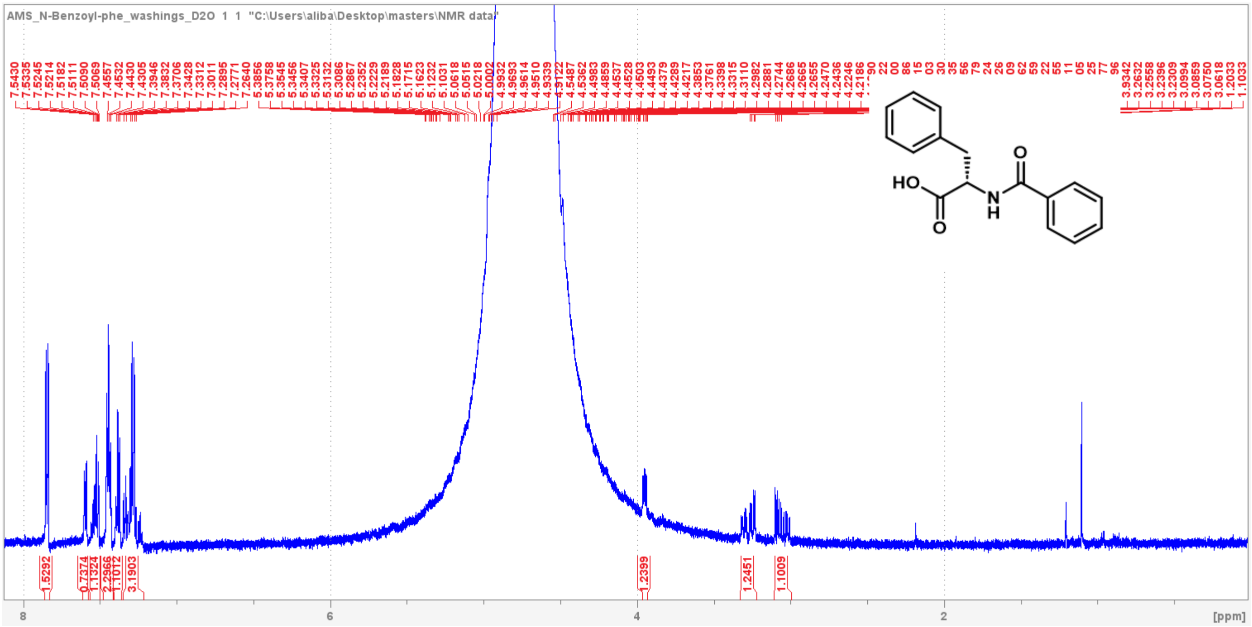

6) Synthesis of *N*-acetyl-β-phenylalanine

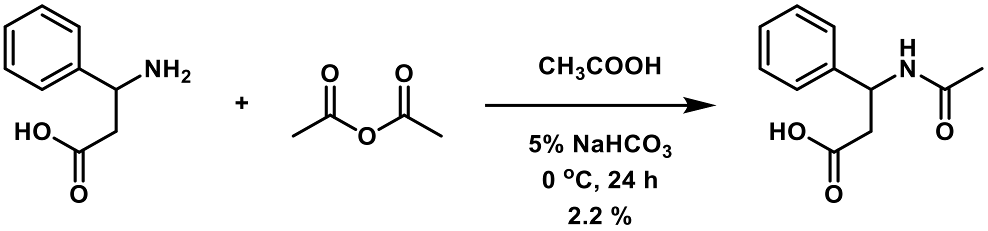

β-phenylalanine (0.3003 g, 1.82 mmol) was dissolved in 5.00 mL of 5% $NaHCO_3$ in $H_2O$. Subsequently, acetic anhydride (0.206 mL, 2.18 mmol) was added to the solution and stirred at 0 °C overnight. Reaction completion was tested using TLC; if the reaction was incomplete, additional acetic anhydride was added. Once the reaction was completed, the solution was acidified to a pH of 2 by adding 6 M HCl dropwise, which caused the product to precipitate. The resulting mixture was then refrigerated overnight, followed by filtration and washing with cold H2O. The acquired white solid was then dried under vacuum and weighed. *N*-acetyl-β-phenylalanine (0.0083 g, 0.040 mmol) was obtained, with a total yield of 2.2%. [89] $^1$H NMR (600 MHz, acetone-d6): δ 7.43-7.46 (m, 2H), 7.34-7.39 (m, 2H), 7.26-7.30 (m, 1H), 5.42-5.46 (t, *J* = 7.1 Hz, 1H), 2.90-2.95 (dd, *J* = 8.3, 7.5 Hz, 1H), 2.81-2.86 (dd, *J* = 8.3, 7.5 Hz, 1H), 1.33-1.35 (s, 3H) ppm.

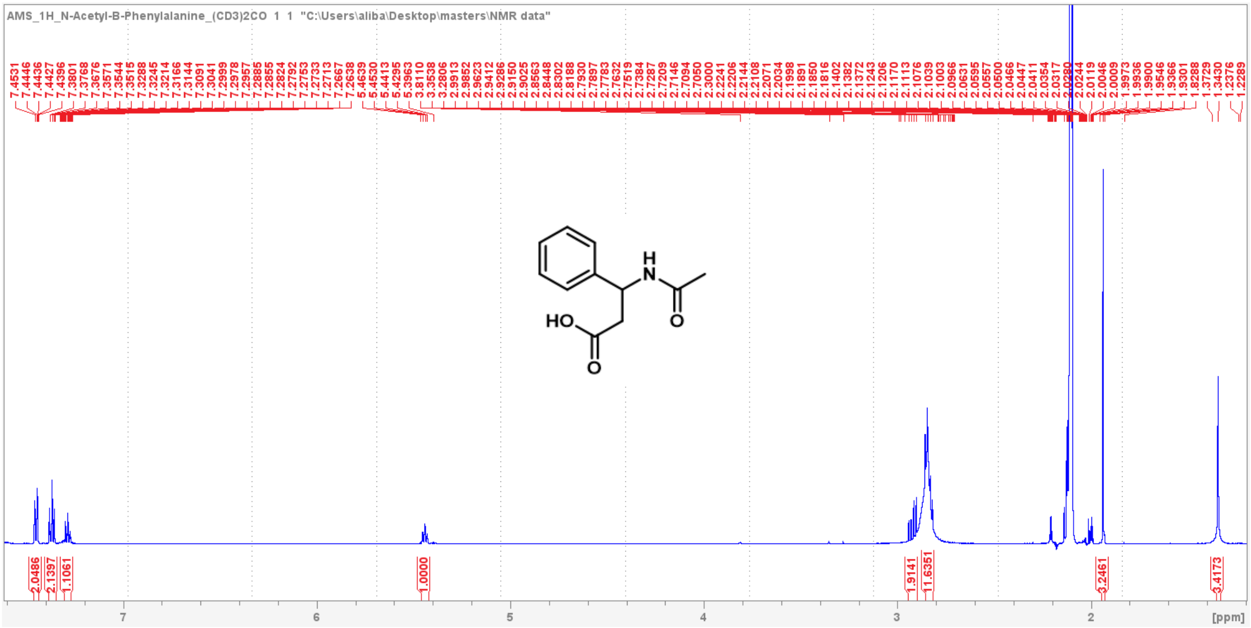

7) Synthesis of *N*-isobutyric-β-phenylalanine

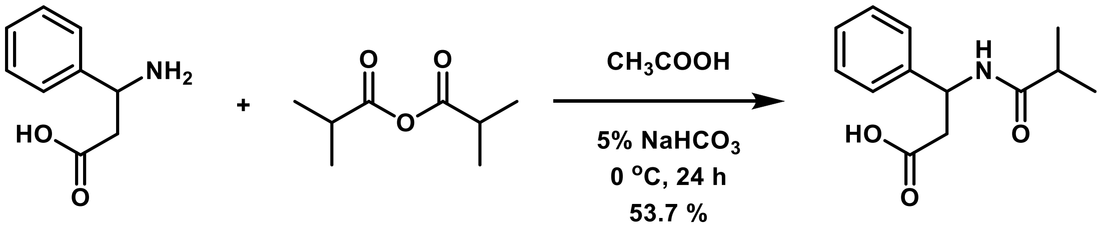

β-phenylalanine (0.2989 g, 1.81 mmol) was dissolved in 5.00 mL of 5% $NaHCO_3$ in $H_2O$. Subsequently, isobutyric anhydride (0.344 mL, 2.17 mmol) was added to the solution and stirred at 0 °C overnight. Reaction completion was tested using TLC; if the reaction was incomplete, additional isobutyric anhydride was added. Once the reaction was completed, the solution was acidified to a pH of 2 by adding 6 M HCl dropwise, which caused the product to precipitate. The resulting mixture was then refrigerated overnight, followed by filtration and washing with cold H2O. The acquired white solid was then dried under vacuum and weighed. *N*-isobutyric-β-phenylalanine (0.2268 g, 0.972 mmol) was obtained, with a total yield of 53.7%. [89] $^1$H NMR

(600 MHz, $D_2O$): δ 7.29-7.41 (m, 5H), 5.21-5.26 (t, *J* = 7.1 Hz, 1H), 2.81-2.91 (m, 2H), 2.45-2.54 (sept, *J* = 6.8 Hz, 1H), 1.04-1.08 (d, *J* = 6.8 Hz, 3H), 1.00-1.03 (d, *J* = 6.8 Hz, 3H) ppm.

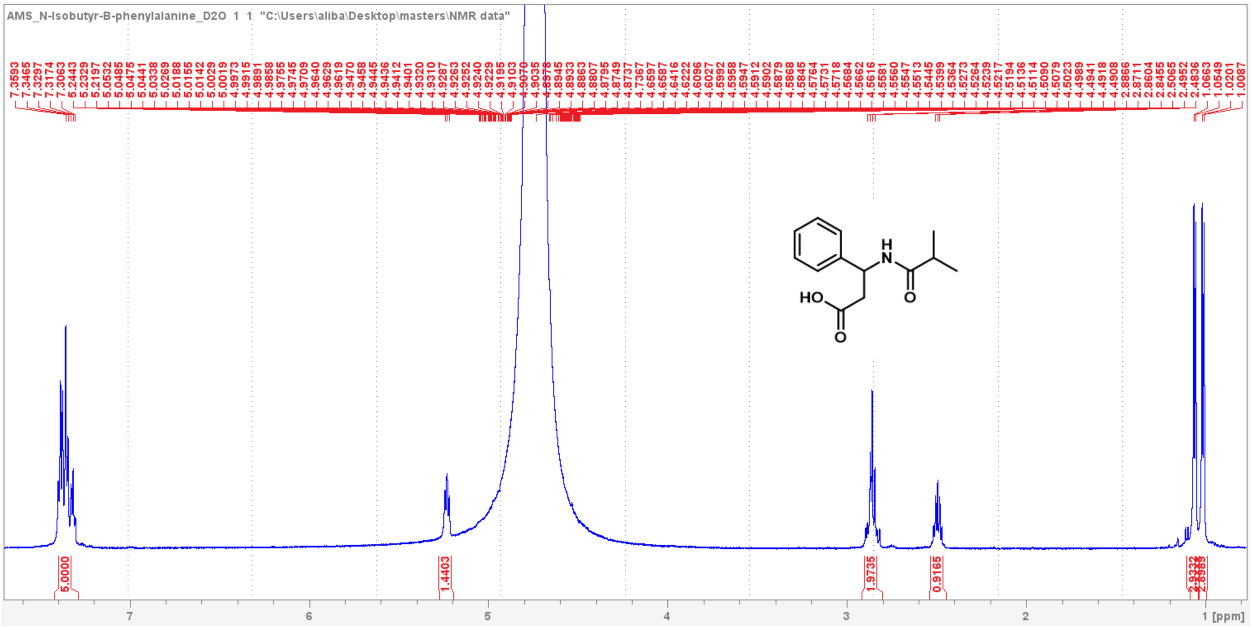

## 8) Synthesis of Boc-β-phenylalanine

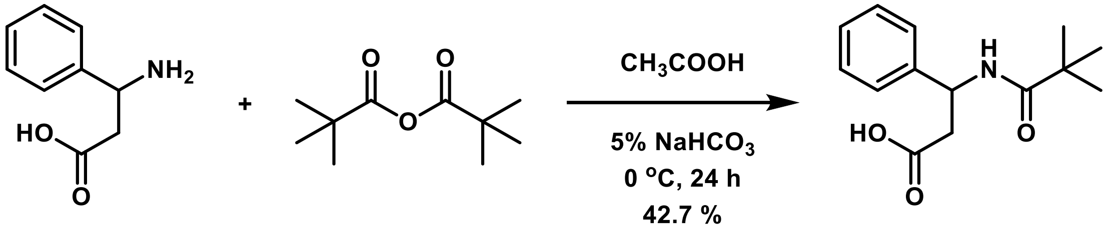

β-phenylalanine (0.2993 g, 1.81 mmol) was dissolved in 5.00 mL of 5% $NaHCO_3$ in $H_2O$. Subsequently, trimethylacetic anhydride (0.643 mL, 3.17 mmol) was added to the solution and stirred at 0 °C overnight. Reaction completion was tested using TLC; if the reaction was incomplete, additional trimethylacetic anhydride was added. Once the reaction was completed, the solution was acidified to a pH of 2 by adding 6 M HCl dropwise, which caused the product to precipitate. The resulting mixture was then refrigerated overnight, followed by filtration and washing with cold H2O. The acquired white solid was then dried under vacuum and weighed. Boc-β-phenylalanine (0.1925 g, 0.772 mmol) was obtained, with a total yield of 42.7%. [89] $^1$H NMR (600 MHz, $CDCl_3$): δ 7.24-7.29 (m, 2H), 7.18-7.22 (m, 3H), 6.66-6.70 (d, *J* = 8.0 Hz, 1H), 5.31-5.35 (dt, *J* = 5.8, 2.3 Hz, 1H), 2.87-2.92 (dd, *J* = 10.3, 5.8 Hz, 1H), 2.78-2.83 (dd, *J* = 10.3, 5.8 Hz, 1H), 1.13-1.14 (s, 9H) ppm. $^{13}$C NMR (600 MHz, DMSO-d6): δ 174.8, 140.4, 128.8, 127.7, 126.1, 49.2, 39.5, 38.8, 27.5 ppm.

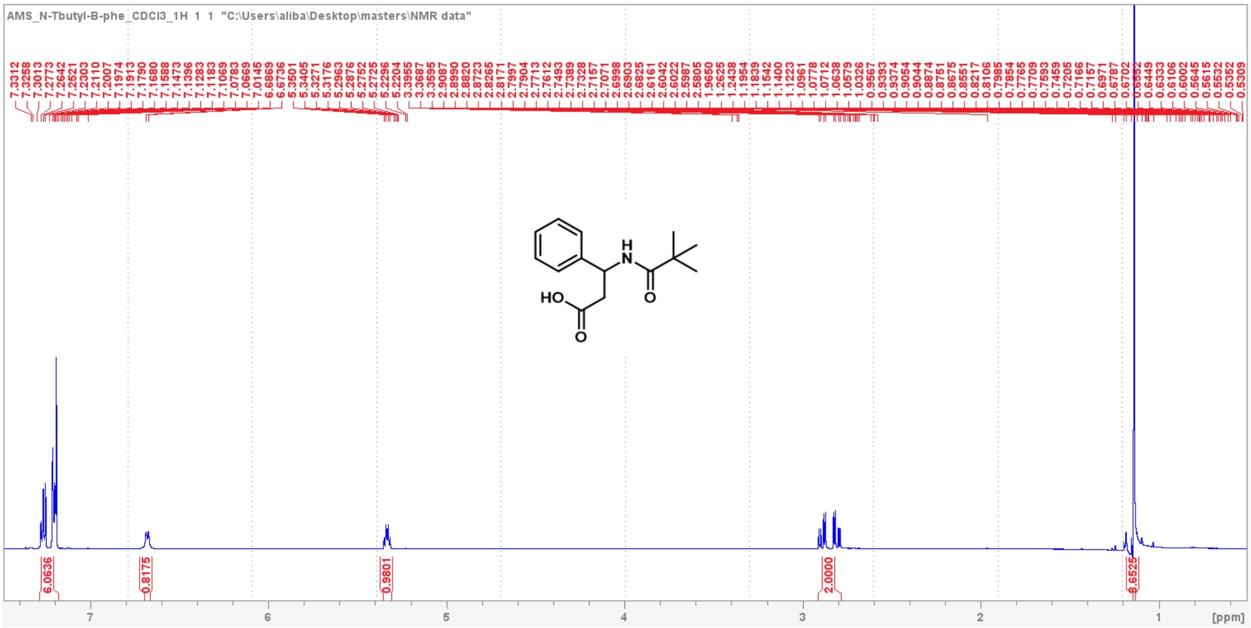

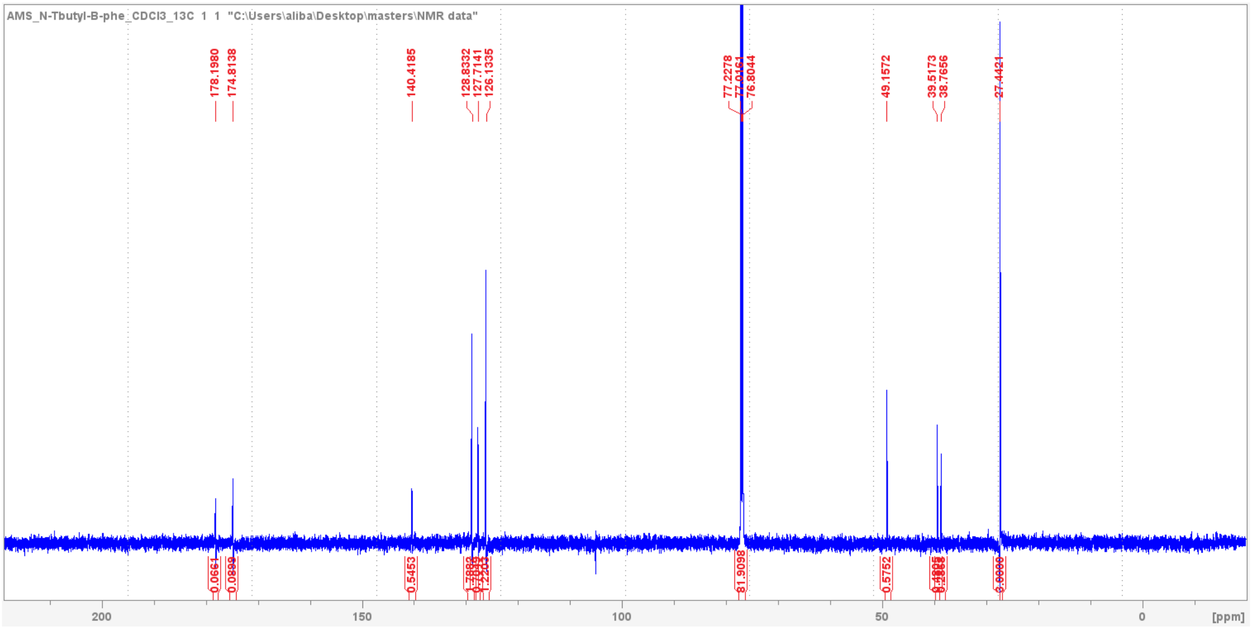

## 9) Synthesis of *N*-butyric-β-phenylalanine

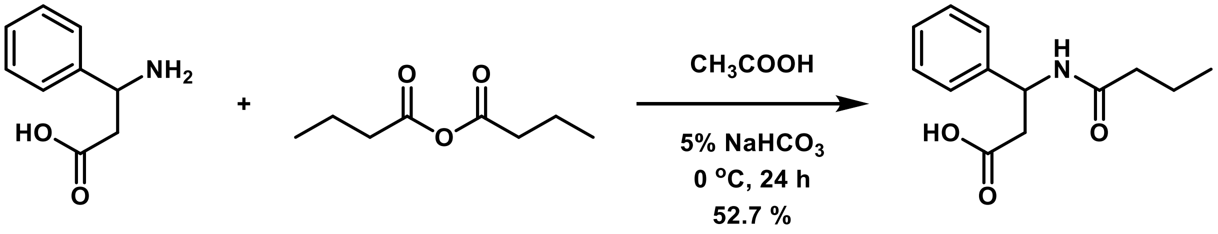

β-phenylalanine (0.3030 g, 1.83 mmol) was dissolved in 5.00 mL of 5% $NaHCO_3$ in $H_2O$. Subsequently, butyric anhydride (0.360 mL, 2.20 mmol) was added to the solution and stirred at 0 °C overnight. Reaction completion was tested using TLC; if the reaction was incomplete, additional butyric anhydride was added. Once the reaction was completed, the solution was acidified to a pH of 2 by adding 6 M HCl dropwise, which caused the product to precipitate. The resulting mixture was then refrigerated overnight, followed by filtration and washing with cold H2O. The acquired white solid was then dried under vacuum and weighed. *N*-butyric-β-phenylalanine (0.2271 g, 0.970 mmol) was obtained, with a total yield of 52.7%. [89] $^1$H

NMR (600 MHz, DMSO-d6): $\delta$ 12.16-12.27 (br s, 1H), 8.27-8.31 (d, $J$ = 8.3 Hz, 1H), 7.28-7.33 (m, 4H), 7.20-7.24 (m, 1H), 5.16-5.22 (q, $J$ = 7.6 Hz, 1H), 2.65-2.69 (dd, $J$ = 8.2, 3.8 1H), 2.61-2.69 (dd, $J$ = 8.2, 3.8 1H), 2.03-2.07 (td, $J$ = 4.6, 2.8 Hz, 2H), 1.44-1.52 (sx, $J$ = 7.1 Hz, 2H), 0.79-0.84 (t, $J$ = 7.4 Hz, 3H) ppm. $^{13}$C NMR (600 MHz, DMSO-d6): δ 171.1 170.5, 142.2, 127.7, 126.3, 125.8, 48.7, 40.5, 36.7, 18.1, 12.9 ppm.

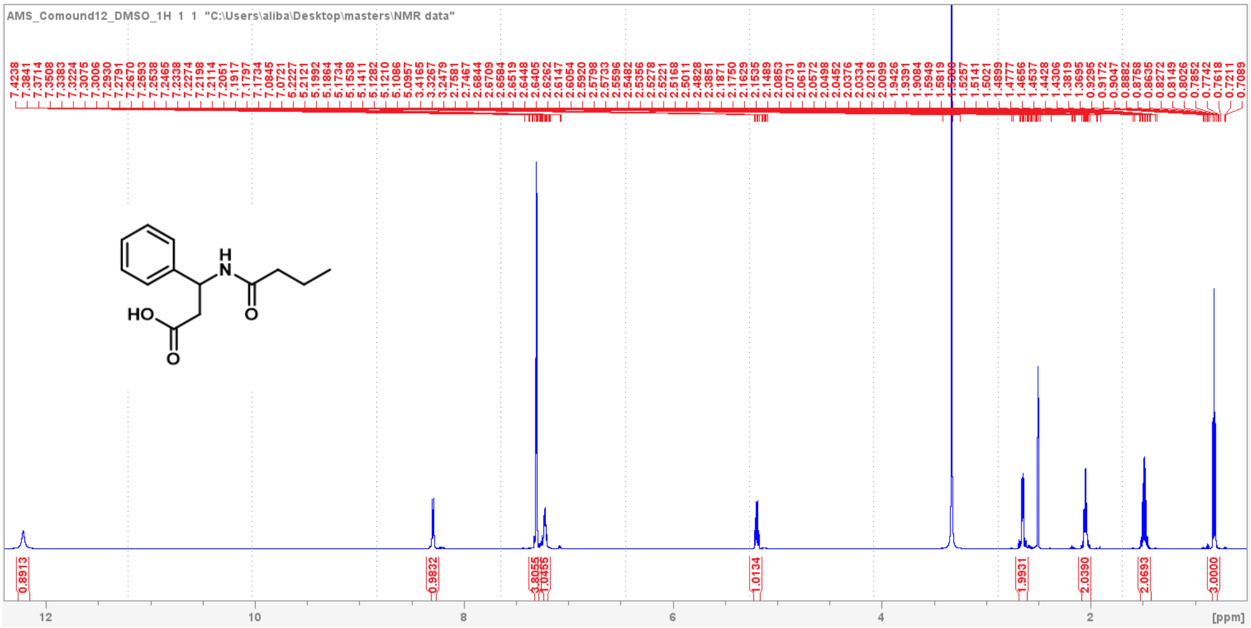

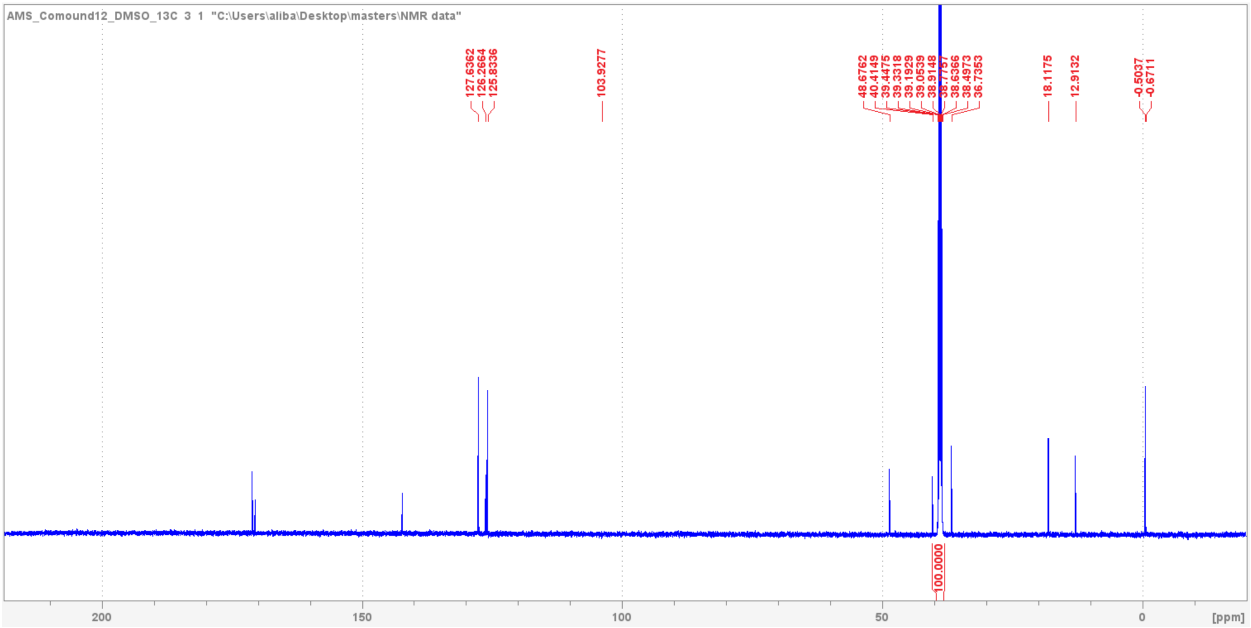

10) Synthesis of *N*-benzoyl-β-phenylalanine

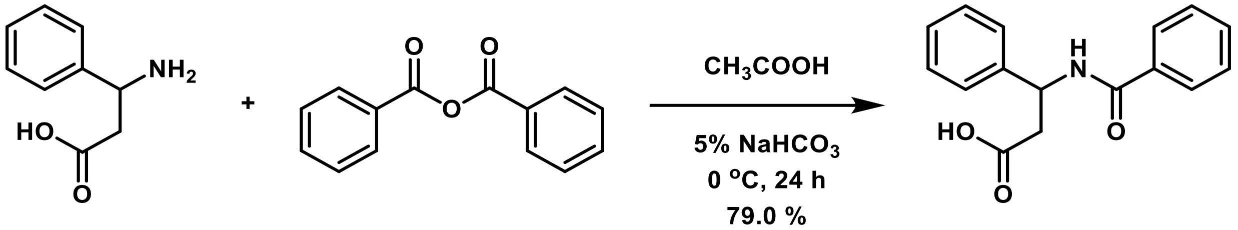

β-phenylalanine (0.3323 g, 1.98 mmol) was dissolved in 5.00 mL of 5% $NaHCO_3$ in $H_2O$. Subsequently, butyric anhydride (0.26.8 g, 1.65 mmol) was added to the solution and stirred at 0 °C overnight. Reaction completion was tested using TLC; if the reaction was incomplete, additional butyric anhydride was added. Once the reaction was completed, the solution was acidified to a pH of 2 by adding 6 M HCl dropwise, which caused the product to precipitate. The resulting mixture was then refrigerated overnight, followed by filtration and washing with cold H2O. The acquired white solid was then dried under vacuum and weighed. *N*-butyric-β-phenylalanine (0.3483 g, 1.30 mmol) was obtained, with a total yield of 79.0%. [89] $^1$H NMR (600 MHz, acetone-d6): $\delta$ 8.10-8.11 (m, 2H), 7.93-7.96 (m, 2H), 7.67-7.71 (m, 1H), 7.47-7.52 (m, 2H) , 7.37-7.41 (m, 2H), 7.28-7.32 (m, 1H), 5.69-5.73 (t, *J* = 7.3 Hz, 1H), 3.08-3.13 (dd, *J* = 8.0, 7.8 1H), 2.97-3.02 (dd, *J* = 9.4, 6.4 1H) ppm.

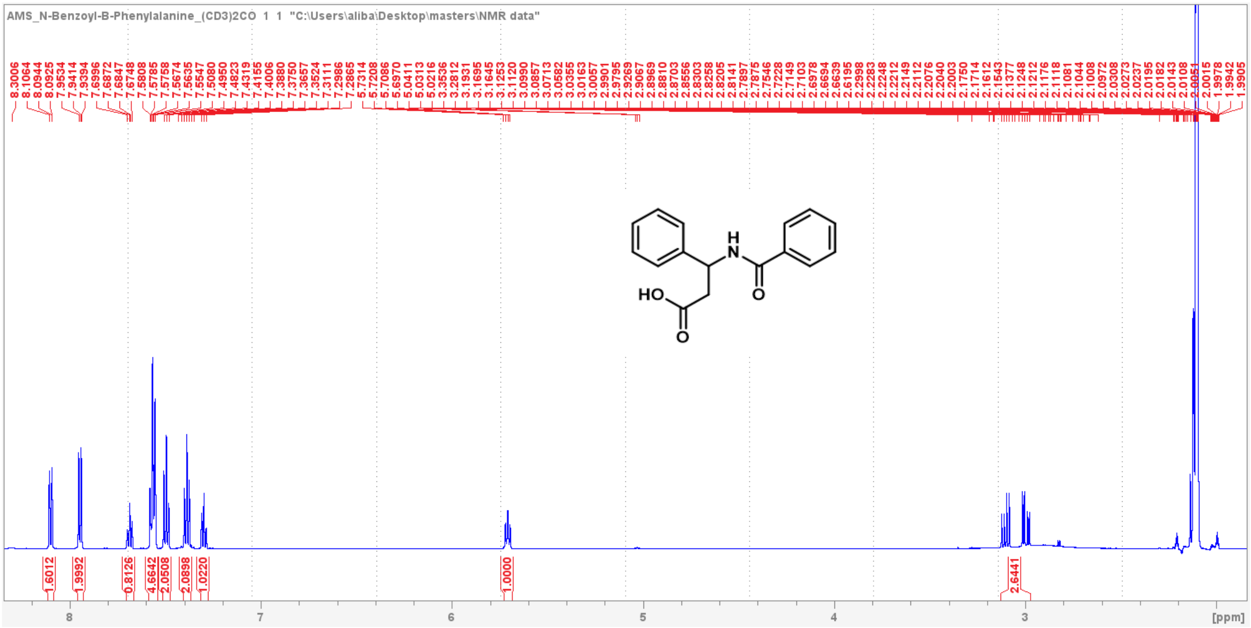
AMS_N-Benzoyl-B-Phenylalanine_(CD3)2CO 1 1 "C:\Users\aliba\Desktop\masters\NMR data"
8.3006
8.1064
8.0944
8.0925
7.9534
7.9414
7.9394
7.6996
7.6872
7.6847
7.6748
7.5808
7.5785
7.5758
7.5674
7.5635
7.5547
7.5080
7.4950
7.4823
7.4319
7.4155
7.4006
7.3880
7.3750
7.3657
7.3524
7.3111
7.2986
7.2865
5.7314
5.7208
5.7086
5.6970
5.0411
5.0313
5.0216
3.3536
3.2812
3.1931
3.1695
3.1645
3.1253
3.1120
3.0990
3.0857
3.0713
3.0582
3.0355
3.0163
3.0057
2.9901
2.9795
2.9269
2.9067
2.8969
2.8810
2.8703
2.8556
2.8303
2.8258
2.8205
2.8141
2.7897
2.7875
2.7546
2.7228
2.7149
2.7103
2.6978
2.6694
2.6639
2.6195
2.2998
2.2283
2.2248
2.2212
2.2149
2.2112
2.2076
2.2040
2.2003
2.1750
2.1714
2.1612
2.1543
2.1377
2.1248
2.1212
2.1176
2.1118
2.1081
2.1044
2.1008
2.0972
2.0308
2.0273
2.0237
2.0195
2.0182
2.0143
2.0108
2.0051
2.0015
1.9978
1.9942
1.9905
H
N
HO
O
O
1.6012
1.9992
0.8126
4.6642
2.0508
2.0898
1.0220
1.0000
2.6441
8
7
6
5
4
3
[ppm]

## 4.4 Reductive amination of phenylalanine

The *L*-phenylalanine, β-phenylalanine, sodium cyanoborohydride, acetone, and methanol used in this experiment were purchased from Sigma-Aldrich. The glacial acetic acid used was purchased from ACP chemicals.

1) Synthesis of *N*-isopropyl-*L*-phenylalanine

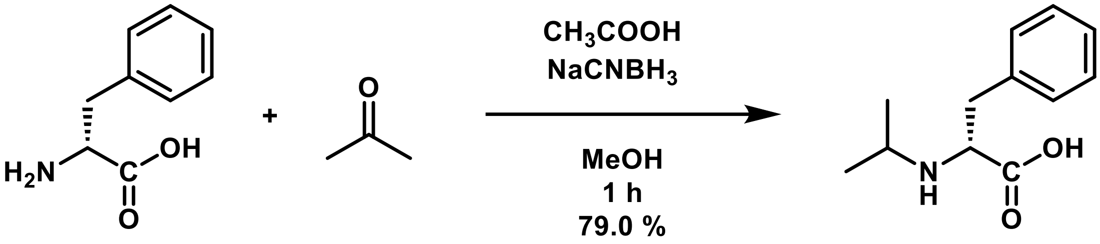

*L*-phenylalanine (0.3058 g, 1.85 mmol) was dissolved in 4 mL dry methanol, along with 2-3 drops of glacial acetic acid. Subsequently, acetone (0.125 mL, 1.56 mmol) and $NaCNBH_3$ (0.1643 g, 2.65 mmol) were added, which was then stirred for 1 hour. Reaction completion was tested using TLC; since the reaction was incomplete, additional acetone (0.125 mL, 1.56 mmol) was added, and stirred for another hour. Upon reaction completion, a white precipitate was observed. The reaction mixture was refrigerated overnight, then filtered and washed with cold methanol. The resulting white solid was dried under vacuum and weighed. *N*-isopropyl-*L*-phenylalanine (0.3029 g, 1.46 mmol) was obtained, with a total yield of 79.0%.[91] $^1$H NMR (600 MHz, $D_2O$): $\delta$ 7.35-7.39 (m, 2H), 7.30-7.34 (m, 2H), 7.26-7.30 (m, 1H), 3.89-3.92 (t, $J$ = 7.2 Hz, 1H), 3.34-3.41 (sept, $J$ = 6.6 Hz, 1H), 3.19-3.14 (dd, $J$ = 7.7, 6.4 1H), 3.10-3.14 (dd, $J$ = 7.4, 6.7 1H), 1.25-1.27 (d, $J$ = 6.6 Hz, 3H), 1.22-1.24 (d, $J$ = 6.6 Hz, 3H) ppm. $^{13}$C NMR (600 MHz, $D_2O$): δ 173.2 129.3, 129.0, 127.6, 105.1, 61.1, 50.5, 36.3, 18.9, 17.8 ppm.

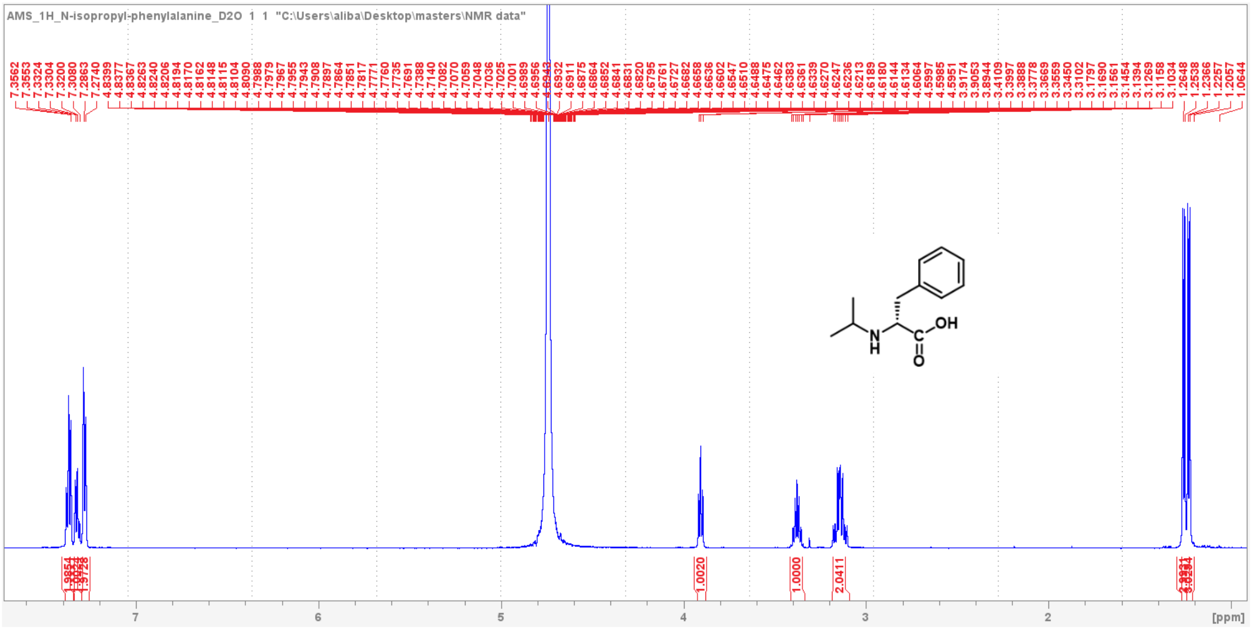
AMS_1H_N-isopropyl-phenylalanine_D2O 1 1 "C:\Users\aliba\Desktop\masters\NMR data"
7.3562
7.3553
7.3324
7.3304
7.3200
7.3080
7.2863
7.2740
4.8399
4.8377
4.8367
4.8263
4.8240
4.8206
4.8194
4.8170
4.8162
4.8148
4.8115
4.8104
4.8090
4.7988
4.7979
4.7967
4.7955
4.7943
4.7908
4.7897
4.7864
4.7851
4.7817
4.7771
4.7760
4.7735
4.7691
4.7388
4.7140
4.7082
4.7070
4.7059
4.7048
4.7036
4.7025
4.7001
4.6989
4.6956
4.6943
4.6932
4.6911
4.6875
4.6864
4.6852
4.6841
4.6831
4.6820
4.6795
4.6761
4.6727
4.6682
4.6658
4.6636
4.6602
4.6547
4.6510
4.6488
4.6475
4.6462
4.6383
4.6361
4.6339
4.6270
4.6247
4.6236
4.6213
4.6189
4.6180
4.6144
4.6134
4.6064
4.5997
4.5985
4.5951
3.9174
3.9053
3.8944
3.4109
3.3997
3.3888
3.3778
3.3669
3.3559
3.3450
3.3102
3.1797
3.1690
3.1561
3.1454
3.1394
3.1269
3.1158
3.1034
1.2648
1.2538
1.2366
1.2257
1.2057
1.0644
N
H
OH
C
O
1.9854
1.9728
1.0020
1.0000
2.0411
7
6
5
4
3
2
[ppm]

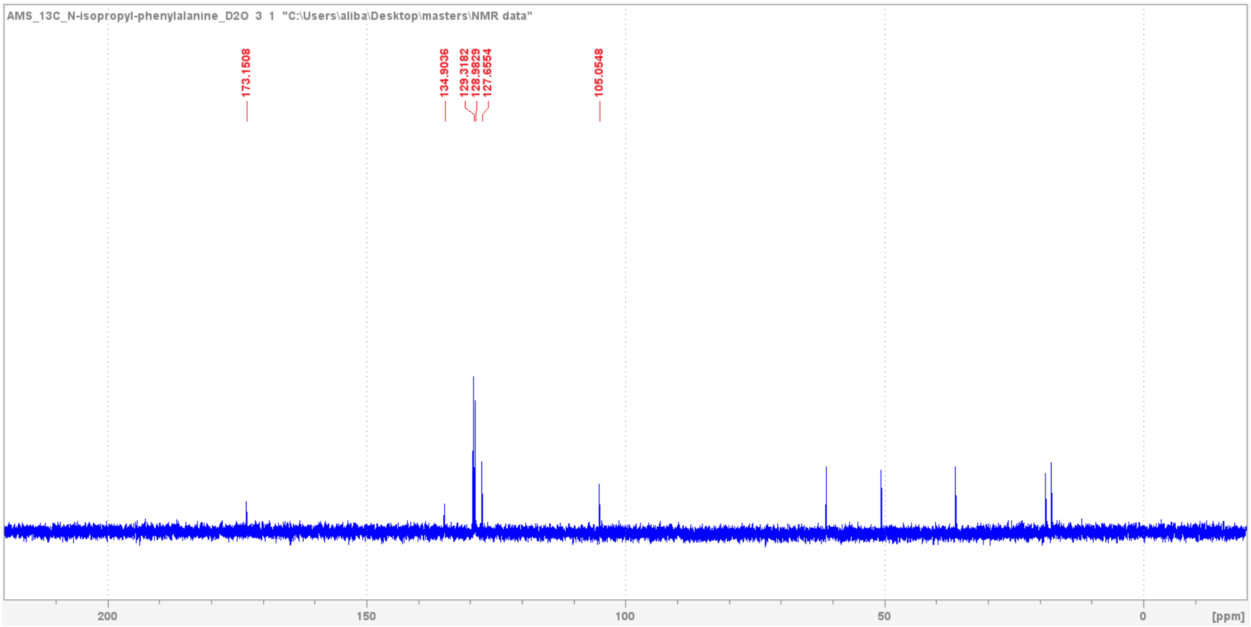
AMS_13C_N-isopropyl-phenylalanine_D2O 3 1 "C:\Users\aliba\Desktop\masters\NMR data"
173.1508
134.9036
129.3182
128.9829
127.6554
105.0548
200
150
100
50
0
[ppm]

2) Synthesis of *N*-isopropyl-β-phenylalanine

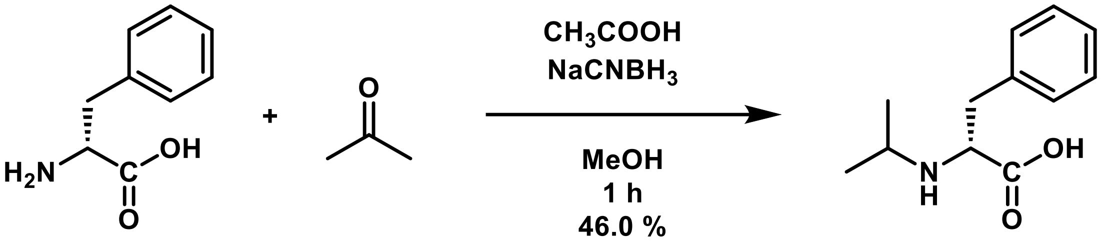

β-phenylalanine (0.3010 g, 1.82 mmol) was dissolved in 4 mL dry methanol, along with 2-3 drops of glacial acetic acid. Subsequently, acetone (0.16 mL, 2.13 mmol) and $NaCNBH_3$ (0.1370 g, 2.19 mmol) were added, which was then stirred for 1 hour. Reaction completion was tested using TLC; since the reaction was incomplete, additional acetone (0.16 mL, 2.13 mmol) was added, and stirred for another hour. Upon reaction completion, a white precipitate was observed. The reaction mixture was refrigerated overnight, then filtered and washed with cold methanol. The resulting white solid was dried under vacuum and weighed. *N*-isopropyl-β-phenylalanine (0.1764 g, 0.85 mmol) was obtained, with a total yield of 46.0%. [91] $^1H$ NMR (600 MHz, DMSO-d6): $\delta$ 7.37-7.40 (m, 2H), 7.29-7.33 (m, 2H), 7.20-7.24 (m, 1H), 4.08-4.12 (dd, $J$ = 5.1, 4.4 Hz, 1H), 2.52-2.59 (sept, $J$ = 6.3 Hz, 1H), 2.30-2.36 (dd, $J$ = 9.6, 5.6 1H), 2.19-2.25 (dd, $J$ = 10.8, 4.4 1H), 0.98-1.01 (d, $J$ = 6.3 Hz, 3H), 0.92-0.94 (d, $J$ = 6.3 Hz, 3H) ppm. $^{13}C$ NMR (600 MHz, DMSO-d6): δ 171.3 127.6, 126.5, 126.3, 103.9, 56.4, 44.6, 43.1, 22.7, 20.3 ppm.

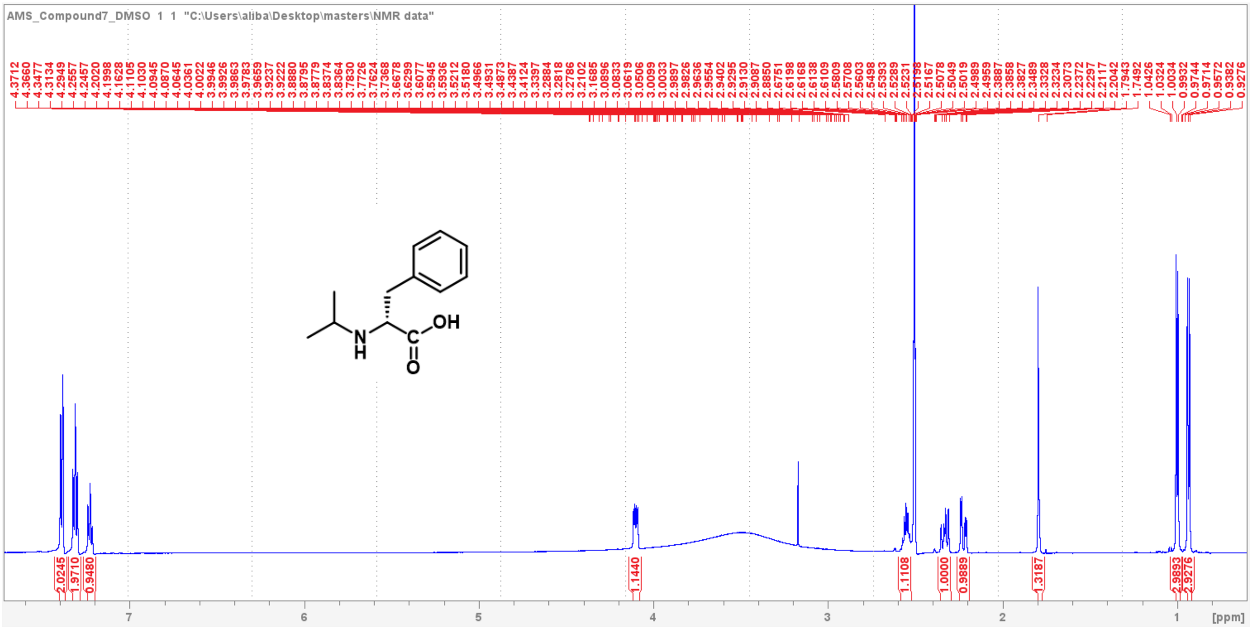
AMS_Compound7_DMSO 1 1 "C:\Users\aliba\Desktop\masters\NMR data"
4.3712
4.3660
4.3477
4.3134
4.2949
4.2557
4.2457
4.2020
4.1998
4.1628
4.1105
4.1030
4.0945
4.0870
4.0645
4.0361
4.0022
3.9946
3.9926
3.9863
3.9783
3.9659
3.9237
3.9222
3.8880
3.8795
3.8779
3.8374
3.8364
3.7830
3.7726
3.7624
3.7368
3.6678
3.6299
3.6077
3.5945
3.5936
3.5212
3.5180
3.4966
3.4931
3.4873
3.4387
3.4124
3.3397
3.2884
3.2818
3.2786
3.2102
3.1685
3.0896
3.0833
3.0619
3.0506
3.0099
3.0033
2.9897
2.9826
2.9636
2.9554
2.9402
2.9295
2.9130
2.9087
2.8850
2.6751
2.6198
2.6168
2.6138
2.6109
2.5809
2.5708
2.5603
2.5498
2.5393
2.5289
2.5231
2.5198
2.5167
2.5078
2.5049
2.5019
2.4989
2.4959
2.3887
2.3858
2.3827
2.3489
2.3328
2.3234
2.3073
2.2372
2.2297
2.2117
2.2042
1.7943
1.7492
1.0426
1.0324
1.0034
0.9932
0.9744
0.9714
0.9572
0.9382
0.9276
N
H
C
OH
O
2.0245
1.9710
0.9480
1.1440
1.1108
1.0000
0.9889
1.3187
2.9893
2.9276
7
6
5
4
3
2
1
[ppm]

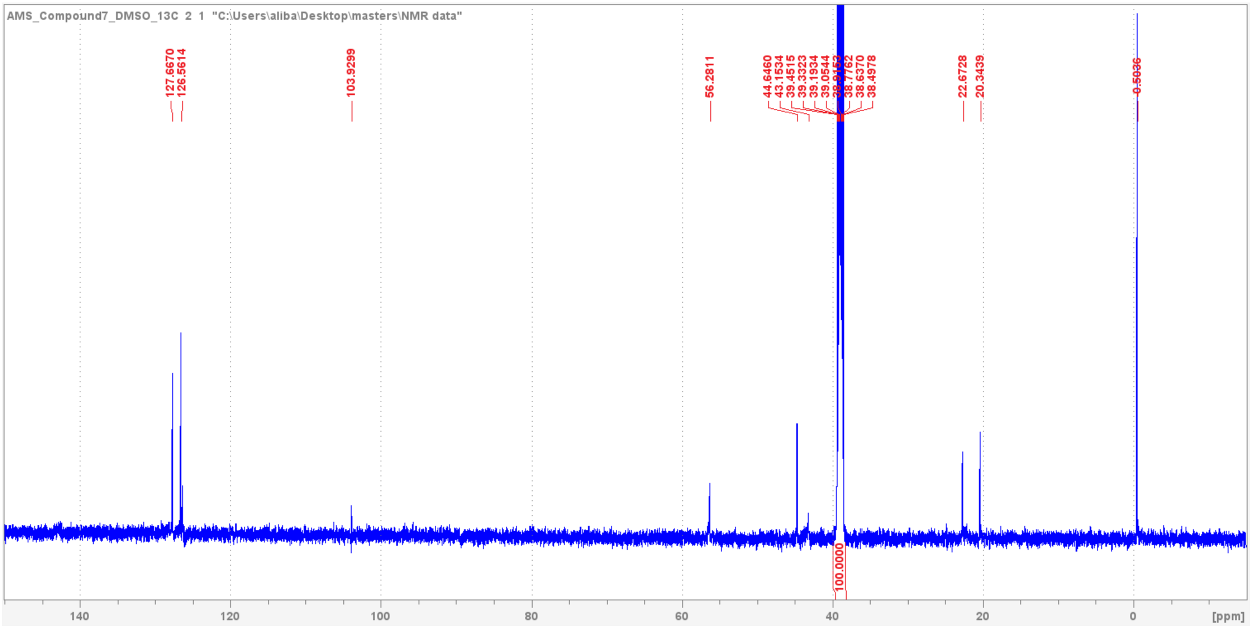
AMS_Compound7_DMSO_13C 2 1 "C:\Users\aliba\Desktop\masters\NMR data"
127.6670
126.5614
103.9299
56.2811
44.6460
43.1534
39.4515
39.3323
39.1934
39.0544
38.9153
38.7762
38.6370
38.4978
22.6728
20.3439
0.5036
100.0000
140
120
100
80
60
40
20
0
[ppm]

### 4.5 *N*-(2-fluorophenyl)-d-gluconamide (2FA) synthesis

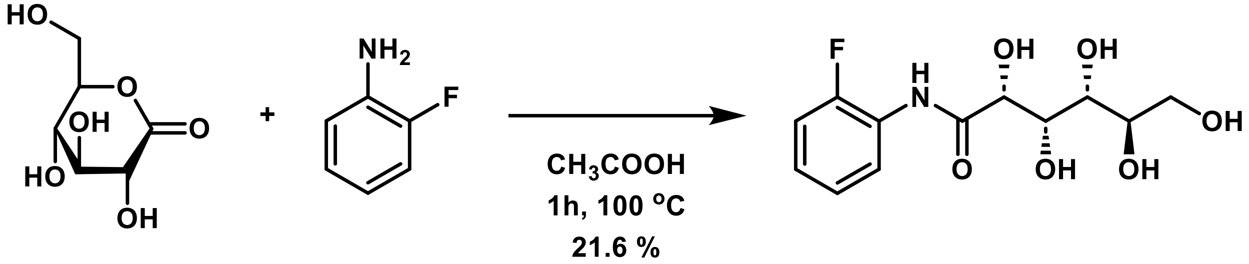

D-gluconic acid-d-lactone (2.0696 g, 11.6 mmol, 1 eq) was dissolved in acetic acid (20 mL), followed by the addition of 2-fluoroaniline (3.2 mL, 33.3 mmol, 3 eq). The reaction mixture was stirred under reflux at 100 °C for 1 hour, resulting in a brown sludge. The crude product was then recrystalized using ethanol solvent, filtered, and dried under vacuum. Obtaining a final mass of 0.7262 g, 2.51 mmol 2FA, with a total yield of 21.6 %.[41] $^1$H NMR (600 MHz, DMSO-d6): δ 9.20 (br. s, 1H), 8.08-8.16 (td, *J* = 11.3 Hz, 4.7 Hz, 1H), 7.22-7.33 (m, 1H), 7.07-722 (m, 2H), 5.90-6.00 (d, *J* = 9.4 Hz, 1H), 4.65-4.70 (d, *J* = 14.7 Hz, 1H), 4.58-4.65 (t, *J* = 10.2 Hz, 2H), 4.35-4.42 (t, *J* = 10.5 Hz, 1H), 4.21-4.26 (t, *J* = 7.2 Hz, 1H), 3.99-4.05 (m, 1H), 3.45-3.64 (m, 3H), 3.44-3.36 (m, 1H) ppm.

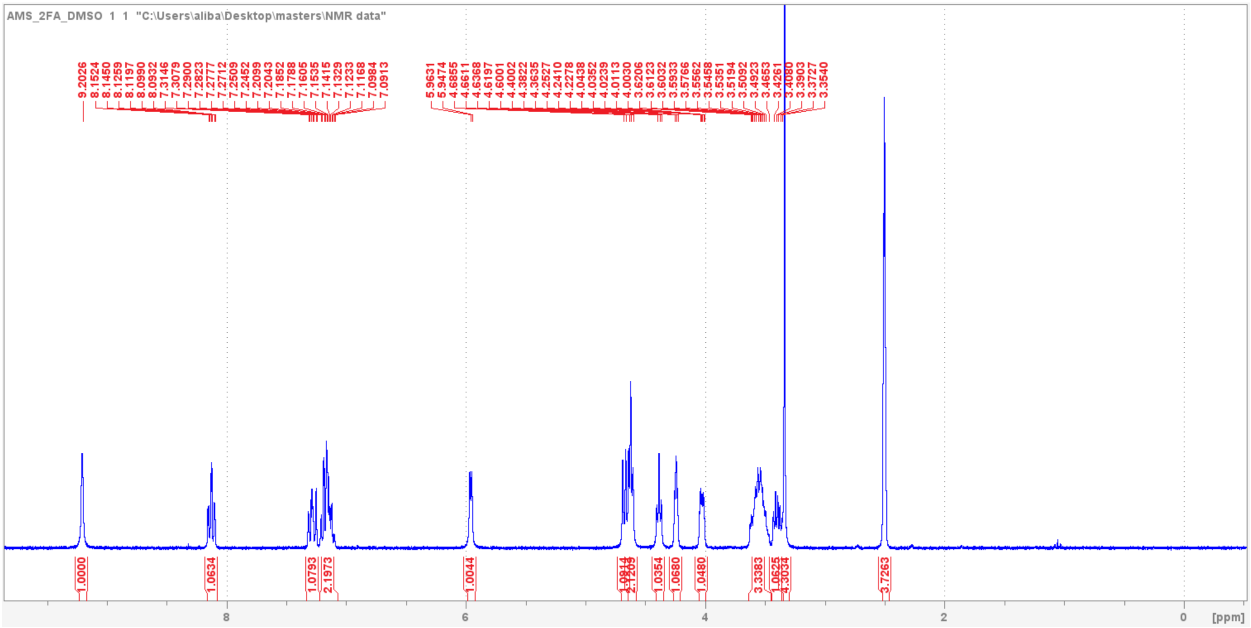
AMS_2FA_DMSO 1 1 "C:\Users\aliba\Desktop\masters\NMR data"
9.2026
8.1524
8.1450
8.1259
8.1197
8.0990
8.0932
7.3146
7.3079
7.2900
7.2823
7.2777
7.2712
7.2509
7.2452
7.2099
7.2043
7.1852
7.1788
7.1605
7.1535
7.1415
7.1329
7.1233
7.1168
7.0984
7.0913
5.9631
5.9474
4.6855
4.6611
4.6368
4.6197
4.6001
4.4002
4.3822
4.3635
4.2527
4.2410
4.2278
4.0438
4.0352
4.0239
4.0113
4.0030
3.6206
3.6123
3.6032
3.5933
3.5766
3.5562
3.5458
3.5351
3.5194
3.5092
3.4923
3.4653
3.4261
3.4080
3.3903
3.3727
3.3540
1.0000
1.0634
1.0793
2.1973
1.0044
1.0914
2.1209
1.0354
1.0680
1.0480
3.3383
1.0625
4.3034
3.7263
8
6
4
2
0
[ppm]

# 5 References

(1) Valeri, C. R.; Ragno, G. Cryopreservation of Human Blood Products. *Transfusion and Apheresis Science* **2006**, *34* (3). https://doi.org/10.1016/j.transci.2005.11.010.

(2) Scott, K. L.; Lecak, J.; Acker, J. P. Biopreservation of Red Blood Cells: Past, Present, and Future. *Transfus Med Rev* **2005**, *19* (2), 127–142. https://doi.org/10.1016/j.tmrv.2004.11.004.

(3) Baust, J. M.; Van Buskirk, R.; Baust, J. G. Gene Activation of the Apoptotic Caspase Cascade Following Cryogenic Storage. *Cell Preserv Technol* **2003**, *1* (1). https://doi.org/10.1089/15383440260073301.

(4) Pegg, D. E. Principles of Cryopreservation. *Methods in Molecular Biology* **2015**, *1257*. https://doi.org/10.1007/978-1-4939-2193-5_1.

(5) Jang, T. H.; Park, S. C.; Yang, J. H.; Kim, J. Y.; Seok, J. H.; Park, U. S.; Choi, C. W.; Lee, S. R.; Han, J. Cryopreservation and Its Clinical Applications | Elsevier Enhanced Reader. *Integr Med Res* **2017**, *6* (1).

(6) Fahy, G. M.; Wowk, B. Principles of Cryopreservation by Vitrification. *Methods in Molecular Biology* **2015**, *1257*. https://doi.org/10.1007/978-1-4939-2193-5_2.

(7) Fahy, G. M.; MacFarlane, D. R.; Angell, C. A.; Meryman, H. T. Vitrification as an Approach to Cryopreservation. *Cryobiology* **1984**, *21* (4). https://doi.org/10.1016/0011-2240(84)90079-8.

(8) Fahy, G. M.; Levy, D. I.; Ali, S. E. Some Emerging Principles Underlying the Physical Properties, Biological Actions, and Utility of Vitrification Solutions. *Cryobiology* **1987**, *24* (3). https://doi.org/10.1016/0011-2240(87)90023-X.

(9) Fahy, G. M.; Wowk, B. Principles of Cryopreservation by Vitrification. *Methods in Molecular Biology* **2015**, *1257*. https://doi.org/10.1007/978-1-4939-2193-5_2.

(10) Fahy, G. M.; Levy, D. I.; Ali, S. E. Some Emerging Principles Underlying the Physical Properties, Biological Actions, and Utility of Vitrification Solutions. *Cryobiology* **1987**, *24* (3). https://doi.org/10.1016/0011-2240(87)90023-X.

(11) Fahy, G. M.; MacFarlane, D. R.; Angell, C. A.; Meryman, H. T. Vitrification as an Approach to Cryopreservation. *Cryobiology* **1984**, *21* (4). https://doi.org/10.1016/0011-2240(84)90079-8.

(12) Briard, J. G.; Poisson, J. S.; Turner, T. R.; Capicciotti, C. J.; Acker, J. P.; Ben, R. N. Small Molecule Ice Recrystallization Inhibitors Mitigate Red Blood Cell Lysis during Freezing, Transient Warming and Thawing. *Sci Rep* **2016**, *6*. https://doi.org/10.1038/srep23619.

(13) Elliott, G. D.; Wang, S.; Fuller, B. J. Cryoprotectants: A Review of the Actions and Applications of Cryoprotective Solutes That Modulate Cell Recovery from Ultra-Low Temperatures. *Cryobiology*. 2017. https://doi.org/10.1016/j.cryobiol.2017.04.004.

(14) Lovelock, J. E. The Haemolysis of Human Red Blood-Cells by Freezing and Thawing. *BBA - Biochimica et Biophysica Acta* **1953**, *10* (C). https://doi.org/10.1016/0006-3002(53)90273-X.

(15) Bakhach, J. The Cryopreservation of Composite Tissues: Principles and Recent Advancement on Cryopreservation of Different Type of Tissues. *Organogenesis*. 2009. https://doi.org/10.4161/org.5.3.9583.

(16) Ampaw, A. A.; Sibthorpe, A.; Ben, R. N. Use of Ice Recrystallization Inhibition Assays to Screen for Compounds That Inhibit Ice Recrystallization. In *Methods in Molecular Biology*; 2021; Vol. 2180. https://doi.org/10.1007/978-1-0716-0783-1_9.

(17) Yang, J.; Pan, C.; Zhang, J.; Sui, X.; Zhu, Y.; Wen, C.; Zhang, L. Exploring the Potential of Biocompatible Osmoprotectants as Highly Efficient Cryoprotectants. *ACS Appl Mater Interfaces* **2017**, *9* (49). https://doi.org/10.1021/acsami.7b12189.

(18) Mazur, P. Freezing of Living Cells: Mechanisms and Implications. *The American journal of physiology*. 1984. https://doi.org/10.1152/ajpcell.1984.247.3.C125.

(19) Mazur, P. Basic Problems in Cryobiology. In *Advances in Cryogenic Engineering*; 1964. https://doi.org/10.1007/978-1-4757-0525-6_4.

(20) Mazur, P.; Leibo, S. P.; Chu, E. H. Y. A Two-Factor Hypothesis of Freezing Injury. *Exp Cell Res* **1972**, *71* (2). https://doi.org/10.1016/0014-4827(72)90303-5.

(21) Scott, K. L.; Lecak, J.; Acker, J. P. Biopreservation of Red Blood Cells: Past, Present, and Future. *Transfus Med Rev* **2005**, *19* (2). https://doi.org/10.1016/j.tmrv.2004.11.004.

(22) Zhao, R.; Liu, X.; Ekpo, M. D.; He, Y.; Tan, S. Exploring the Cryopreservation Mechanism and Direct Removal Strategy of TAPS in Red Blood Cell Cryopreservation. *ACS Biomater Sci Eng* **2024**, *10* (7), 4259–4268. https://doi.org/10.1021/acsbiomaterials.3c01701.

(23) Meryman, H. T. Cryoprotective Agents. *Cryobiology* **1971**, *8* (2). https://doi.org/10.1016/0011-2240(71)90024-1.

(24) Valeri, C. R.; Ragno, G. Cryopreservation of Human Blood Products. *Transfusion and Apheresis Science* **2006**, *34* (3). https://doi.org/10.1016/j.transci.2005.11.010.

(25) Ben, R.; Capicciotti, C.; Briard, J. Small Molecule Ice Recrystallization Inhibitors and Methods of Use Thereof. 10,004,222, June 26, 2018.

(26) Chantelle Capicciotti; Robert Ben. The Rational Design of Potent Ice Recrystallization Inhibitors for Use as Novel Cryoprotectants, University of Ottawa, Ottawa, 2014.

(27) Jennie G. Briard; Robert N. Ben. The Rational Design and Use of Novel Small-Molecule Ice Recrystallization Inhibitors for the Cryopreservation of Hematopoietic Stem Cells and Red Blood Cells, University of Ottawa, Ottawa, 2016.

(28) Pegg, D. E. Principles of Cryopreservation. *Methods in Molecular Biology* **2015**, *1257*. https://doi.org/10.1007/978-1-4939-2193-5_1.

(29) Scott, K. L.; Lecak, J.; Acker, J. P. Biopreservation of Red Blood Cells: Past, Present, and Future. *Transfus Med Rev* **2005**, *19* (2). https://doi.org/10.1016/j.tmrv.2004.11.004.

(30) Meryman, H. T. Cryoprotective Agents. *Cryobiology* **1971**, *8* (2). https://doi.org/10.1016/0011-2240(71)90024-1.

(31) Cregan, P.; Gotelli, G. Hemolytic Transfusion Reaction Following Transfusion of Frozen and Washed Autologous Red Cells. *Transfusion (Paris)* **1991**, *31* (2). https://doi.org/10.1046/j.1537-2995.1991.31291142950.x.

(32) Rudolph, A. S.; Crowe, J. H. Membrane Stabilization during Freezing: The Role of Two Natural Cryoprotectants, Trehalose and Proline. *Cryobiology* **1985**, *22* (4). https://doi.org/10.1016/0011-2240(85)90184-1.

(33) J., C.; Doshi, M.; N., R. Ice Recrystallization Inhibitors: From Biological Antifreezes to Small Molecules. In *Recent Developments in the Study of Recrystallization*; 2013. https://doi.org/10.5772/54992.

(34) Jang, T. H.; Park, S. C.; Yang, J. H.; Kim, J. Y.; Seok, J. H.; Park, U. S.; Choi, C. W.; Lee, S. R.; Han, J. Cryopreservation and Its Clinical Applications | Elsevier Enhanced Reader. *Integr Med Res* **2017**, *6* (1).

(35) Mazur, P. Basic Problems in Cryobiology. In *Advances in Cryogenic Engineering*; 1964. https://doi.org/10.1007/978-1-4757-0525-6_4.

(36) Pegg, D. E. Principles of Cryopreservation. *Methods in Molecular Biology* **2015**, *1257*. https://doi.org/10.1007/978-1-4939-2193-5_1.

(37) Bakhach, J. The Cryopreservation of Composite Tissues: Principles and Recent Advancement on Cryopreservation of Different Type of Tissues. *Organogenesis*. 2009. https://doi.org/10.4161/org.5.3.9583.

(38) Briard, J. G.; Fernandez, M.; De Luna, P.; Woo, T. K.; Ben, R. N. QSAR Accelerated Discovery of Potent Ice Recrystallization Inhibitors. *Sci Rep* **2016**, *6*. https://doi.org/10.1038/srep26403.

(39) Bank, H. Visualization of Freezing Damage. II. Structural Alterations during Warming. *Cryobiology* **1973**, *10* (2). https://doi.org/10.1016/0011-2240(73)90023-0.

(40) Balcerzak, A. K.; Capicciotti, C. J.; Briard, J. G.; Ben, R. N. Designing Ice Recrystallization Inhibitors: From Antifreeze (Glyco)Proteins to Small Molecules. *RSC Advances*. 2014. https://doi.org/10.1039/c4ra06893a.

(41) Briard, J. G.; Jahan, S.; Chandran, P.; Allan, D.; Pineault, N.; Ben, R. N. Small-Molecule Ice Recrystallization Inhibitors Improve the Post-Thaw Function of Hematopoietic Stem and Progenitor Cells. *ACS Omega* **2016**, *1* (5). https://doi.org/10.1021/acsomega.6b00178.

(42) Knight, C. A.; Wen, D.; Laursen, R. A. Nonequilibrium Antifreeze Peptides and the Recrystallization of Ice. *Cryobiology* **1995**, *32* (1). https://doi.org/10.1006/cryo.1995.1002.

(43) Fayter, A. E. R.; Hasan, M.; Congdon, T. R.; Kontopoulou, I.; Gibson, M. I. Ice Recrystallisation Inhibiting Polymers Prevent Irreversible Protein Aggregation during Solvent-Free

Cryopreservation as Additives and as Covalent Polymer-Protein Conjugates. *Eur Polym J* **2020**, *140*. https://doi.org/10.1016/j.eurpolymj.2020.110036.

(44) Alley, R. B.; Perepezko, J. H.; Bentley, C. R. Grain Growth in Polar Ice: I. Theory. *Journal of Glaciology* **1986**, *32* (112). https://doi.org/10.3189/s0022143000012120.

(45) Alley, R. B.; Perepezko, J. H.; Bentley, C. R. Grain Growth in Polar Ice: II. Application. *Journal of Glaciology* **1986**, *32* (112). https://doi.org/10.3189/s0022143000012132.

(46) J., C.; Doshi, M.; N., R. Ice Recrystallization Inhibitors: From Biological Antifreezes to Small Molecules. In *Recent Developments in the Study of Recrystallization*; 2013. https://doi.org/10.5772/54992.

(47) Fukunaga, Y.; Okada, T. Essential Role of Methyl Groups in Ice Recrystallization Inhibition of Antifreeze Silver Nanoparticles Studied by Surface-Enhanced Raman Scattering. *The Journal of Physical Chemistry C* **2024**, *128* (19), 8068–8076.

(48) Budke, C.; Koop, T. Ice Recrystallization Inhibition and Molecular Recognition of Ice Faces by Poly(Vinyl Alcohol). *ChemPhysChem* **2006**, *7* (12). https://doi.org/10.1002/cphc.200600533.

(49) Abraham, S.; Keillor, K.; Capicciotti, C. J.; Perley-Robertson, G. E.; Keillor, J. W.; Ben, R. N. Quantitative Analysis of the Efficacy and Potency of Novel Small Molecule Ice Recrystallization Inhibitors. *Cryst Growth Des* **2015**, *15* (10). https://doi.org/10.1021/acs.cgd.5b00995.

(50) Wharton, D. A.; Wilson, P. W.; Mutch, J. S.; Marshall, C. J.; Lim, M. Recrystallization Inhibition Assessed by Splat Cooling and Optical Recrystallometry. *Cryo-Letters* **2007**, *28* (1).

(51) Alley, R. B.; Perepezko, J. H.; Bentley, C. R. Grain Growth in Polar Ice: I. Theory. *Journal of Glaciology* **1986**, *32* (112). https://doi.org/10.3189/s0022143000012120.

(52) Alley, R. B.; Perepezko, J. H.; Bentley, C. R. Grain Growth in Polar Ice: II. Application. *Journal of Glaciology* **1986**, *32* (112). https://doi.org/10.3189/s0022143000012132.

(53) Georgiou, P. G.; Marton, H. L.; Baker, A. N.; Congdon, T. R.; Whale, T. F.; Gibson, M. I. Polymer Self-Assembly Induced Enhancement of Ice Recrystallization Inhibition. *J Am Chem Soc* **2021**, *143* (19). https://doi.org/10.1021/jacs.1c01963.

(54) Abraham, S.; Keillor, K.; Capicciotti, C. J.; Perley-Robertson, G. E.; Keillor, J. W.; Ben, R. N. Quantitative Analysis of the Efficacy and Potency of Novel Small Molecule Ice Recrystallization Inhibitors. *Cryst Growth Des* **2015**, *15* (10). https://doi.org/10.1021/acs.cgd.5b00995.

(55) Wharton, D. A.; Wilson, P. W.; Mutch, J. S.; Marshall, C. J.; Lim, M. Recrystallization Inhibition Assessed by Splat Cooling and Optical Recrystallometry. *Cryo-Letters* **2007**, *28* (1).

(56) Wharton, D. A.; Wilson, P. W.; Mutch, J. S.; Marshall, C. J.; Lim, M. Recrystallization Inhibition Assessed by Splat Cooling and Optical Recrystallometry. *Cryo-Letters* **2007**, *28* (1).

(57) Gibson, M. I.; Barker, C. A.; Spain, S. G.; Albertin, L.; Cameron, N. R. Inhibition of Ice Crystal Growth by Synthetic Glycopolymers: Implications for the Rational Design of Antifreeze Glycoprotein Mimics. *Biomacromolecules* **2009**, *10* (2). https://doi.org/10.1021/bm801069x.

(58) Inada, T.; Lu, S. S. Thermal Hysteresis Caused by Non-Equilibrium Antifreeze Activity of Poly(Vinyl Alcohol). *Chem Phys Lett* **2004**, *394* (4–6). https://doi.org/10.1016/j.cplett.2004.07.021.

(59) Biggs, C. I.; Bailey, T. L.; Ben Graham; Stubbs, C.; Fayter, A.; Gibson, M. I. Polymer Mimics of Biomacromolecular Antifreezes. *Nature Communications*. 2017. https://doi.org/10.1038/s41467-017-01421-7.

(60) Biggs, C. I.; Stubbs, C.; Graham, B.; Fayter, A. E. R.; Hasan, M.; Gibson, M. I. Mimicking the Ice Recrystallization Activity of Biological Antifreezes. When Is a New Polymer "Active"? *Macromolecular Bioscience*. 2019. https://doi.org/10.1002/mabi.201900082.

(61) Mitchell, D. E.; Lilliman, M.; Spain, S. G.; Gibson, M. I. Quantitative Study on the Antifreeze Protein Mimetic Ice Growth Inhibition Properties of Poly(Ampholytes) Derived from Vinyl-Based Polymers. *Biomater Sci* **2014**, *2* (12). https://doi.org/10.1039/c4bm00153b.

(62) Mitchell, D. E.; Cameron, N. R.; Gibson, M. I. Rational, yet Simple, Design and Synthesis of an Antifreeze-Protein Inspired Polymer for Cellular Cryopreservation. *Chemical Communications* **2015**, *51* (65). https://doi.org/10.1039/c5cc04647e.

(63) Inada, T.; Lu, S. S. Inhibition of Recrystallization of Ice Grains by Adsorption of Poly(Vinyl Alcohol) onto Ice Surfaces. *Cryst Growth Des* **2003**, *3* (5). https://doi.org/10.1021/cg0340300.

(64) Congdon, T.; Notman, R.; Gibson, M. I. Antifreeze (Glyco)Protein Mimetic Behavior of Poly(Vinyl Alcohol): Detailed Structure Ice Recrystallization Inhibition Activity Study. *Biomacromolecules* **2013**, *14* (5). https://doi.org/10.1021/bm400217j.

(65) Rajan, R.; Jain, M.; Matsumura, K. Cryoprotective Properties of Completely Synthetic Polyampholytes via Reversible Addition-Fragmentation Chain Transfer (RAFT) Polymerization and the Effects of Hydrophobicity. *J Biomater Sci Polym Ed* **2013**, *24* (15). https://doi.org/10.1080/09205063.2013.801703.

(66) Matsumura, K.; Hyon, S. H. Polyampholytes as Low Toxic Efficient Cryoprotective Agents with Antifreeze Protein Properties. *Biomaterials* **2009**, *30* (27). https://doi.org/10.1016/j.biomaterials.2009.05.025.

(67) Stubbs, C.; Lipecki, J.; Gibson, M. I. Regioregular Alternating Polyampholytes Have Enhanced Biomimetic Ice Recrystallization Activity Compared to Random Copolymers and the Role of Side Chain versus Main Chain Hydrophobicity. *Biomacromolecules* **2017**, *18* (1). https://doi.org/10.1021/acs.biomac.6b01691.

(68) Olijve, L. L. C.; Hendrix, M. M. R. M.; Voets, I. K. Influence of Polymer Chain Architecture of Poly(Vinyl Alcohol) on the Inhibition of Ice Recrystallization. *Macromol Chem Phys* **2016**, *217* (8). https://doi.org/10.1002/macp.201500497.

(69) Mitchell, D. E.; Fayter, A. E. R.; Deller, R. C.; Hasan, M.; Gutierrez-Marcos, J.; Gibson, M. I. Ice-Recrystallization Inhibiting Polymers Protect Proteins against Freeze-Stress and Enable Glycerol-Free Cryostorage. *Mater Horiz* **2019**, *6* (2). https://doi.org/10.1039/c8mh00727f.

(70) Jain, M.; Rajan, R.; Hyon, S. H.; Matsumura, K. Hydrogelation of Dextran-Based Polyampholytes with Cryoprotective Properties via Click Chemistry. *Biomater Sci* **2014**, *2* (3). https://doi.org/10.1039/c3bm60261c.

(71) Deller, R. C.; Congdon, T.; Sahid, M. A.; Morgan, M.; Vatish, M.; Mitchell, D. A.; Notman, R.; Gibson, M. I. Ice Recrystallisation Inhibition by Polyols: Comparison of Molecular and Macromolecular Inhibitors and Role of Hydrophobic Units. *Biomater Sci* **2013**, *1* (5). https://doi.org/10.1039/c3bm00194f.

(72) Phillips, M.; Romeo, F.; Bitsaktsis, C.; Sabatino, D. B7H6-Derived Peptides Trigger TNF-α-Dependent Immunostimulatory Activity of Lymphocytic NK92-MI Cells. *Biopolymers* **2016**. https://doi.org/10.1002/bip.22879.

(73) Wincott, F. E. Strategies for Oligoribonucleotide Synthesis According to the Phosphoramidite Method. *Curr Protoc Nucleic Acid Chem* **2000**, *00* (1). https://doi.org/10.1002/0471142700.nc0305s00.

(74) Hermkens, P. H. H.; Ottenheijm, H. C. J.; Rees, D. C. Solid-Phase Organic Reactions II: A Review of the Literature Nov 95-Nov 96. *Tetrahedron* **1997**, *53* (16). https://doi.org/10.1016/S0040-4020(97)00279-2.

(75) Camarero, J. A.; Cotton, G. J.; Adeva, A.; Muir, T. W. Chemical Ligation of Unprotected Peptides Directly from a Solid Support. *Journal of Peptide Research* **1998**, *51* (4). https://doi.org/10.1111/j.1399-3011.1998.tb00428.x.

(76) Stawikowski, M.; Fields, G. B. Introduction to Peptide Synthesis. *Curr Protoc Protein Sci* **2012**, *1* (SUPPL.69). https://doi.org/10.1002/0471140864.ps1801s69.

(77) Meldal, M.; Auzanneau, F. I.; Hindsgaul, O.; Palcic, M. M. A PEGA Resin for Use in the Solid-Phase Chemical-Enzymatic Synthesis of Glycopeptides. *J Chem Soc Chem Commun* **1994**, No. 16. https://doi.org/10.1039/C39940001849.

(78) Coin, I.; Beyermann, M.; Bienert, M. Solid-Phase Peptide Synthesis: From Standard Procedures to the Synthesis of Difficult Sequences. *Nat Protoc* **2007**, *2* (12). https://doi.org/10.1038/nprot.2007.454.

(79) Lagerberg, J. W. Cryopreservation of Red Blood Cells. In *Cryopreservation and Freeze-Drying Protocols*; Wolkers Willem F. and Oldenhof, H., Ed.; Springer New York: New York, NY, 2015; pp 353–367. https://doi.org/10.1007/978-1-4939-2193-5_17.

(80) Capicciotti, C. J.; Leclère, M.; Perras, F. A.; Bryce, D. L.; Paulin, H.; Harden, J.; Liu, Y.; Ben, R. N. Potent Inhibition of Ice Recrystallization by Low Molecular Weight Carbohydrate-Based Surfactants and Hydrogelators. *Chem Sci* **2012**, *3* (5). https://doi.org/10.1039/c2sc00885h.

(81) Gibson, M. I. Slowing the Growth of Ice with Synthetic Macromolecules: Beyond Antifreeze(Glyco) Proteins. *Polymer Chemistry*. 2010. https://doi.org/10.1039/c0py00089b.

(82) McMunn, L. E.; Walsh, E. M.; Ben, R. N. TARGETED DEVELOPMENT AND OPTIMIZATION OF SMALLMOLECULE ICE RECRYSTALLIZATION INHIBITORS (IRIs) FOR THE CRYOPRESERVATION OF

BIOLOGICAL SYSTEMS. *Cryo-Letters* **2024**, *45* (2), 69–87. https://doi.org/10.54680/fr24210110112.

(83) Warren, M. T.; Galpin, I.; Bachtiger, F.; Gibson, M. I.; Sosso, G. C. Ice Recrystallization Inhibition by Amino Acids: The Curious Case of Alpha- and Beta-Alanine. *Journal of Physical Chemistry Letters* **2022**, *13* (9). https://doi.org/10.1021/acs.jpclett.1c04080.

(84) Sakai, K.; Hirayama, N.; Tamura, R. *Novel Optical Resolution Technologies*, 1st ed.; Springer: Berlin, 2007; Vol. 269.

(85) Tulashie, S. K.; Lorenz, H.; Hilfert, L.; Edelmann, F. T.; Seidel-Morgenstern, A. Potential of Chiral Solvents for Enantioselective Crystallization. 1. Evaluation of Thermodynamic Effects. *Cryst Growth Des* **2008**, *8* (9). https://doi.org/10.1021/cg800356v.

(86) Hyone-Myong Eun. *Enzymology Primer for Recombinant DNA Technology*; Academic Press, 1996; Vol. 1. https://doi.org/10.1016/b978-0-12-243740-3.x5000-5.

(87) Graham, B.; Fayter, A. E. R.; Houston, J. E.; Evans, R. C.; Gibson, M. I. Facially Amphipathic Glycopolymers Inhibit Ice Recrystallization. *J Am Chem Soc* **2018**, *140* (17). https://doi.org/10.1021/jacs.8b02066.

(88) Jeon, N.; Choi, I.; Lee, P. C. W.; Lee, E. Gold Nanoparticle-Tethered Peptide Nanofibrils for Monitoring Ice Recrystallization Inhibition: Implications for Cryopreservation. *ACS Appl Nano Mater* **2022**, *5* (10). https://doi.org/10.1021/acsanm.2c03469.

(89) Nathanael, J. G.; White, J. M.; Richter, A.; Nuske, M. R.; Wille, U. Oxidative Damage of Proline Residues by Nitrate Radicals ($NO_3^{\cdot}$): A Kinetic and Product Study. *Org Biomol Chem* **2020**, *18* (35), 6949–6957. https://doi.org/10.1039/D0OB01337D.

(90) Ouellette, R. J.; Rawn, J. D. *Principles of Organic Chemistry*; 2015. https://doi.org/10.1097/00010694-193910000-00008.

(91) Ando, A.; Shioiri, T. Enantioselective Synthesis of β-Hydroxy-α-Methyl Carbonyl Compounds by Aldol Reaction. *Tetrahedron* **1989**, *45* (16). https://doi.org/10.1016/S0040-4020(01)81078-4.

# 6 Contribution to research

- Simon Sinn helped in the synthesis, solubility testing in PBS, and IRI analysis of *N*-acetyl-*L*-phenylalanine, *N*-isobutyric-*L*-phenylalanine, Synthesis of Boc-*L*-phenylalanine, *N*-butyric-β-phenylalanine, and *N*-isopropyl-β-phenylalanine.